Innovative Tuneable Optical Devices Based on Smart Electroactive Elastomers

Leihao Chen

Submitted in partial fulfilment of the requirements of the

Degree of Doctor of Philosophy

School of Engineering and Materials Science

Queen Mary University of London

November 2019

Statement of originality

I, Leihao Chen, confirm that the research included within this thesis is my own work or that where it has been carried out in collaboration with, or supported by others, that this is duly acknowledged below and my contribution indicated. Previously published material is also acknowledged below.

I attest that I have exercised reasonable care to ensure that the work is original, and does not to the best of my knowledge break any UK law, infringe any third party's copyright or other Intellectual Property Right, or contain any confidential material.

I accept that the College has the right to use plagiarism detection software to check the electronic version of the thesis.

I confirm that this thesis has not been previously submitted for the award of a degree by this or any other university.

Signature:

Date:

Abstract

Electroactive polymers that deform in response to electrical stimulation have been a significant area of interest under development over the last decade. Recently, so-called dielectric elastomer actuators (DEAs), which consist of a dielectric elastomer membrane sandwiched between two compliant electrodes, have been shown as a promising technology for the development of new adaptive optical devices. This thesis presents research into tuneable optical transparency devices using DEA technology, which are capable of reversibly controlling light transmittance by electrically changing the surface topography using transparent electrodes. The deformable poly(3,4-ethylenedioxythiophene) polystyrene sulfonate (PEDOT:PSS) conducting polymer is selected as the optimal transparent conductor amongst a diversity of electronic materials, owing to its high transparency, environmental stability and surface wrinkling reversibility. In this work, the concept to make the surface transparency electrically tuneable to both higher and lower values within the same device is presented. This concept is applicable to any soft insulating membrane, by coating both of its surfaces with a circular transparent stretchable conductor, surrounded by a stretchable annular conductor. The two conductors are used as independently addressable electrodes to generate a dielectric elastomer-based actuation of the membrane, so as to electrically control its surface topography. The optical transmittance can thus be modulated within a broad range between 25% and 83%. Furthermore, another concept to achieve the electrically-induced directional control of light diffusion on soft elastomer membranes is demonstrated. The uniaxial pre-strain of elastomer membranes contributes to the alignment of surface wrinkles upon

electrical activation to directionally scatter light. This concept provides a dual function that can not only electrically spread light in a desired direction but also tune the optical transmittance within an even broader range between 4% and 75%. Those tuneable optical devices using dielectric elastomer actuation have shown thin structures, low specific weight and acoustically silent operation. They could be potentially useful in electrically operated smart windows, controllable light diffusers and directional beam spreaders with light shaping.

Acknowledgements

First and foremost, I would like to express my greatest appreciation to my principal supervisor Prof James Busfield, for his constant encouragement, valuable suggestions and enlightening instructions through all the stages of my PhD study. Truly, without his help in revising and polishing my drafts, the completion of this thesis would not have been possible. I feel so lucky and honoured to be his student. It has been an invaluable experience to work with him.

Secondly, I would like to show my sincere gratitude to Prof Federico Carpi, who has been acting as the external supervisor for my entire PhD study. He has been always very enthusiastic about research and inspired me a lot in this research project. His consistent support, insightful guidance and professional advice have contributed greatly to the completion of this thesis.

I would also like to give special thanks to my second supervisor Dr Nuria Gavara, as well as other academic staff and technicians at Queen Mary University of London, for their useful advice and kind discussion with me on the research project.

Many thanks to all the members of Soft Matter Group and all my friendly colleagues in SEMS, for their suggestions and assistance on the experimental work, and making my time in the UK joyful and unforgettable.

I gratefully acknowledge the financial support from the China Scholarship Council and Queen Mary University of London, for providing me this amazing opportunity to study in London and making my PhD research work possible.

Last but not least, my sincere thanks go to my beloved family, who have always been helping me out of difficulties, and consistently caring and encouraging me all through my PhD period.

Table of contents

List of figures

List of tables

List of symbols and abbreviations

Symbols:

A	Area
C	Capacitance
E	Electric field
I	Current
Q	Amount of heat added to the system
R_s	Surface resistance
T_d	Near-field diffuse transmittance
T_f	Far-field transmittance
T_t	Near-field total transmittance
U	Stored electrostatic energy
V	Voltage
W	Amount of work done by the system
Y	Elastic modulus
p	Electrostatic pressure or Maxwell pressure
q	Electric charge
s_A	Area strain
s_r	Radial strain
s_z	Thickness strain
z	Thickness
ε_0	Dielectric permittivity of vacuum
ε_r	Dielectric constant

Abbreviations:

AFM	Atomic force microscopy
AgNW	Silver nanowire
APS	Ammonium persulphate
CNT	Carbon nanotube
DE	Dielectric elastomer
DEA	Dielectric elastomer actuator
DMA	Dynamic mechanical analysis
DMSO	Dimethyl sulfoxide
DSC	Differential scanning calorimetry
EAC	electroactive ceramic
EAP	Electroactive polymer
IPA	Isopropanol
IPMC	Ionic polymer-metal composite
ITO	Indium tin oxide
LiCl	Lithium chloride
MBAA	*N,N'*-methylenebisacrylamide
PAAm	Polyacrylamide
PDLC	Polymer-dispersed liquid crystals
PDMS	Poly(dimethylsiloxane)
PDVF	Poly(vinylidene fluoride)
PEDOT:PSS	Poly(3,4-ethylenedioxythiophene) polystyrene sulfonate
PET	Polyethylene terephthalate

PMMA	Polymethyl methacrylate
PTFE	Polytetrafluoroethylene
PU	Polyurethane
SEM	Scanning electron microscopy
SMA	Shape memory alloy
SPD	Suspended particle devices
SWCNT	Single-walled carbon nanotube
TEMED	*N,N,N',N'*-tetramethylethylenediamine

Chapter 1 Introduction

1.1 Background and objectives

Electroactive devices that deform in response to electrical stimulation are currently at the forefront of developing tuneable optical systems, tactile interfaces and bioinspired robots (Carpi, Bauer, & De Rossi, 2010). A mechanical device that can move or control a mechanism or system is defined as an actuator, which is operated by converting a source of energy, for example, electric current, hydraulic fluid pressure, or pneumatic pressure, into motion. As an emerging class of smart electromechanical devices, electroactive polymer (EAP) actuators are able to undergo deformations when stimulated by electricity (O'Halloran, O'Malley, & McHugh, 2008). Compared with conventional actuating systems, such as electric motors, hydraulic cylinders, piezoelectric actuators and pneumatic actuators, EAP actuators exhibit many advantages, including large active strains when electrically stimulated, light weight, relatively fast response speed, high mechanical compliance, structural simplicity, scalability, acoustically silent operation and a reasonably low cost (Carpi, Kornbluh, Sommer-Larsen, & Alici, 2011). Furthermore, EAP actuators are normally regarded as "artificial muscles" because of their characteristics to mimic the motion of natural muscles and therefore popularly used for various biomimetic motion applications (Anderson, Gisby, McKay, O'Brien, & Calius, 2012).

As a distinct type of EAP actuators, dielectric elastomer actuators (DEAs) have been playing an important role in the development of electrically stretchable materials and devices since a remarkable study in the year 2000. Research conducted at SRI International found an unprecedented electromechanical transduction performance of dielectric elastomers (DE) that could undergo electrically induced actuation with high speeds and giant strains over 100% (R. Pelrine, Kornbluh, Pei, & Joseph, 2000). In general, DEAs are composed of a dielectric elastomer thin film, such as acrylic elastomer, silicone elastomer or polyurethane, sandwiched between two compliant electrodes. By applying a voltage between the electrodes, the DE thin film experiences a surface expansion and a thickness compression due to purely electrostatic pressure. Similarly to other EAP actuators, DEAs also show fast response, long lifetime, high resilience, light weight, scalability, shock tolerance, free from noise and heat, as well as low costs (Carpi et al., 2010). With those exceptional actuation characteristics, DEAs can be potentially useful for smart adaptive devices in various fields, varying from tuneable optics to haptic interfaces, soft robotics, biomedical applications, microfluidics, energy harvesting and sensing applications (Rosset & Shea, 2016).

Recently, DEAs for electrically tuneable optical systems have attracted an increasing interest. Several studies have been focused on such smart optical devices based on miniaturised soft actuators. As an example, electrically tuneable lenses were developed by using DEAs to control the curvature radius of soft lenses to thereby change the focal length (Carpi, Frediani, Turco, & De Rossi, 2011; Maffli, Rosset, Ghilardi, Carpi, & Shea, 2015; Shian, Diebold, & Clarke, 2013; Son et al., 2012; Wei, Domicone, & Zhao, 2014). Also, DEA-

based tuneable diffraction gratings were devised to change the grating period by electrically deforming a soft grating pattern mounted on the elastomer membrane (Aschwanden, Beck, & Stemmer, 2007; Fang, Punckt, Leung, Schniepp, & Aksay, 2010; Ji, Rosset, & Shea, 2016; Rosset et al., 2013; Y. Wang, Zhou, Sun, Wu, & Zhang, 2014). Early prototypes of tuneable window devices that consist of clear dielectric elastomers that use nearly transparent electrodes have been proposed which electrically modulate the optical transparency of soft elastomeric membranes (Ong, Shrestha, & Lau, 2015; Shian & Clarke, 2016). Other examples include the electrically tuneable phase retarders that allowed arbitrary phase shifts of an optical beam (Beck, Fiolka, & Stemmer, 2009) and the electrically tuneable photonic crystals that produced marked colour changes (Q. Zhao et al., 2012). Owing to its ability to tune the optical properties by deformation, DEA technology has started to become of practical use in the optics industry. For instance, the Swiss company Optotune has commercialised a series of electrically tuneable optics based on DEAs for different optical applications (Carpi, Kornbluh, et al., 2011; Rosset & Shea, 2016).

The use of conductive transparent electrode materials is another significant aspect of developing DEA-based devices particularly for adaptive optical applications. Transparent electrodes are a new emerging functional conductor. They can not only exhibit conductivity and compliance that conventional carbon-based electrodes normally have but also provide an additional essential feature of optical transparency. Previous research has summarised a diversity of available transparent electronic materials, such as silver nanowires, metal oxide thin films, carbon nanotubes, graphene, conducting

hydrogels and conducting polymers (McCoul, Hu, Gao, Mehta, & Pei, 2016). However, their compatibility, environmental stability and electro-optical transduction performance when integrated with dielectric elastomers still need to be further evaluated to obtain reliable DEA-based tuneable optical devices.

Thus, the aims of this research are to first deepen the investigation on the selection of optimal transparent electrode materials used for transparent DEAs, and then develop novel variable optical transmission devices based on DEAs which use reliable transparent conductors to achieve the electrically-induced reversible and continuous tuning of surface transparency.

The light modulating devices developed in this work are thin structures, with fast response, low specific weight and acoustically silent operation. Therefore, they could be potentially useful in electrically tuneable privacy windows, controllable light diffusers and directional light beam spreaders.

1.2 Outline of thesis

The rest of this thesis is structured as follows. In Chapter 2, the general background of electroactive polymer technology is first introduced. A literature review on the fundamental aspects of DEAs (including working principles, examples of different dielectric elastomer materials, compliant electrode materials, the effects of pre-stretch on actuation, the role of electromechanical instability and a discussion of different device configurations) is then conducted. Following that, state-of-the-art technologies such as electrochromics, polymer-dispersed liquid crystals, suspended particles and

DEA-based devices that can be used to electrically modulate the optical transparency are summarised and compared.

Chapter 3 investigates a variety of transparent electronic materials, including silver nanowires (AgNWs), conducting hydrogels, ionogels, PEDOT:PSS conducting polymer and PEDOT:PSS/AgNWs compounds, used as transparent electrodes for fabricating DEA-based devices with variable optical transmission. The material's properties, electrode preparation methods, fabrication techniques and the electrical tuning performance of each of the different DEA device are described. Furthermore, the benefits and drawbacks for each transparent electrode are compared, and the optimal electrode materials are selected.

Chapter 4 presents a concept to make the optical transparency electrically tuneable to both higher and lower values, within a single device. The concept is applicable to any soft insulating membrane, by coating both of its surfaces with a circular transparent stretchable conductor, surrounded by a stretchable annular conductor. The two conductors are used as independently addressable electrodes to generate a dielectric elastomer-based actuation of the membrane, so as to electrically control its surface topography. Such device shows that the surface transparency can be modulated electrically between opaque and transparent.

In Chapter 5, a DEA-based device is developed to obtain the electrically-induced directional control of light diffusion on soft elastomer membranes. The uniaxial pre-strain of elastomer membranes allows the alignment of surface wrinkles upon electrical activation to directionally scatter light. Multi-directional

light diffusion is also achieved by attaching two single directional light diffusers orthogonally to each other. This design provides a dual function that can not only electrically spread light in a desired direction but also tune the optical transmittance within an even broader range than that of the dual-mode device described in Chapter 4.

Chapter 6 presents the conclusions made from this thesis. Furthermore, possible future work on this topic is described, with some promising routes to make the tuneable optical transparency devices using dielectric elastomer actuation obtain a broader tuning range and a faster response speed.

Chapter 2 Literature review

2.1 Overview of electroactive polymer technology

Electroactive polymers (EAPs) are an emerging class of materials for actuation technology, capable of undergoing a substantial change in size or shape when stimulated by an electric field. EAPs are therefore recognised as a type of artificial muscle which can mimic the motion of natural muscle. When used in artificial muscle applications, EAPs exhibit better actuation performance than other conventional actuator technologies, such as shape memory alloys (SMA), electroactive ceramics (EAC) and McKibben actuators. The comparison between EAP and other existing transducer actuators is listed in Table 2.1. EAP actuators offer more predictable movement and faster response speed than SMA. Also, EAPs provide greater mechanical compliance and larger actuation strain in comparison with EAC. In addition, EAP actuators are superior to McKibben actuators which usually use heavy electric motors and pneumatics (O'Halloran et al., 2008). Furthermore, the low force and high strain generated by EAPs are well suited to the optical applications explored in the thesis. In general, the exceptional characteristics of EAP actuators include large active strains when activated by an applied voltage, light weight, fast response speed, high mechanical compliance, structural simplicity, scalability, free from acoustic noise and mostly low cost (Carpi, Kornbluh, et al., 2011).

Table 2.1 Comparison between EAP and other established transducer actuators (O'Halloran et al., 2008).

Property	EAP	SMA	EAC
Actuation strain	Over 300%	<8%	0.1%-0.3%
Force	0.1-25 MPa	200 MPa	30-40 MPa
Reaction speed	µs to min	ms to min	µs to sec
Density	1-2.5 g/cc	5-6 g/cc	6-8 g/cc
Drive voltage	Ionic-EAP: 1-7 V Elec-EAP: 10-150 V/µm	5 V	50-800 V
Fracture behaviour	Resilient, elastic	Resilient, elastic	Fragile

- EAP classification

Depending on different actuation mechanism, EAPs can be broadly categorised into two major classes: ionic and electronic. Table 2.2 summarises the EAP classification and the type of materials that are involved in each subdivision. Ionic EAPs are activated by electrically-induced diffusion or mobility of ions and/or molecules, while electronic EAPs are driven by an electrostatic pressure. Polymer gels, ionic polymer-metal composites (IPMC), conjugated polymers and carbon nanotubes are typical examples of ionic EAPs, whereas piezoelectric polymers, electrostrictive polymers, dielectric elastomers, liquid crystal elastomers and carbon nanotube aerogels fall under the electronic EAPs (Carpi, Kornbluh, et al., 2011; O'Halloran et al., 2008).

Table 2.2 EAP classification (Carpi, Kornbluh, et al., 2011).

EAP class	Materials
Ionic EAPs	Polymer gels
	Ionic polymer-metal composites (IPMC)
	Conjugated polymers
	Carbon nanotubes
Electronic EAPs	Piezoelectric polymers
	Electrostrictive polymers
	Dielectric elastomers
	Liquid crystal elastomers
	Carbon nanotube aerogels

- Ionic EAPs

The primary advantage of ionic EAPs is that they can be activated by relatively low driving voltages normally in the order of 1 V. However, since they are driven by electromechanical energy transduction mechanism, the electro-diffusion of ions and solvent may not only cause material degradations under a cyclic loading but will also lead to a slower response speed. Thus, the use of ionic EAP actuators is constrained by short lifetime and long response time (Carpi, Kornbluh, et al., 2011). A schematic representation of the actuation mechanism of an IPMC actuator is demonstrated in Figure 2.1. At the neutral state, the IPMC actuator is flat. Application of a bias voltage causes cations to migrate to the cathode, generating a bending motion. As the voltage is released, the build-up pressure gradient will cause water to flow towards the anode, resulting in the IPMC actuator relaxing back to the flat state (Madden et al., 2004).

Figure 2.1 Actuation mechanism of an IPMC actuator (Madden et al., 2004).

- Electronic EAPs

In contrast to the features of ionic EAPs, electronic EAPs present several advantages including relatively large actuation strain and stress, fast response speed and long lifetime even under cyclic loading. However, since the actuation mechanism is due to the electrostatic nature, electronic EAP actuators often require high driving voltages up to the order of 100 V/μm. The

applicable approaches to enable electronic EAP actuators operated at low voltages are usually through the modification of materials with high dielectric constant and the fabrication of thin layers of EAP. A schematic representation of the basic functional element and typical response of an electronic EAP actuator is shown in Figure 2.2. The applied electric field causes an increase in the stress and corresponding strain of the electronic EAP actuator. If the applied voltage results in the reorientation of a crystalline structure that changes the material permittivity, then the EAP is called an electrostrictive polymer, such as poly(vinylidene fluoride) (PVDF) and certain polyurethanes (PU). If the applied voltage leads to the interaction of the electrostatic charges on the electrodes, then the EAP can be regarded as a dielectric elastomer (Carpi, Kornbluh, et al., 2011). The fundamental aspects of dielectric elastomer actuators are described in greater details in the following section.

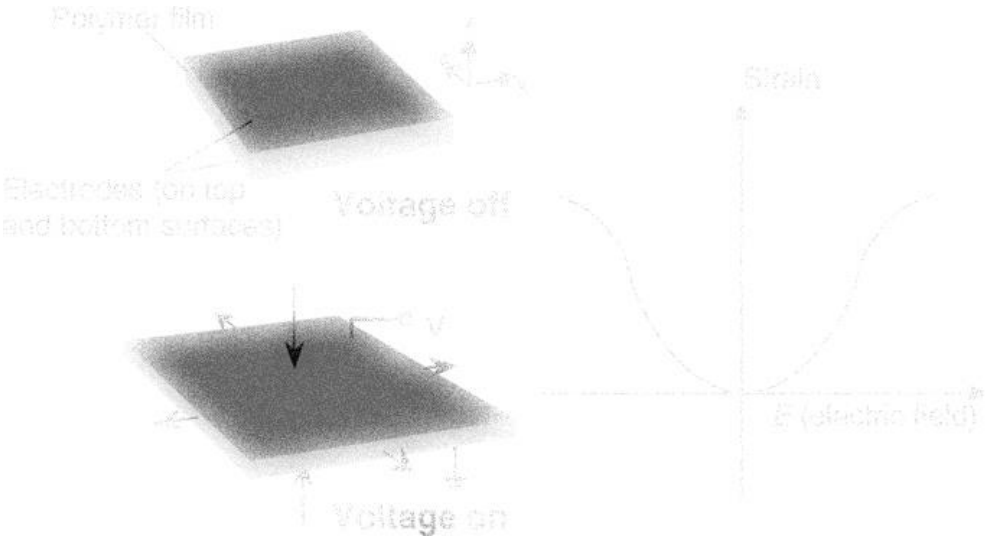

Figure 2.2 Functional element and typical response of an electronic EAP actuator (Carpi, Kornbluh, et al., 2011).

2.2 Fundamental aspects of dielectric elastomer actuators

2.2.1 Introduction

The concept that a solid material deforms in response to electrical stimulation can be dated back to 1880, when a natural rubber sample was demonstrated to change in shape when a large voltage was applied through it. This was believed to be the first observation of actuation associated with a dielectric elastomer (Roentgen, 1880). Dielectric elastomer actuators (DEAs) have become a promising technology to manufacture electrically stretchable devices since their unprecedented electromechanical transduction performance was discovered by researchers from the SRI International in the 1990s (Carpi et al., 2010). In this study, electrically actuated elastomers with high speed and giant strains over 100% were observed (R. Pelrine, Kornbluh, Pei, et al., 2000). DEAs are essentially compliant variable capacitors composed of a dielectric elastomer film sandwiched between two compliant electrodes. By applying an electric field across electrodes, purely electrostatic forces cause the elastomer film to compress in thickness and expand in area. When the electric field is released, the elastomer film will return to its original shape. As shown in Figure 2.3, a typical DEA is fabricated by stretching the elastomer film on a rigid frame and applying electrode patterns on a small portion of the pre-stretched film on both sides. The electrodes are then connected with an external power source to create the actuation (R. Pelrine, Kornbluh, & Kofod, 2000).

Figure 2.3 Circular dielectric elastomer actuator with biaxial pre-strain, inactivated when voltage is off and activated when voltage is on (R. Pelrine, Kornbluh, & Kofod, 2000).

The exceptional actuation characteristics of DEAs include fast response, high resilience, light weight, scalability, shock tolerance, noise- and heat-free, and low costs (Carpi et al., 2010). Therefore, smart devices based on DEAs have been a subject of interest undergoing continuous development throughout the last two decades and this research area has experienced substantial growth. Possible future application areas of DEAs exist in adaptive optics, haptic interfaces, soft robotics, biomedical applications, microfluidics, energy harvesting and sensing applications (Rosset & Shea, 2016). The greatest challenge in the development of DEAs currently is the requirement for high electric fields owing to the actuation mechanism being electrostatic in nature. Actuation voltages required for DE films 10-100 µm in thickness often vary from 500 V to 10 kV (Brochu & Pei, 2010). However, the high voltage issue can be strategically addressed by developing high dielectric constant elastomers and manufacturing them as thin films (Carpi et al., 2010).

2.2.2 Working principles

A schematic representation of the operating principle of DEAs is demonstrated in Figure 2.4. As an electric field is applied across compliant electrodes that are coated on both sides of the DE film, the electrostatic attraction between the opposing charges on the two electrodes creates a compressive stress which causes the film to contract in the thickness direction, whereas the electrostatic repulsion of the like charges on the two electrodes generates a tensile stress which results in the film stretching in the length and width directions. When the electric field is discharged, the interactions of electrostatic charges will no longer exist and hence the elastomer film will reversibly return back to its initial shape. The actuation deformation results from the approximate incompressibility of most dielectric elastomers, which means the film volume remains constant during the actuation cycle. Therefore, any reduction in thickness is accompanied by an increase in planar area (Brochu & Pei, 2010; R. Pelrine, Kornbluh, Pei, et al., 2000). The adjustment of driving voltages can be used to control the amount of generated electrostatic forces and corresponding actuation strains and DEAs can thus be potentially useful to design adaptive devices for achieving voltage-induced continuous shape changes between different states.

Figure 2.4 Working principle of dielectric elastomer actuators. An electric field applied across compliant electrodes coated on both sides of a dielectric elastomer film causes the surface expansion and thickness compression (Bar-Cohen, 2004).

The primary mechanism contributing to the deformation of actuation is attributed to the electrostatic pressure, also known as the Maxwell pressure. The derivation of the relationship between the Maxwell pressure and actuation voltage is illustrated as follows (Brochu & Pei, 2010; R. E. Pelrine, Kornbluh, & Joseph, 1998).

According to the first law of thermodynamics, within a closed system the change in internal energy $\mathrm{d}U$ is equal to the amount of heat added to the system δQ minus the amount of work done $\mathrm{d}W$ by the system.

$$\mathrm{d}U = \delta Q - \mathrm{d}W \tag{2.1}$$

Provided that a DEA is operated at a constant temperature ($\delta Q = 0$) and the Maxwell pressure p causes the film with an area A to change in thickness $\mathrm{d}z$, the change in electrostatic energy is then given by

$$\mathrm{d}U = -\mathrm{d}W = pA\mathrm{d}z \tag{2.2}$$

Thus, the Maxwell pressure can be written as

$$p = \frac{1}{A}\frac{\mathrm{d}U}{\mathrm{d}z} \tag{2.3}$$

As a DEA is regarded as a capacitor, the stored electrostatic energy *U* on the DE film is given by

$$U = 0.5\frac{q^2}{C} = 0.5\frac{q^2 z}{\varepsilon_0 \varepsilon_r A} \tag{2.4}$$

where q is the charge on the electrodes, C is the capacitance ($C = \varepsilon_0 \varepsilon_r A/z$), ε_0 is the dielectric permittivity of vacuum ($8.85 \times 10^{-12} F/m$), ε_r is the elastomer's dielectric constant and z is the film thickness.

Provided that dielectric elastomers are incompressible, where the material volume remains a constant during the actuation cycle, thus

$$volume = Az = constant \tag{2.5}$$

which can be expressed as

$$A\mathrm{d}z + z\mathrm{d}A = 0$$

or

$$\frac{\mathrm{d}A}{A} = -\frac{\mathrm{d}z}{z} \tag{2.6}$$

The change in the stored electrostatic energy $\mathrm{d}U$ for a change in thickness $\mathrm{d}z$ and a change in area $\mathrm{d}A$ can be derived from Equation (2.4) as

$$\mathrm{d}U = \frac{0.5q^2}{\varepsilon_0 \varepsilon_r A}\mathrm{d}z - \frac{0.5q^2 z}{\varepsilon_0 \varepsilon_r A^2}\mathrm{d}A \tag{2.7}$$

Substituting Equation (2.6) into Equation (2.7) gives

$$\mathrm{d}U = \frac{q^2}{\varepsilon_0 \varepsilon_r A}\mathrm{d}z \tag{2.8}$$

Then, substituting Equation (2.8) into Equation (2.3) gives

$$p = \frac{q^2}{\varepsilon_0 \varepsilon_r A^2} \tag{2.9}$$

Since the relationships between the charge q, voltage V and electric field E are given by

$$q = CV = \frac{\varepsilon_0 \varepsilon_r A}{z} V = \varepsilon_0 \varepsilon_r AE \tag{2.10}$$

By substituting Equation (2.10) into Equation (2.9), the Maxwell pressure can finally be expressed as

$$p = \varepsilon_0 \varepsilon_r E^2 = \varepsilon_0 \varepsilon_r (\frac{V}{z})^2 \tag{2.11}$$

Therefore, the Maxwell pressure induced on the elastomer film is directly proportional to both the material's dielectric constant and the square of the applied electric field or voltage, while inversely proportional to the square of the film thickness.

Assuming linear-elasticity and free boundary approximations, which are only valid at small strains, the thickness strain s_z can be written as

$$s_z = -\frac{p}{Y} = -\frac{\varepsilon_0 \varepsilon_r E^2}{Y} = -\frac{\varepsilon_0 \varepsilon_r (V/z)^2}{Y} \tag{2.12}$$

where Y is the elastic modulus. It can be noted from above equations that developing high dielectric constant elastomers and processing them as thin films are important when trying to increase the electrostatic pressure or actuation strains without significantly increasing the driving voltages.

2.2.3 Dielectric elastomer materials

The general material requirements for a polymer film to demonstrate dielectric elastomer actuation under the Maxwell pressure include a need for a relatively soft material with low modulus of elasticity together with good electrical insulation and a high dielectric strength in order to sustain high electric fields. Different types of polymers, such as polyacrylics, silicones, polyurethanes (PUs), isoprene and fluoroelastomers, have been evaluated for their suitability as dielectric elastomers since the late 1990s. Among them, acrylic elastomers, silicone elastomers and PUs are three promising classes of DE materials because of their excellent actuation performance and therefore they have been extensively used for the fabrication of DEA-based devices (Brochu & Pei, 2010; Carpi, Kornbluh, et al., 2011). Table 2.3 compares relevant properties of those popular DE materials, which are described in more details as follows.

Table 2.3 Comparison of commercially available dielectric elastomer material properties (Brochu & Pei, 2010).

Property	Acrylic (3M VHB 4910)	Silicone (Nusil CF19-2186)	Polyurethane (Deerfield PT6100S)
Pre-strain (x%, y%)	(300, 300)	(45, 45)	-
Energy density (MJ/m^3)	3.4	0.75	0.087
Actuation stress (MPa)	7.2	3	1.6
Thickness strain (%)	61	39	11
Area strain (%)	158	64	-
Young's modulus (MPa)	3.0	1.0	17
Electric field strength (MV/m)	412	350	160
Dielectric constant (at 1 kHz)	4.8	2.8	7
Dielectric loss factor (at 1 kHz)	90	6.3	21
Mechanical loss factor (at 80 Hz)	<0.005	0.005	0.5
Coupling efficiency k^2 (%)	0.18	0.05	0.08
Efficiency (at 80 Hz) (%)	80	79	-
Total strain ($\frac{\varepsilon_r E^2}{Y}$) ($\times 10^9$ m/F)	271	339	10.6
Strain per field ($\frac{\varepsilon_r}{Y}$) (MPa^{-1})	1.6	2.8	0.41

- Acrylic elastomers

Commercially available 3M acrylic VHB elastomers (VHB 4910 and VHB 4905) in the form of transparent and viscoelastic tapes are some of the most commonly used dielectric materials for DEAs. The outstanding performance of acrylic elastomers is the significantly large actuation strains, which have been reported in excess of 380% (Kornbluh et al., 2002). Such giant deformation is primarily attributed to the application of a large pre-strain before actuation, leading to the increased dielectric breakdown strength (Carpi, Kornbluh, et al., 2011). The theoretical energy density of acrylic elastomers is impressively high at 3.4 MJ/m^3, greater than that of any other conventional field-induced actuator technology. Also, acrylics have high coupling coefficients and their efficiencies are possible to reach 90% (Brochu & Pei, 2010). Additionally, due to high surface energy and viscoelastic phenomenon, acrylic elastomers which are supplied in the form of double-sided adhesive tapes offer good adhesion and are therefore easy to handle with most compliant electrodes. Nevertheless, the drawbacks of acrylic elastomers due to their relatively high glass transition temperature are a large variation in mechanical behaviour with temperature and high viscoelastic losses with substantial creep and stress relaxation (O'Halloran et al., 2008). The glass transition temperature of acrylic VHB 4910 can be determined by differential scanning calorimetry (DSC) to be around -40°C, while dynamic mechanical analysis (DMA) on the same material shows a broad glass transition range from -50°C to 60°C (Sheng, Chen, Qiang, Li, & Wang, 2012). The viscoelastic behaviour of acrylic elastomers unfortunately constrains the response speed

and reliability in practical use, although they have been mostly used in laboratorial tests when large actuation strains are needed.

- Silicone elastomers

Silicone elastomers or polydimethylsiloxane (PDMS) are another widely used group of DE materials. They are optically clear and generally inert, non-toxic and non-flammable. Commercially available silicone products that have been used for DEAs include PDMS CF19-2186 from Nusil, silicone HS3 from Dow Corning and soft silicone TC-5005 A/BC from BJB Enterprises (O'Halloran et al., 2008). Silicone elastomers exhibit modest actuation strains, with reported values of over 100% when pre-strained. Although silicones fall short of acrylics in terms of actuation strains, the primary advantage of silicone elastomers is the much lower viscoelasticity, and thus silicone-based DEAs can be operated with faster response time and higher frequencies with lower mechanical and electrical losses (Brochu & Pei, 2010). Furthermore, silicone elastomers are highly stable over a wide temperature range, due to the glass transition temperature normally being less than -100°C (Madsen, Daugaard, Hvilsted, & Skov, 2016). Therefore, silicones are more suitable for applications operating with significant temperature variation. However, since silicone elastomers have lower dielectric constant than acrylics, further improvement could be made by increasing their dielectric permittivity.

- Polyurethanes

Polyurethanes (PUs) are considered as a group of DE materials primarily because they offer larger force output and particularly higher dielectric

constant than acrylics and silicones. Those features enable PUs to be actuated at relatively low electric fields. However, the major limitation of PUs is that the elastic modulus is usually high, so they can only generate limited actuation strains (Brochu & Pei, 2010). Therefore, the use of PUs for DEAs is not as widespread as acrylic elastomers and silicone elastomers.

2.2.4 Compliant electrode materials

Applicable electrodes are another key component for the fabrication of DEAs. Since electrodes are coated on both sides of the DE film, they must be compliant and conductive to be able to deform or stretch with the soft elastomer during repeated actuation cycles, without severely losing conductivity or generating an opposing stress (O'Halloran et al., 2008). There are three major groups of compliant electrodes often used for DEAs: carbon-based electrodes, metal thin-film electrodes and some new emerging unconventional electrodes (Rosset & Shea, 2013).

- Carbon-based electrodes

Carbon-based electrodes are the most commonly used with DEAs and can be classified into three main types: loose carbon powder, carbon grease and conductive rubber, as shown in Figure 2.5. Loose carbon powders, such as conductive carbon black and graphite, are usually applied directly on the elastomer membrane. As there is no strong binding force between the particles, carbon powders are possible to detach from the electrode and difficult to sustain full coverage at large strains, adversely affecting the electrode lifetime,

although loose powders do not add to the stiffness of soft actuators. In addition, loose powders are quite difficult to handle owing to their high sensitivity to static charges. Therefore, loose carbon powders are mostly found in combination with adhesive acrylic VHB films, which are intrinsically sticky to bind carbon particles (Rosset & Shea, 2013).

Carbon grease is developed to solve above issues by binding carbon particles into a viscous oil or grease. The primary benefits are that carbon grease is easier to handle than loose carbon powders and can maintain large strains without losing conductivity. Nevertheless, carbon grease could either evaporate or diffuse into the DE film in the long term, leading to short circuits or swelling of the elastomer. Furthermore, carbon grease tends to creep under gravity due to its viscous nature and can be subject to mechanical abrasion, both of which could limit the lifetime of such electrodes (Rosset & Shea, 2013).

Conductive rubber refers to a polymer-carbon conductive composite, consisting of carbon particles incorporated into a crosslinked elastomer such as silicone. The quantity of carbon particles in conductive rubber must exceed the percolation threshold, which typically varies from 1% to 24% (volume fraction) depending on the shape and size of the carbon powders used in the elastomer matrix, to make the composite electrode conductive. Conductive rubber electrodes can be firmly bound to the DE film reducing their opportunities to detach or migrate with time compared to carbon powders or carbon grease, and thus have longer electrode lifetime. However, conductive rubber is more likely to contribute to the stiffness of soft actuators owing to the elastomeric matrix. This effect is more prominent with thinner DE films,

because on this occasion the electrode stiffness cannot be neglected in comparison to the stiffness of the elastomer film (Rosset & Shea, 2013).

Figure 2.5 Three main types of carbon-based electrodes: (a) loose carbon powders, (b) carbon grease and (c) conductive rubber (Rosset & Shea, 2013).

- Metallic thin-film electrodes

While metallic thin-film electrodes are widely used in the microelectronics industry, they have also been employed in the fabrication of DEAs. With the microfabrication technologies such as electron beam evaporation, cathodic sputtering and electroplating, metals can be deposited directly on DE substrates to form conductive thin films. The primary advantage of metallic thin-film electrodes is that the electrode shape can be precisely defined using patterning techniques, including shadow masking or photolithography using a metal etching and lift-off process. The metallic electrodes can be patterned down to the nanometre scale. However, a major constraint of using metallic electrodes in DEAs is the modulus of metals (50-100 GPa), which is several

orders of magnitude greater than that of dielectric elastomers (0.2-1 MPa). Another obstacle is the low limit of elasticity for metals at around 2-3%, and therefore metallic electrodes tend to fracture when they are strained above their elastic limit. Nevertheless, some strategies have been used to create stretchable metallic thin-film electrodes for greater actuation, as demonstrated in Figure 2.6. They include patterned metal electrodes defined by photolithography, out-of-plane bucked metal electrodes created by relaxing from pre-stretched elastomer films, and metallic thin-film electrodes deposited directly onto corrugated elastomer films (Rosset & Shea, 2013).

Figure 2.6 Different methods to create stretchable metallic thin-film electrodes through (a) patterned electrodes, (b) out-of-plane buckled electrodes and (c) corrugated electrodes (Rosset & Shea, 2013).

- Novel techniques for compliant electrodes

Some emerging techniques have been used to develop new types of compliant electrodes with additional specific characteristics. For instance, photo-patternable electrodes are created to promote the ease of patterning. Self-clearing electrodes are used to sustain a certain amount of localised dielectric breakdowns so as to prolong the lifetime of DEAs (Rosset & Shea, 2013). Table 2.4 summarises the main advantages and disadvantages of novel

compliant electrodes in comparison with conventional carbon-based electrodes and metallic thin-film electrodes.

Table 2.4 Main advantages and disadvantages of the principal types of compliant electrodes used for DEAs (Rosset & Shea, 2013).

Electrode technology	Advantages	Disadvantages
Carbon electrodes	Low impact on stiffness	High resistivity
	Cheap and rapidly made	Easily damaged
Metallic electrodes	High conductivity	High impact on stiffness
	Pattern-ability	
	Large-scale production	
Novel techniques	New specific features	Complex process
		Expensive

Transparent materials for electrodes are another class of material that has recently emerged which have increasingly become a subject of interest. In addition to conductivity and compliance that conventional electrodes possess, transparent electrodes offer the additional characteristic of transparency that allows DEAs to be potentially useful in some specific applications such as with a flexible screen with haptic feedback and adaptive optics. Stretchable and transparent electrode materials that have been investigated for use with DEAs include silver nanowires (AgNWs) (Yun et al., 2012), carbon nanotubes (CNT) (Shian, Diebold, McNamara, & Clarke, 2012), AgNW-CNT hybrid electrodes (Lee, Kwon, Lee, & Lee, 2017), graphene-AgNW hybrid electrodes (Jun, Kim, Jung, & Oh, 2017), poly(3,4-ethylenedioxythiophene) polystyrene sulfonate (PEDOT:PSS) (Vosgueritchian, Lipomi, & Bao, 2012), ionogels (B. Chen, Lu,

et al., 2014), hydrogels (Keplinger et al., 2013), indium tin oxide (ITO) (Ong et al., 2015), gold and palladium implanted electrodes (Rosset, Niklaus, Dubois, & Shea, 2009), as well as extremely thin layers of loose carbon black (Kovacs & Düring, 2009). The transmittance of light highly depends on the quantity of transparent electrodes applied to the DE films. Reducing the amount of electrode material or electrode layer thickness can positively improve the transparency, although it can also negatively restrict the maximal actuation strain as the electrodes may not have sufficient conductivity to operate. Additionally, light scattering induced by imperfectly transparent electrodes may also have an adverse impact on optical transparency, making imaging applications impractical (Rosset & Shea, 2013).

2.2.5 Effects of pre-stretch

Dielectric elastomer materials are usually pre-stretched before undergoing actuation. One major beneficial effect is that pre-straining a DE film can increase its dielectric breakdown strength and inhibit the electromechanical or pull-in instability (Brochu & Pei, 2010), which is described in more detail in the next section. Furthermore, a pre-stretch reduces the thickness of the DE film and consequently the Maxwell pressure to drive the actuator is increased according to Equation (2.11), which means a specific actuation strain can be achieved at a lower applied voltage. Although the mechanism where pre-stretch increases breakdown strength is still not completely known, it has been suggested that pre-stretch leads to the structural alignment in the polymer chains, which prevents the flow of charges through the DE film from gaining

sufficient energy to cause dielectric breakdown (Anderson et al., 2012). Additionally, pre-stretch results in the stiffening of the DE film, shifting the voltage-stretch response curve as illustrated in Figure 2.7, and thus reduces or removes pull-in effects (Koh et al., 2011). A 400% biaxial pre-stretch is seen to be optimal for acrylic VHB films, since pull-in instability is highly suppressed at this pre-stretch (Figure 2.7). In contrast, silicone elastomers tend to be stiffer than acrylic elastomers and therefore have a lower limiting pre-stretch. A 30% biaxial pre-stretch is usually applied for silicone films (Rosset, Araromi, Schlatter, & Shea, 2016). Other advantages of pre-straining DE films have been observed to remove the boundary constraints of the inactive region (O'Halloran et al., 2008), increase mechanical efficiency (Palakodeti & Kessler, 2006), enhance the response speed of most DE materials by reducing their viscoelastic feature (Choi et al., 2005) and obtain the direction-controlled actuation via the application of a high pre-strain perpendicular to the actuation direction (R. Pelrine, Kornbluh, Pei, et al., 2000). However, pre-stretch has a significant disadvantage in that it requires a rigid frame to sustain the tension of the pre-stretched elastomer film. This will increase the complexity and total mass of the actuator, leading to reduced effective work density and power to mass ratio. In addition, because of possible stress relaxation and fatigue of pre-stretched elastomer films over time the shelf life of DEAs can be adversely affected (Brochu & Pei, 2010).

Figure 2.7 Voltage-stretch response of dielectric elastomer film at various levels of pre-stretch λ_{pre} (blue lines). Red dots represent pull-in instability while intersections between blue lines and breakdown field line (red line) represent electrical breakdown (Koh et al., 2011).

2.2.6 Electrical breakdown and electromechanical instability

The performance of DEAs is often limited by electrical failure, which inhibits them from charging and deforming. One predominant failure mode is electrical breakdown due to an excessive electric field applied through the DE membrane. Electrical breakdown usually arises around a flaw or defect in the DE membrane and occurs when a conductive track is created to enable charges to flow through the membrane, resulting in electrical short circuiting and heat generation. Increased charge leakage and localised temperature growth will finally cause the permanent damage of the DE membrane (Anderson et al., 2012; Rosset & Shea, 2013). Aside from taking extra care in the fabrication and handling of DE materials to protect them from potential damage, one strategical approach to avoid breakdown failure is through pre-stretching DE membranes to increase their dielectric breakdown strength, as previously stated in Section 2.2.5. The dielectric strength of 3M VHB 4910 acrylic film was reported to increase from 20 MV/m when unstretched to 220

MV/m with 500% equiaxial pre-stretch (Kofod, Sommer-Larsen, Kornbluh, & Pelrine, 2003). Another approach to address the breakdown issue is using self-clearing electrodes. Such electrodes can be burnt off around the defect site during an electrical breakdown, effectively isolating the short-circuited zone from the rest of the electrode and allowing the actuator to continue operating. Self-clearing electrodes are therefore able to survive a number of localised breakdowns and significantly prolong the lifetime of DEAs (Rosset & Shea, 2013). Electrode materials that have been observed to exhibit self-clearing characteristic on dielectric elastomers include single-walled carbon nanotubes (SWCNT) (Yuan et al., 2008), silver thin films that are formed by electroless deposition on a VHB substrate (Lau, Goh, & Shiau, 2011) and doped conductive polymers made with poly(3-dodoxylthiophene) or polyaniline nanofibers (Lam et al., 2008; Yuan et al., 2007).

Electromechanical or pull-in instability is another failure mode of DE materials. According to Equation (2.11), the Maxwell stress on the elastomer film is directly proportional to the square of the applied voltage while inversely proportional to the square of the elastomer thickness. The voltage-induced Maxwell pressure will cause the reduction of the elastomer thickness. At a certain high level of driving voltage, the Maxwell stress will further increase while the elastomer become even thinner. Pull-in instability will usually occur if the Maxwell stress is greater than the resisting elastic stress, leading to the DE membrane collapsing into a complex of wrinkling patterns as shown in Figure 2.8. Pull-in instability will eventually result in electrical breakdown and material failure when the elastomer membrane continues to be driven thinner and thinner until the Maxwell stress exceeds the dielectric strength of the

material (Anderson et al., 2012; Plante & Dubowsky, 2006). Pull-in instability is commonly observed in soft dielectric elastomers such as acrylic VHB membranes, whereas stiffer dielectric elastomers that only undergo a small actuation deformation typically suffer electrical breakdown prior to pull-in instability (X. Zhao & Suo, 2010).

Figure 2.8 Typical wrinkling patterns of dielectric elastomer membrane caused by pull-in instability (Plante & Dubowsky, 2006).

As mentioned in Section 2.2.5, pre-stretching the DE membrane improves the resistance to pull-in instability, as the stiffening of the DE membrane due to the increased modulus of the material at larger pre-strains which can suppress these pull-in effects and therefore a stable state is reached prior to electrical breakdown (Koh et al., 2011). Also, operating viscoelastic DE materials at high pre-stretch rates and actuating them quickly at intermittent or high frequencies also creates a greater resistance to pull-in instability (Plante & Dubowsky, 2006). Furthermore, pull-in effects can be avoided by suitable materials design.

As shown in Figure 2.9d, a modified material that is compliant at small stretches and then stiffens substantially at higher stretches can theoretically eliminate the pull-in instability producing a large and safe actuation before electrical breakdown (X. Zhao & Suo, 2010).

Figure 2.9 Three types of DE materials distinguished by intersections between voltage-stretch curves $\Phi(\lambda)$ (blue lines) and electric breakdown voltage-stretch curves $\Phi_B(\lambda)$ (red lines). (a) nonmonotonic voltage-stretch curve of typical DE; (b) Type I DE that may fail by electrical breakdown with small actuation strain; (c) Type II DE that may fail at the point where pull-in instability occurs; (d) Type III DE that may fail by electrical breakdown with large and stable actuation strain (X. Zhao & Suo, 2010).

2.2.7 Configurations and applications

DEAs designed with different configurations can lead to various specific applications. Figure 2.10 demonstrates a number of widely used configurations for DEAs, including planar, extender, diaphragm, stacked, folded, rolled, tube, stretched-frame, bowtie, spider, unimorph and bimorph

(Carpi, De Rossi, Kornbluh, Pelrine, & Sommer-Larsen, 2008; Kornbluh et al., 2002). Most actuator designs use the surface expansion when DEAs are under actuation, whereas stacked actuators are primarily actuated through the thinning of multilayer DE films (Brochu & Pei, 2010). Simple planar actuators that were firstly developed by SRI International in the late 1990s have been amongst the most common configurations in use today for both experimental testing and device fabrication (R. Pelrine, Kornbluh, & Kofod, 2000). For instance, planar actuators were found in applications for tuneable optical gratings and variable optical transmission devices when incorporated with transparent electrodes (Ji et al., 2016; Ong et al., 2015). In addition, planar annular actuators were used to encapsulate a soft deformable lens so as to change focal length in optical systems (Carpi, Frediani, et al., 2011; Maffli et al., 2015). Therefore, planar configuration is chosen for the fabrication of DEA-based tuneable optical transparency devices in this thesis as such configuration is simple and well suited to optical applications. Diaphragm actuators with rigid constraints at the edge of the DE film could produce an out-of-plane deformation of actuation which can be used in wearable tactile displays (Ig Mo Koo et al., 2008). Multilayer stacked actuators that exhibited voltage-induced thickness contraction were used to lift an external load up to 4.5 kg (Kovacs & Düring, 2009). DEAs could also be rolled into a scroll to create multiple-degrees-of-freedom walking robots or arm-wrestling robots producing 200 N unidirectional force (Kovacs, Lochmatter, & Wissler, 2007; Pei, Rosenthal, Stanford, Prahlad, & Pelrine, 2004). Bowtie actuators are linear framed actuators in which the frame flexes and these have found applications as robotic legs in the self-contained hexapod robot (Bar-Cohen,

2004). Unimorph and bimorph actuators that generate bending displacement upon electrical activation could have potential applications as low force robotic grippers (O'Halloran et al., 2008).

Figure 2.10 Basic configurations for dielectric elastomer actuators (Carpi et al., 2008).

2.3 Electrically tuning optical transparency

Smart membranes with optical transparency that can be electrically tuned are gathering growing interest for possible applications in different fields, varying from smart dimmable windows to switchable privacy glass and controllable light diffusing filters (Mortimer, Rosseinsky, & Monk, 2015; Ohzono, Suzuki, Yamaguchi, & Fukuda, 2013; Williamson & Venables, 2013). There are several technologies that can be used to electrically change the surface transparency, including electrochromics, liquid crystals and suspended

particle displays (Bonsor, 2001). More recently, DEAs have been shown as an alternative promising technology to achieve large and continuous voltage-induced changes in optical transparency (Ong et al., 2015; Shian & Clarke, 2016). Those state-of-the-art strategies to achieve electrically tuneable optical transparency are described as follows.

2.3.1 Electrochromic devices

In electrochromic devices, an electric field-driven transport of ions between an ion storage layer and an electrochromic layer is used to modulate the optical transmittance (Claes G. Granqvist, 2014; Claes Goran Granqvist, 2005; Mortimer et al., 2015; Niklasson & Granqvist, 2007). Figure 2.11 illustrates the basic configuration and working principle of electrochromic devices. At electrical rest, an electrochromic window remains transparent, allowing light to pass through. When a voltage of the order of one volt is applied, positive ions will transport from the ion storage layer through the ion conducting layer into the electrochromic layer. These ions in the electrochromic layer allow it to absorb and reflect light, causing the electrochromic window to change from transparent to opaque. When the applied electric filed is released, the ions are driven out of the electrochromic layer and into the ion storage layer. Thus, the electrochromic window becomes transparent again (Bonsor, 2001; Claes Goran Granqvist, 2005). In general, electrochromic devices operate to electrically darken the surface transparency through the electrochemical reaction. Electrochromic windows can be continuously tuned to allow varying degrees of visibility.

Figure 2.11 Basic design and working principle of electrochromic devices (Bonsor, 2001).

2.3.2 Polymer-dispersed liquid crystals devices

In polymer-dispersed liquid crystals (PDLC) devices, the electrically-induced alignment of liquid crystal molecules is used to change the optical transparency (Cupelli et al., 2009; Hosseinzadeh Khaligh, Liew, Han, Abukhdeir, & Goldthorpe, 2015; M. Kim et al., 2015; Nicoletta et al., 2005). Figure 2.12 demonstrates the basic design and operating principle of PDLC devices. At electrical rest, the liquid crystals within the window are randomly oriented, producing an opaque surface. When an electric field is applied, the liquid crystals respond to the field by aligning in a parallel direction, which allows light to pass through (Bonsor, 2001; Cupelli et al., 2009). Therefore, PDLC devices operate to electrically increase the surface transparency, which reverses the process of electrochromic devices. Also, PDLC devices usually provide an on-off switch of optical transparency between opaque and transparent, without any intermediate settings.

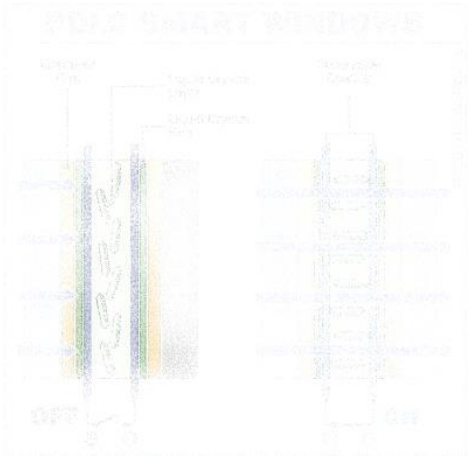

Figure 2.12 Basic design and working principle of polymer-dispersed liquid crystals (PDLC) devices (Bonsor, 2001).

2.3.3 Suspended particle devices

Suspended particle devices (SPD) use small light-absorbing microscopic particles that can be used to adjust the optical transmittance. The basic design and working principle of SPD windows are shown in Figure 2.13. Millions of suspended particles are situated between two glass plates coated with transparent conductors. At electrical rest, the suspended particles form a random pattern and block light, making the surface completely dark. When a voltage is applied through the conductors, the suspended particles line up in a straight line which allows light to pass through (Bonsor, 2001). Thus, operating similarly as PDLC devices, SPD windows can electrically increase the surface transparency. In addition, SPD windows can be continuously tuned to allow varying degrees of visibility, in the same way that electrochromic devices can operate.

Figure 2.13 Basic design and working principle of suspended particle devices (SPD) (Bonsor, 2001).

2.3.4 Dielectric elastomer actuator-based devices

DEA-based devices have also been used to electrically tune the optical transparency of soft insulating membranes, with three main different strategies, which are discussed below.

- Approach I

The first approach consists in coating the soft dielectric membrane with stretchable transparent electrodes, whose surfaces are initially made with wrinkled patterns by applying the electrodes to a pre-stretched membrane and partially reducing the pre-strain. The formation of electrode wrinkles is due to the dissimilar stiffness with the elastomer membrane. At electrical rest, the wrinkled electrodes scatter light, thereby showing low transmittance. Upon electrical activation, voltage-induced surface expansions are used to flatten the wrinkles, so as to increase the optical transparency (Jun et al., 2017; Ong et al., 2015; Shrestha, Asundi, & Lau, 2018). An example of DEA-based device

using transparent indium-tin-oxide (ITO) electrodes to electrically tune the surface transparency is given in Figure 2.14. In general, a DEA-based device operating with this approach can increase the optical transparency with the increase in electric fields. Also, the transparency can be continuously tuned to allow varying degrees of transmissibility.

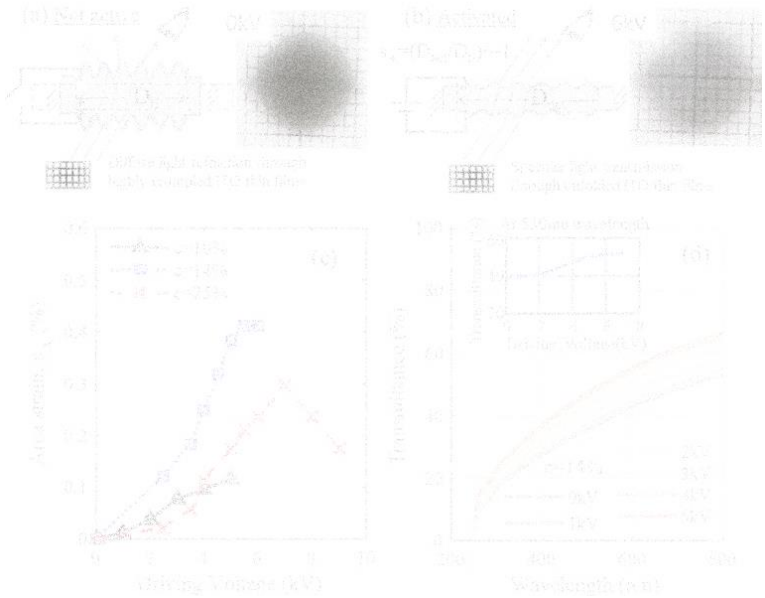

Figure 2.14 Working principle of DEA-based tuneable transparency devices, through the expansion of a soft membrane with wrinkled stretchable transparent electrodes (Ong et al., 2015).

- Approach II

In a second approach, the structure is made of transparent electrodes covering the elastomer membrane fixed to a rigid substrate. At electric rest, the flat and clear surfaces allow light to pass through. Upon electrical activation, the active region is constrained from deforming in the plane of actuation due to the fixed substrate. Instead, the electrode surfaces will form a pattern of creases or

craters due to the electromechanical instability when the electric field reaches a critical value prior to electrical breakdown (Q. Wang, Tahir, Zang, & Zhao, 2012). Consequently, the cratering-type surface instability of transparent electrodes causes light diffusion which in turn reduces the optical transparency (Lin, Wang, Zhang, & Smoukov, 2017; Shian & Clarke, 2016; Shian, Kjeer, & Clarke, 2018; Van Den Ende, Kamminga, Boersma, Andritsch, & Steeneken, 2013). Figure 2.15 shows an example of DEA-based device using silver nanowires (AgNWs) electrodes to electrically modulate the transparency. In this approach, optical transmittance can be decreased by using electrical means. Also, the transparency can be continuously tuned, although very high electric fields (around 600 V/μm) are typically required.

Figure 2.15 Working principle of DEA-based tuneable transparency devices, using a surface cratering-type of instability on a constrained soft membrane with transparent electrodes (Shian & Clarke, 2016).

- Approach III

In a third approach, voltage-controlled light shutters are obtained by encapsulating liquid crystals into the elastomer membrane and sandwiching it between transparent electrodes, to achieve an operation similar to that of PDLC windows, producing the electrically-induced on-off switching of optical transparency between opaque and transparent, without intermediate settings (Yang, Zhou, Shian, Clarke, & Suo, 2017), as the example given in Figure 2.16.

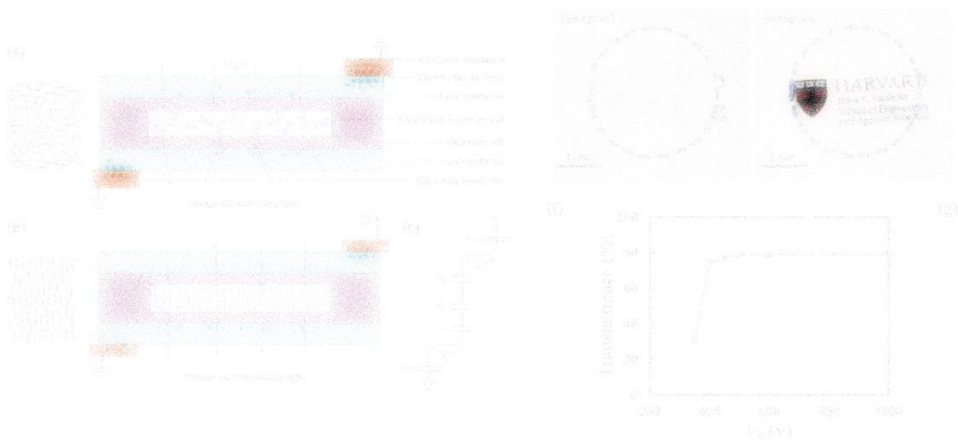

Figure 2.16 Working principle of DEA-based tuneable transparency devices, through the alignment of liquid crystals encapsulated within a soft matrix sandwiched between transparent electrodes (Yang et al., 2017).

According to all those state-of-the-art approaches, by using electrical means the optical transparency can only be either increased or decreased. Table 2.5 summarises various types of DEA-based tuneable optical transparency devices and compares their design with different transparent electrodes, working principle based on above three described approaches and the tuning range of optical transmittance at 550 nm.

Table 2.5 Literature on electrically tuneable optical transparency devices based on dielectric elastomer actuators.

Device structure	Working principle	Tuning range of transmittance at 550 nm	Reference
ITO/acrylic elastomer/ITO	Approach I	Electrically increased from 39% to 52%	(Ong et al., 2015)
Graphene-AgNWs/acrylic elastomer/graphene-AgNWs	Approach I	Electrically increased from 15% to 30%	(Jun et al., 2017)
TiO_2/acrylic elastomer/ TiO_2	Approach I	Electrically increased from 3% to 78%	(Shrestha et al., 2018)
Au/acrylic elastomer/ITO/glass	Approach II	Electrically decreased from 32% to 28%	(Van Den Ende et al., 2013)
AgNWs/acrylic elastomer/PET/acrylic elastomer/AgNWs	Approach II	Electrically decreased from 62% to 8%	(Shian & Clarke, 2016)
Au/silicone elastomer/rigid Kapton/Au/glass	Approach II	Electrically decreased from 39% to 11%	(Lin et al., 2017)
LiCl hydrogel /acrylic elastomer/LiCl hydrogel	Approach II	Electrically decreased from 88% to 77%	(Tang, Li, Zou, Liu, & Chen, 2018)
CNT/soft silicone elastomer/stiff silicone elastomer/ITO/glass	Approach II	Electrically decreased from 80% to 10%	(Shian et al., 2018)
LiCl hydrogel/acrylic elastomer/liquid crystal/acrylic elastomer/LiCl hydrogel	Approach III	Electrically on-off switch from 30% to 80%	(Yang et al., 2017)

2.4 Conclusions

In this chapter, the fundamental aspects of DEAs, including working principles, dielectric elastomer materials, compliant electrode materials, pre-stretch effects, electromechanical instability and device configurations, are carefully reviewed. Then, state-of-the art technologies used to electrically control light transmittance, such as commercially available electrochromic, PDLC and SPD smart windows, as well as more recently developed DEA-based electrically tuneable transparency devices, are summarised and compared. This research is focused on the development of variable optical transmission devices using the DEA technology. In contrast to the electrochromic technology where the operation is primarily based on the complex electrochemical reaction which usually takes time, the DEA technology that relies on a physical process can achieve the transparency change within a second. In comparison with the PDLC technology, which only provides an on-off switch between two states without any intermediate settings, the DEA-based devices are able to achieve the continuous tuning of optical transparency to allow varying degrees of visibility. According to all these state-of-the-art approaches using the DEA technology, by using electrical means the optical transparency can be either only increased or only decreased. Therefore, in this work the first concept to make the optical transparency of soft elastomer membranes electrically tuneable to both higher and lower values within the same device is proposed and it is described in more detail in Chapter 4. Additionally, some DEA-based devices (adopting the approaches I and III) have applied the equi-biaxial pre-stretch of DE membranes, while some others (adopting the approach II) have been built without any pre-stretch. Consequently, the uniform actuation in all

directions when activated by an applied voltage has led to those devices with isotropic changes in optical transparency over the entire elastomer membrane surface. Thus, another new concept is to be proposed here with the aim of achieving directionally-controlled light diffusion based on dielectric elastomer actuation. The directional control of optical transmittance can be obtained by uniaxially pre-stretching a DE membrane. Such directional light diffusing devices are further described in Chapter 5. Therefore, the main aims of the thesis are listed below:

- investigate the optimal transparent electrode materials used for making transparent DEAs
- achieve the electrically-induced reversible and continuous tuning of surface transparency using DEA technology
- develop DEA-based devices to electrically tune soft membranes to both a higher and a lower transparency
- develop DEA-based devices to make light diffusion directionally-controlled for light shaping applications

Chapter 3 Transparent electrode materials used for devices with variable optical transmission

3.1 Introduction

Transparent electrodes are an area of increasing interest for the DEA technology. Apart from conductivity and compliance, transparent electrodes provide an additional feature of optical transparency, making them useful in the development of DEA-based adaptive optical devices. The state of the art offers a range of different transparent electronic materials (McCoul et al., 2016), including silver nanowires (Shian & Clarke, 2016), gold thin films (Lin et al., 2017; Van Den Ende et al., 2013), metal oxide thin films (Ong et al., 2015; Shrestha et al., 2018), carbon nanotubes (Shian et al., 2018; Yuan et al., 2008), graphene (Zang et al., 2013), conducting hydrogels (B. Chen, Bai, et al., 2014; Keplinger et al., 2013), ionogels (B. Chen, Lu, et al., 2014; Ji et al., 2016) and conducting polymers (Son et al., 2012; Vosgueritchian et al., 2012).

One of the most challenging aspects in this work is the selection of the optimal transparent deformable electrode. A preliminary experiment was conducted to examine the reliability and performance of some available transparent electrodes for use with DEAs. Several types of devices with variable optical transmission were developed based on planar DEAs made of clear dielectric elastomer membranes and deformable transparent electrodes. They were proposed to reversibly control light transmittance by electrically changing the

surface roughness of DEAs. According to a principle of operation described in the literature (Ong et al., 2015), the process for device fabrication and device evaluation under driving voltages using an expansion mode are illustrated in Figure 3.1. The devices were fabricated by initially biaxially pre-stretching a DE membrane, applying transparent electrodes on both sides of the membrane, and then partially reducing the pre-strain to create micro-wrinkles due to the dissimilar moduli between the elastomer membrane and the electrodes, and finally fixing the membrane to a holding frame to maintain elastic tension. At electrical rest, light is scattered from actuator surfaces that are intentionally made with wrinkles. Upon electrical activation, the voltage-induced in-plane expansion flattens the wrinkled DEA surfaces, allowing more light to pass through the elastomer membrane, so as to increase the optical transparency. The performance of devices operated using the expansion mode (Figure 3.1) made using different transparent electrode materials, including silver nanowires (AgNWs), conducting hydrogels, ionogels, PEDOT:PSS and AgNWs/PEDOT:PSS compound, to electrically tune the optical transparency is evaluated and compared in the following sections.

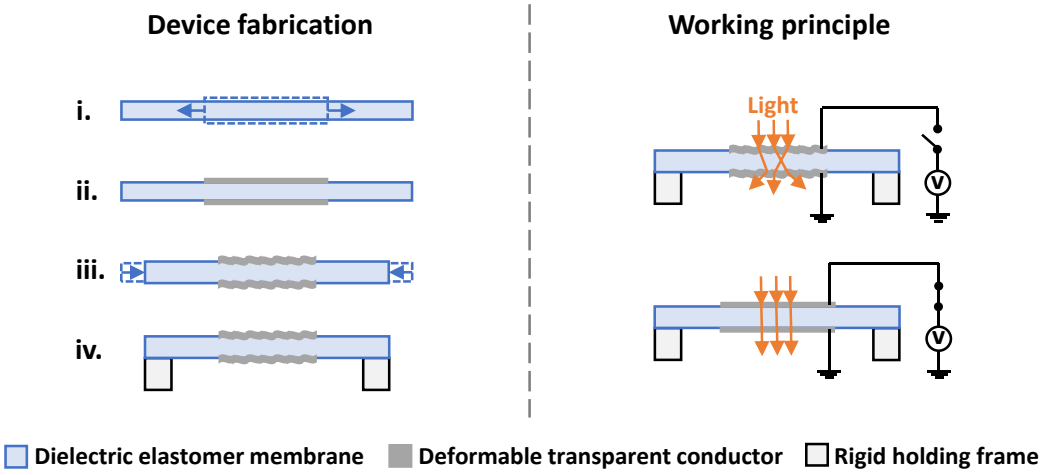

Figure 3.1 Fabrication process and working principle of electrically tuneable optical transparency devices operating with an expansion mode.

3.2 Experimental

3.2.1 Electrode materials and device fabrication

The preparation of AgNWs electrodes followed to a protocol described in the literature (Huang et al., 2016; Shian et al., 2012). The raw AgNW-isopropanol suspension with a concentration of 10 mg/mL (SLV-NW-40, Blue Nano Inc., USA) was diluted to 0.5 mg/mL in isopropanol and then vacuum filtered through polytetrafluoroethylene (PTFE) filters with 100 nm pore size to form mats of AgNWs on the filter. After the solvent was evaporated, the AgNWs/PTFE filter was cut into a circle with a 20-mm diameter. The PTFE filter was used as a transfer medium to print AgNWs onto both sides of a biaxially pre-stretched (to an initial biaxial pre-stretch of 3.5) acrylic dielectric elastomer membrane (VHB4910, 3M, USA). The pre-stretch reduced the membrane thickness from 1000 μm to 81.6 μm (calculated value). As the surface of VHB is sticky, AgNWs were easily transferred to the elastomer surface by uniformly pressing the filter onto the membrane for about 10 s. The

PTFE filter was then peeled off leaving the circular AgNWs electrodes firmly attached to the VHB membrane. The surface area density of the coated AgNWs was calculated to be approximately 200 mg/m^2. After that, the pre-stretch of the VHB membrane was relaxed to 3 times, causing the formation of electrode wrinkles to scatter light. The elastomer membrane was finally fixed onto a rigid holding frame and an aluminium foil was used to connect each electrode to a high voltage source.

The synthesis of hydrogel electrodes followed a protocol described in the literature (B. Chen, Bai, et al., 2014). 9.75 mL of 40% acrylamide (AAm) monomer and 2.9 g lithium chloride (LiCl) powder were dissolved in deionised water to make a 25-mL solution. 5 mg of crosslinking agent *N,N'*-methylenebisacrylamide (MBAA), 21 mg of thermo-initiator ammonium persulphate (APS) and 14 µL of accelerator *N,N,N',N'*-tetramethylethylenediamine (TEMED) were subsequently added into the mixed solution. The uniformly mixed solution was transferred to a mould with the thickness varying from 0.2 mm to 0.5 mm, which was then polymerised in an oven for 2 hours at 50 °C. Finally, the polymerised hydrogel containing LiCl was collected from the mould and pasted onto both sides of a biaxially pre-stretched acrylic dielectric elastomer membrane (VHB4910, 3M, USA) to create a transparent DEA.

The preparation of ionogel electrodes followed a protocol described in the literature (Ji et al., 2016). 1.2 g 1-ethyl-3-methylimidazolium dicyanamide ionic liquid and 0.4 g PMMA were mixed in 10 g acetone to prepare the ionogel solution. The mixed solution was stirred at 45 °C for 5 hours using a hotplate,

and then cooled down to room temperature. After that, the ionogel solution was blade cast using a film applicator with 50 µm gap on a flat PET substrate, which was treated by an oxygen plasma (Zepto Plasma, Diener Electronic GmbH, Germany) at 200 W for 1 min. The cast ionogel sheet was placed in an oven at 80 °C for 2 hours to dry and then cooled down to room temperature. The dried ionogels on the PET substrate were cut into a circular shape and gently pasted onto both sides of a 1.5-time biaxially pre-stretched PDMS film (Elastosil Film 2030 250/50, Wacker, Germany). The pre-stretch reduced the PDMS film thickness from 50 µm to 22.2 µm (calculated value). The PET substrate was then peeled off leaving the ionogel electrodes firmly attached to both sides of the PDMS film. Subsequently, the pre-stretch was relaxed to 1.25 times, causing the formation of electrode wrinkles which scattered the light. The PDMS film was finally fixed onto a rigid holding frame with the help of Kapton tapes. A copper tape and conductive carbon grease (Carbon Conductive Grease 846, M.G. Chemicals, Canada) were used to connect each ionogel electrode to the high voltage source.

The deformable PEDOT:PSS electrodes were prepared by first mixing 10 g aqueous PEDOT:PSS (Clevios PH 1000, Heraeus, Germany) with 0.5 g dimethyl sulfoxide (DMSO, Sigma-Aldrich, UK) and 4 g fluorosurfactant (Capstone FS-30, Apollo Scientific, UK), and then diluting the mixed PEDOT:PSS solution in isopropanol (2-Propanol, Sigma-Aldrich, UK) with a weight ratio of 1:3. The diluted solution was mixed using a vortex mixer (SA8, Stuart Equipment, UK) with a speed of 2000 rpm for 1 minute at room temperature. The diluted solution was then used to spray coat the deformable PEDOT:PSS thin film (using a circular shadow mask) onto both sides of a 3.5-

times biaxially pre-stretched acrylic dielectric elastomer membrane (VHB4910, 3M, USA). The biaxial pre-stretch reduced the membrane thickness from 1000 μm to 81.6 μm (calculated value). Owing to the addition of fluorosurfactant and the sticky surface of VHB, the PEDOT:PSS thin films were uniformly and firmly bonded to the elastomer membrane. Subsequently, the biaxial pre-stretch was relaxed to just 3 times, causing the formation of electrode wrinkles to scatter light. The membrane was then fixed onto a rigid holding frame. After that, the whole structure was oven dried for 30 min at 80°C. A copper tape and conductive carbon grease (Carbon Conductive Grease 846, M.G. Chemicals, Canada) were used to connect each PEDOT:PSS electrode to the high voltage source.

The preparation of AgNWs/PEDOT:PSS compound electrodes was based on the following steps. The compound solution was first made by a mixture of PEDOT:PSS solution and AgNWs solution with a weight ratio of 1:3. The PEDOT:PSS solution was prepared by mixing 10 g aqueous PEDOT:PSS (Clevios PH 1000, Heraeus, Germany) with 0.5 g dimethyl sulfoxide (DMSO, Sigma-Aldrich, UK) and 4 g fluorosurfactant (Capstone FS-30, Apollo Scientific, UK), whilst the AgNWs solution was provided by the AgNW-isopropanol suspension (Silver Nanowire, 40 nm diam. x 35 μm L, Sigma-Aldrich, UK) with a concentration of 0.5 mg/mL. The compound solution was mixed using a vortex mixer (SA8, Stuart Equipment, UK) with a speed of 2000 rpm for 1 minute at room temperature. The fabrication of the device with a single elastomer layer was carried out using the approach that is described above (the device using deformable PEDOT:PSS electrodes), except that the PEDOT:PSS/AgNWs compound solution was used to spray coat the

electrodes. Moreover, another prototype using a multi-layer stacked structure with alternating layers of VHB membranes and PEDOT:PSS/AgNWs compound electrodes was fabricated following a similar process. The device consisted of three layers of VHB with four layers of electrodes stacked together.

3.2.2 Characterisation

In order to drive the devices, a high-voltage AC/DC generator (Model 615-10, Trek, USA) was initially used to produce voltages up to 6 kV, for the tests of the devices using AgNWs, hydrogels and ionogels electrodes. However, the high-voltage generator was broken during the later stage of this research. Therefore, for the rest tests, a DC power supply (TSX1820 18V/20A, Thurlby Thandar Instruments, UK) was used to provide voltages in the order of volts, which were amplified by a compact DC-DC high voltage converter (Q-series, EMCO High Voltage Corporation, USA) to produce voltages up to 6 kV, which were monitored with a high-voltage probe.

The optical transmittance of the tuneable devices was characterised, in the 400-800 nm visible range, using a Perkin Elmer Lambda 950 UV-vis spectrometer with a 10 cm-wide integrating sphere. The transmittance was measured with a near-field method (illustrated in Figure 3.2), where the distance between the sample and detector was 5 cm. For the instrument set-up, the transmission port was covered with the sample, whilst the reflectance port was covered with a white standard plate. Therefore, the measured near-

field total transmittance detects both specular transmitted and diffused transmitted light from the sample.

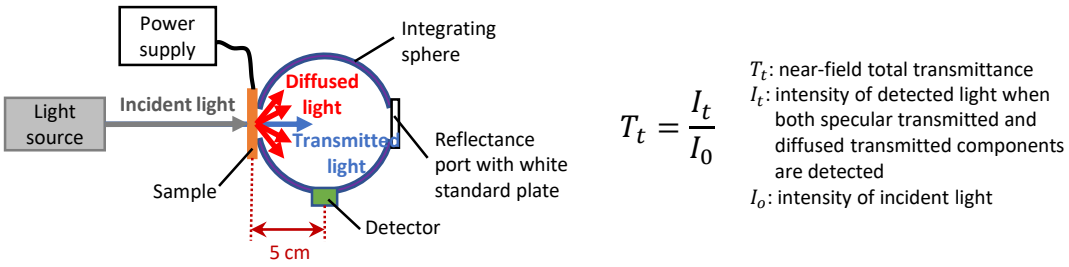

Figure 3.2 Schematic representation of the UV-Vis spectrometer set-up used to characterise the near-field total transmittance, with both specular transmitted and diffused transmitted light detected.

The actuation strains were calculated by processing images (taken at different driving voltages) with the software Image J.

The surface resistance of ionogel electrode was measured following the four-point probes method to avoid the measurement of contact resistances. The electrode surface was contacted by the four probes. A constant current was injected into the electrode sample via the two outer probes. The two inner probes were used for measuring the resulting voltage drop across the surface of the electrode (Carpi et al., 2015). As the measuring instrument contains four probes equally spaced, the surface resistance R_s is thus calculated based on the van-der-Pauw equation: $R_s = \left(\frac{\pi}{\ln 2}\right)\frac{V}{I}$, where V is the voltage drop and I is the applied constant current.

The thickness of ionogel thin film was measured using a contract profilometer (Dektak XT, Bruker, USA), by sensing the deflection of a fine stylus contacted to the electrode surface. The profilometer usually operates a raster scanning over a thin film surface and can detect the height ranging from 1 mm down to 4 Å.

The formation of surface wrinkles that were mechanically induced within the electrode thin films at different strains was investigated by an optical microscope (DMI 4000B, Leica, Germany) using bright field imaging and a confocal microscope (TCS SP2, Leica, Germany). Also, a cross section of the ionogel covering the PDMS film was investigated using the optical microscope.

3.3 Transparent electrode materials and their performance

3.3.1 Silver nanowires

Silver nanowires (AgNWs) have been used as compliant transparent electrodes to fabricate several DEA-based devices for optical applications (Lee et al., 2017; Shian & Clarke, 2016; Yun et al., 2012). Thus, the first prototype of tuneable transparency devices was developed using AgNWs transparent electrodes and clear acrylic dielectric elastomers.

The electro-optical transduction performance was characterised in the 400-800 nm visible range, quantifying how different electrical activations changed the optical transmittance measured with a near-field method (Figure 3.2). As a reference, the transmittance of the 3.5-time pre-stretched acrylic VHB membrane (without any electrodes) was about 92% at 550 nm (Figure 3.3a).

When AgNWs electrodes with a surface density of 200 mg/m^2 were applied on both sides of the pre-stretched membrane, the transmittance reduced to about 64% at 550 nm (Figure 3.3a), due to the fact that AgNWs scatter light even on the flat elastomer. As the pre-stretch of the membrane was partially relaxed from 3.5 to 3 times, which in turn created a 14.3% compressive radial strain on the electrodes, AgNWs wrinkled to further scatter light and thus reduced the transmittance to 47% at 550 nm (Figure 3.3a). The microscopic investigation on the formation of wrinkles owing to the relaxation of the pre-stretch from 3.5 times (0% radial strain on the electrodes) to 3 times (14.3% radial strain on the electrodes) are shown in Figure 3.4. The optical microscopy images show that AgNWs were uniformly dispersed and the formed wrinkles that were randomly oriented, whilst the confocal microscopy images indicate that the height of wrinkles could reach up to 5 µm.

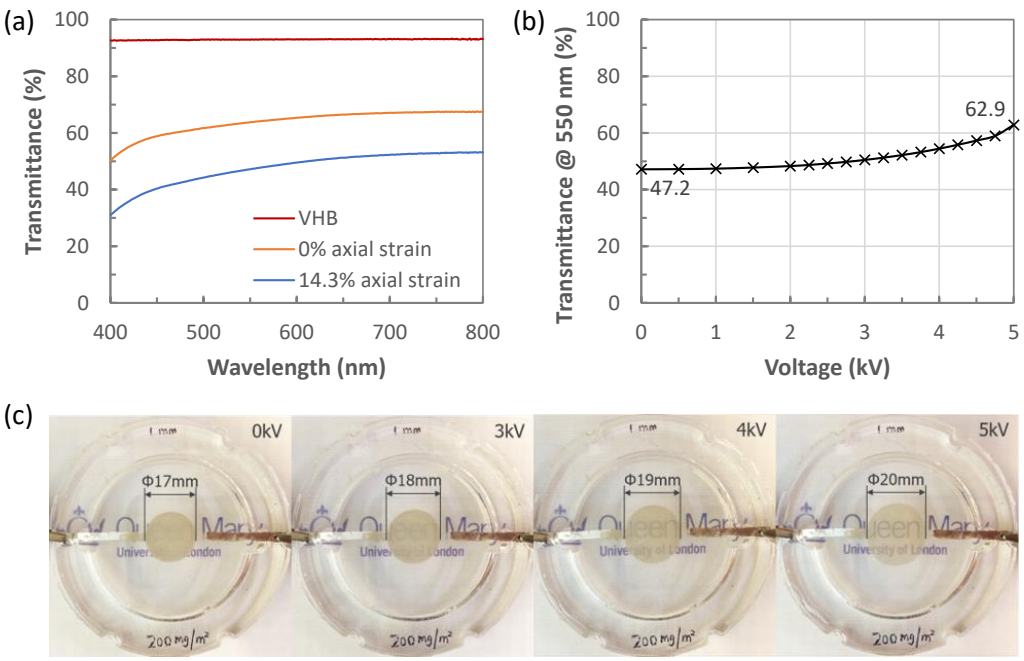

Figure 3.3 Electrical tuning performance of optical transparency using silver nanowires (AgNWs) electrodes. (a) Optical spectra over the visible range for VHB, unwrinkled AgNWs on VHB and wrinkled AgNWs on VHB. (b) Voltage-induced increase in the near-field total transmittance at 550 nm. (c) Changes in surface transparency at various voltages.

Upon electrical activation, the DEA was actuated to create radial strains up to 17.6% (which equates to an area strain of 36.7%). The calculation between the area strain s_A and the radial strain s_r is based on the equation: $s_A = (s_r + 1)^2 - 1$. The voltage-induced surface expansion flattened the electrode wrinkles and the transmittance at 550 nm therefore continuously increased from 47% at electrical rest to 63% at 5 kV, leading to a surface transparency that could be electrically tuned from nearly opaque to translucent, as shown in Figure 3.3c. The logo text was placed 13 mm behind the DEA device. However, even when fully activated the brownish AgNWs electrodes remained in sight and this could not provide a high level of surface transparency. Even if the electrode surfaces were totally unwrinkled, the transmittance at 550 nm was

limited at 64%, which was though insufficient to be effective at achieving a wide tuning range for optical transmittance.

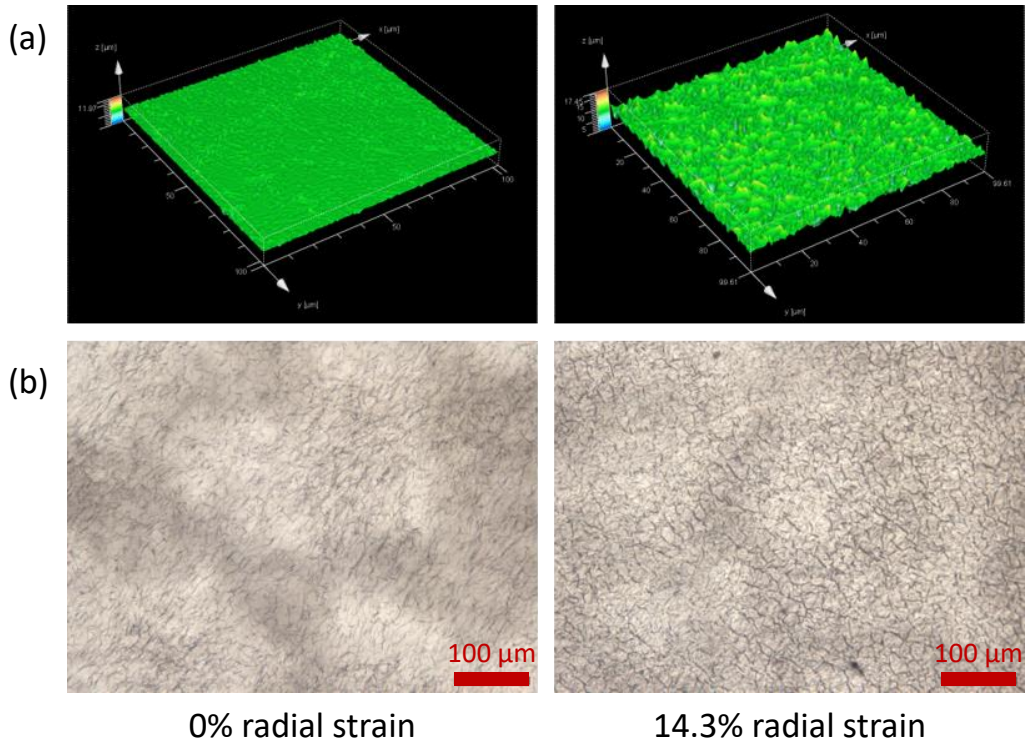

Figure 3.4 Microscopic investigation on the formation of surface wrinkles for AgNWs covering acrylic elastomer when 14.3% radial strain is applied, whilst 0% radial strain indicates AgNWs are unwrinkled. (a) Confocal microscopy images. (b) Optical microscopy images.

3.3.2 Hydrogels

In order to obtain a high degree of surface transparency, a second prototype was considered which combined highly transparent stretchable hydrogel electrodes with clear acrylic dielectric elastomers.

This DEA-based device did not work very well. The first problem was the preparation of hydrogel electrodes. If the thick hydrogels (around 0.5 mm) were prepared, the deformation of actuation was very limited because of the relatively high stiffness of the electrodes. If the thin hydrogels (around 0.2 mm) were prepared, they were firmly attached to the mould surface and very difficult to release for use on the DEA film. For this reason, it was considered to use the blade casting fabrication method to make thin hydrogel films. Nevertheless, due to the high hydrophobicity, the hydrogel solution could not be completely cast on the polyethylene terephthalate (PET) substrate even if an oxygen plasma treatment was used to make the substrate hydrophilic. This gave rise to a second problem. Although the acrylic VHB membrane was sticky, the hydrophobic feature prevented the hydrogels from properly bonding with the elastomer membrane, therefore impairing the electro-optical transduction performance. In addition, it was found that such hydrogels dried out as water evaporated over time, which suggested these types of electrodes were unsuitable for applications in open air. Therefore, the proposed second prototype was also unsuccessful.

3.3.3 Ionogels

Ionogels are a new type of conducting material where an ionic liquid is immobilised inside a polymer matrix. They usually provide high optical transmission combined with high ionic conductivity. Moreover, the use of silicone elastomers as dielectric membranes is expected to lead to devices with the highest possible response speed, due to their low glass transition

temperature and much reduced mechanical losses when compared to acrylic VHB elastomers (Maffli et al., 2015). Thus, the third prototype of tuneable transparency devices was made of silicone film with polymethyl methacrylate (PMMA)-based ionogel electrodes.

The optical behaviours of the ionogel-based DEAs were characterised by measuring the near-field total transmittance in the visible range using a UV-vis spectrometer (Figure 3.2). As a reference, the transmittance at 550 nm of the 1.5-time pre-stretched PDMS film (without any electrodes) was about 93%. When the ionogels were coated on both sides of the PDMS film, the transmittance slightly changed to 92%, owing to the high transparency of the fabricated ionogels. As the pre-stretch was partially relaxed from 1.5 to 1.25 times, which created 16.7% compressive radial strain (or 36.1% area strain) on the electrodes, the ionogels wrinkled which diffused the transmitted light and this reduced the transmittance to 83% at electrical rest. With the increase in applied driving voltages, the electrode circle progressively expanded to flatten the surface wrinkles, making the surface transparency change from translucent to almost transparent, as shown in Figure 3.5. The text logo was placed 20 mm behind the circular DEA device.

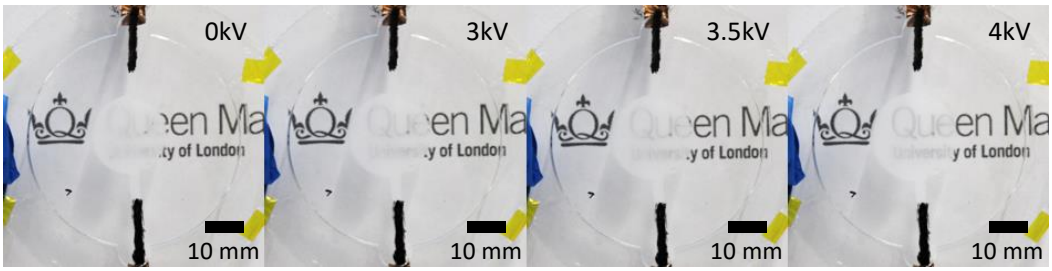

Figure 3.5 Voltage-induced changes in optical transmission for the device made of a PDMS film and ionogel electrodes (after fabrication).

However, an environmental stability test indicated that the ionogel-based DEAs were also not very stable, with the breakdown voltages reducing over time and the actuation area strains (which were measured by processing images taken at different voltages with the software Image J) fluctuating within the monitored time span of 4 weeks (Figure 3.6).

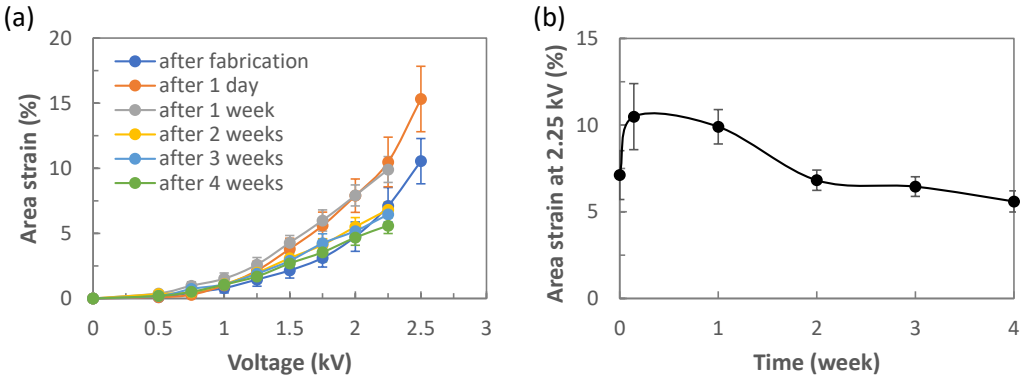

Figure 3.6 Actuation performance stability for ionogel-based DEAs over time. (a) The dependence of the area strain on the applied voltage of the ionogel-coated circle at different times after fabrication. (b) Changes in the area strain at the applied voltage of 2.25 kV with time.

In addition, the investigation on the reversible formation of surface wrinkles within the ionogels at different imposed radial strains was conducted. The PDMS film was first biaxially pre-stretched by 1.5 times and then coated with a thin circular layer of ionogel. The PDMS film was subsequently partially relaxed by reducing the pre-stretch to 1.25 times, such that the ionogel circle was subject to a radial strain of 16.7%. After that, the imposed strain was reversed back to 0% by stretching the PDMS film again, so as to examine the surface wrinkling reversibility. As presented by the confocal microscopy images in Figure 3.7b, the initial smooth surface of the ionogel became randomly wrinkled as the coated area was contracted. However, as the radial strain was mechanically stretched back to 0%, the morphological surface changes were not completely reversible, and a small number of wrinkles remained. This indicates that the electrical tuning of surface transparency using the ionogel-based devices cannot be properly controlled in a reversible manner.

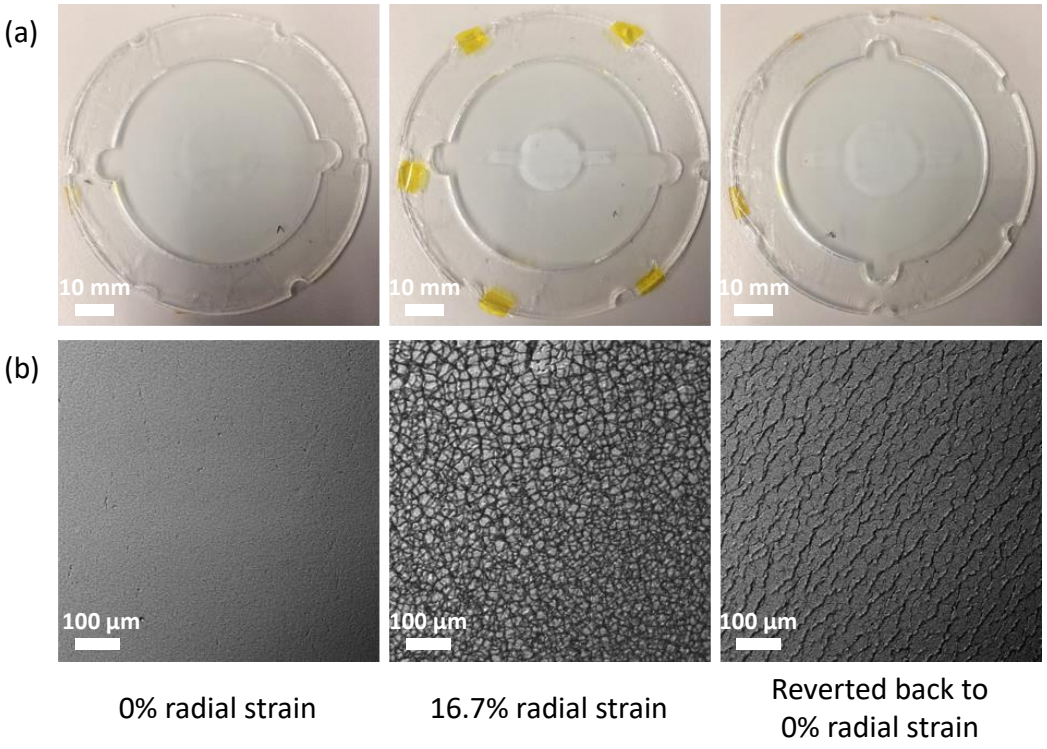

Figure 3.7 Investigation on the surface wrinkling of the ionogel covering a PDMS film, as a result of different imposed compressive radial strains from 0% to 16.7%, and then reverted back to 0%. (a) Photos taken from above. (b) Confocal microscopy images of ionogel coated areas.

Since the ionogel-based DEAs showed unstable actuation strains over time (Figure 3.6), the durability of such electrodes was further investigated by measuring the time-dependent changes in the surface resistance and thickness of the ionogel. The results are presented in Figure 3.8. It was found that the surface resistance of the ionogel on a PDMS film progressively increased with time (Figure 3.8a), which means electrodes produced this way tend to lose their conductivity in open air, presumably owing to ion diffusion.

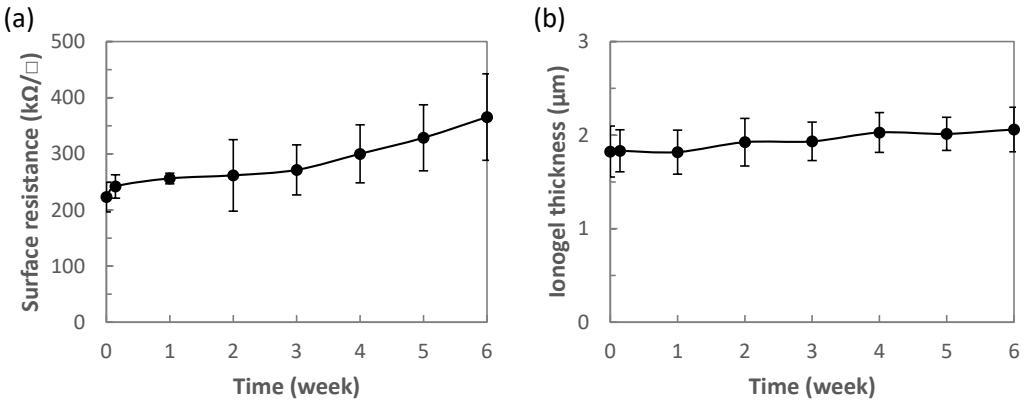

Figure 3.8 Stability of ionogel-based DEAs within the monitored time span of 6 weeks, by quantifying the changes in: (a) the surface resistance and (b) the thickness of the ionogel on a PDMS film.

The thickness of the ionogel was measured by the Bruker Dektak Profilometer. As revealed in Figure 3.8b, the thickness remained constant at approximately 2 µm within 6 weeks, indicating that the penetration or swelling of the ionogel within the PDMS film was unlikely occurred. This was confirmed by the optical microscopy images of a cross section of the ionogel covering the PDMS film. The sample for the optical microscopy was prepared by coating the ionogel thin film on a PDMS film that was placed on a PET substrate. The structure was then manually cut from the middle using a scissors to observe their cross section. It was clear that the ionogel (the first dark layer from the top, shown in Figure 3.9) maintained constant thickness over time.

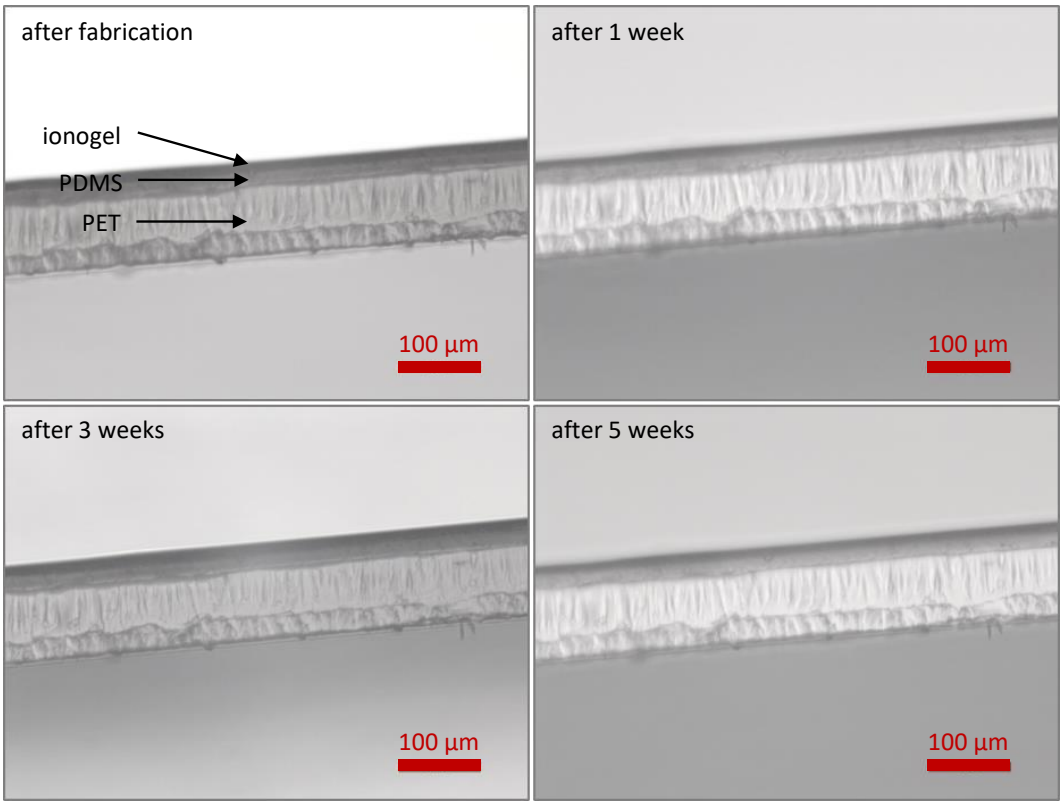

Figure 3.9 Optical microscopy images of a cross section of the ionogel covering a PDMS film, showing the ionogel thickness maintains the constant over time. The first dark layer from the top is the ionogel.

Therefore, based on the experimental results, although PMMA-based ionogels can offer a high transparency, the surface resistance for blade cast ionogels after fabrication is relatively high at about 220 kΩ/□ compared to carbon grease electrodes at about 100 Ω/□. Also, the poor lifetime stability and inadequate surface wrinkling reversibility make these ionogels an inefficient electrode to be used when electrically tuning the optical transmittance. However, a recent study was conducted to develop double network ionogels to obtain a good long-term stability, leading to the constant conductivity of ionogels up to a month (Ding et al., 2017).

3.3.4 PEDOT:PSS

PEDOT:PSS as a conducting polymer has been widely used for transparent electrodes in flexible organic electronic devices (Lipomi et al., 2012). With the doping of dimethyl sulfoxide (DMSO) and zonyl fluorosurfactant solutions, the produced PEDOT:PSS thin films have been shown to be reasonably stretchable, transparent and conductive (Lipomi et al., 2012; Liu, Davis, Liu, & Hammond, 2012; Vosgueritchian et al., 2012). Moreover, PEDOT:PSS has a high refractive index, allowing its wrinkled surfaces to effectively scatter light. Thus, the fourth prototype of tuneable transparency devices was developed using deformable PEDOT:PSS electrodes with clear acrylic elastomer membranes.

The transparency tuning performance was characterised by measuring the near-field total transmittance in the visible range (Figure 3.2). As stated in Section 3.3.1, the transmittance of the 3.5-times pre-stretched acrylic VHB membrane (without any electrodes) was about 92% at a wavelength of 550 nm. When the pre-stretch of the membrane was partially relaxed from 3.5 to 3 times, which created 14.3% compressive radial strain (or 30.6% area strain) on the electrodes, the wrinkled PEDOT:PSS diffused light and therefore reduced the transmittance to 79%. Upon electrical activation up to 5 kV, the DEA experienced a continuous surface expansion, creating the area strains up to around 25% (blue line in Figure 3.10b). The voltage-induced surface expansion thus flattened the electrode wrinkles, causing the transmittance at 550 nm to progressively increase from 79% at electrical rest to 85% at 5 kV (blue line in Figure 3.10a). This could also be observed from the surface

transparency of the elastomer membrane that was electrically tuned from translucent to nearly transparent, as shown in Figure 3.11.

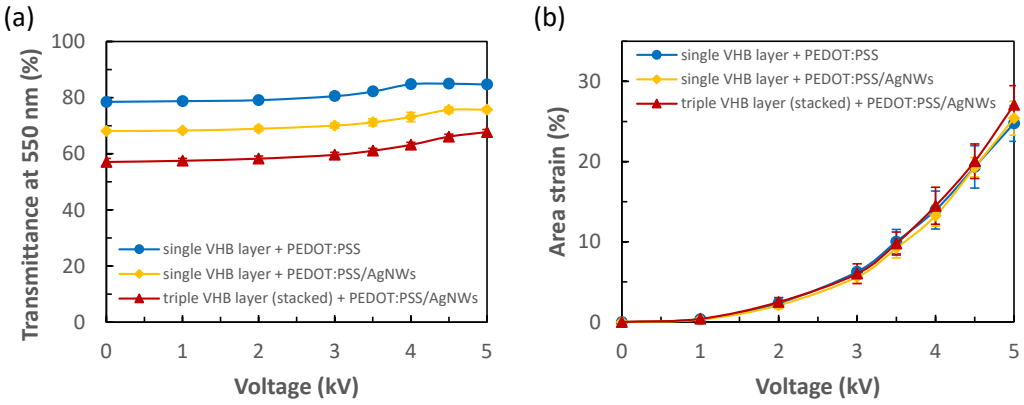

Figure 3.10 Electro-mechano-optical transduction performance of DEA-based tuneable transparency devices using deformable PEDOT:PSS or PEDOT:PSS/AgNWs compound electrodes. (a) The dependence on the applied voltage of the near-field total transmittance at 550 nm. (b) The dependence of the area strain of the PEDOT:PSS-coated circle on the applied voltage.

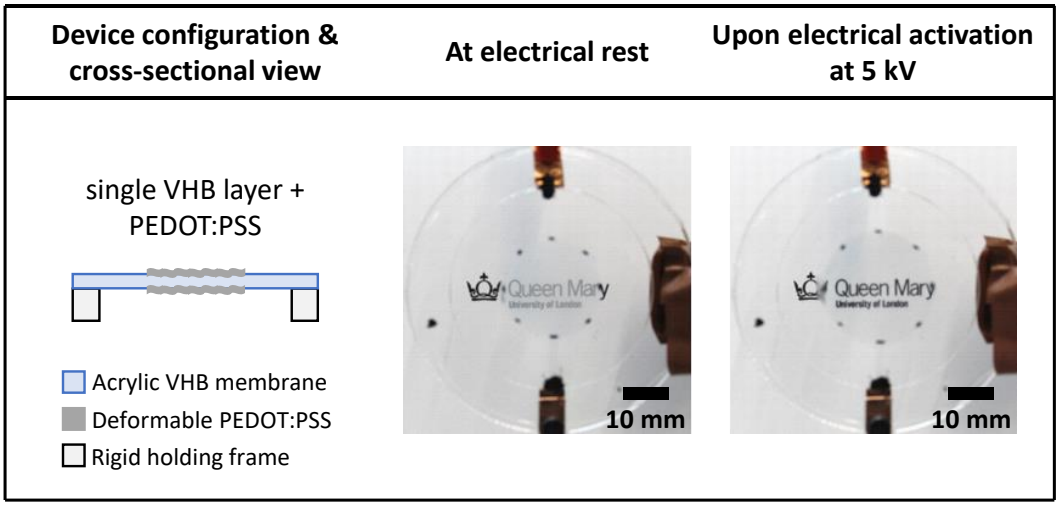

Figure 3.11 Voltage-induced tuning of surface transparency for the DEA-based device using deformable PEDOT:PSS electrodes.

3.3.5 Mixture of PEDOT:PSS and silver nanowires

In order to obtain the tuneable transparency devices with a lower level of optical transmittance (initially opaque surface) at electrical rest, a compound electrode consisting of PEDOT:PSS and silver nanowires was prepared and tested. In addition, a stacked DEA configuration was used to examine the possibility of achieving a wider tuning range of surface transparency.

The addition of AgNWs into PEDOT:PSS increased the light scattering. This therefore reduced the surface transparency at electrical rest (Figure 3.12), with a transmittance of 68% at 550 nm (measured based on the near-field method, Figure 3.2). Upon electrical activation up to 5 kV, such device made of a single elastomer layer and compound electrodes showed an increase in the tuning range of transmittance from 68% to 76% (yellow line in Figure 3.10a), compared to the device using PEDOT:PSS electrodes (blue line in Figure 3.10a), although the actuation area strains remained almost the same (Figure 3.10b).

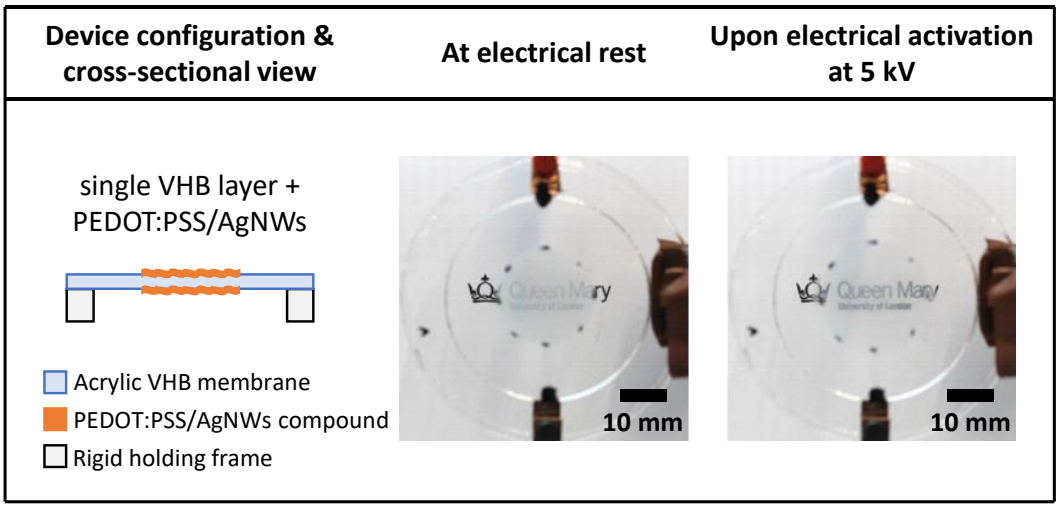

Figure 3.12 Voltage-induced tuning of surface transparency for the DEA-based device using PEDOT:PSS/AgNWs compound electrodes.

For a device with a stacked configuration, the surface was initially opaque at electrical rest (Figure 3.13), as four layers of wrinkled PEDOT:PSS/AgNWs electrodes significantly scattered the transmitted light. Such device exhibited a slightly higher area strain under 5 kV compared to the other two described prototypes (Figure 3.10b), and thus provided an even broader tuning range of transmittance between 58% and 69% (red line in Figure 3.10a), making the surface transparency change from opaque to translucent (Figure 3.13). The higher strain of the triple layer could help explain its wider tuning range, although the fabrication process for the multi-layer stacked structure was more complicated.

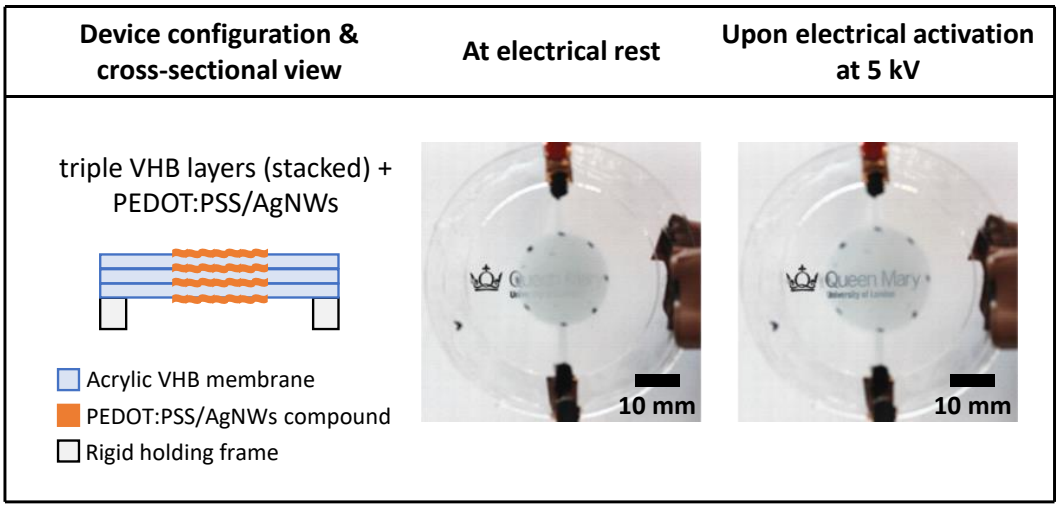

Figure 3.13 Voltage-induced tuning of surface transparency for the DEA-based device using PEDOT:PSS/AgNWs compound electrodes with a stacked configuration.

3.4 Conclusions

Several different types of transparent electrode materials were examined for the electrically-induced tuning performance of surface transparency using DEA technology. Those devices all operated using an expansion-mode working principle (Figure 3.1) to control the optical transmittance. In general, the electrode surfaces were made with wrinkled patterns, by applying the electrodes to a pre-stretched membrane and partially reducing the pre-strain. When the device is at electrical rest, the electrodes scatter light, thereby showing a lower transmittance. Then, voltage-induced surface expansions were used to flatten the corrugations, so as to increase the optical transmission.

It was found that the device using AgNWs electrodes could electrically tune the transmittance at 550 nm from 47% to 63%, changing the surface from

opaque to translucent. However, the brownish AgNWs could not provide a high degree of optical transmittance, because they scattered light even when sitting on a flat elastomer surface. Although PAAm-based hydrogels containing LiCl could offer high transparency, the device using such hydrogel electrodes was not successfully developed, due to the issues that hydrogels are hydrophobic and tend to dry out in open air. In addition, PMMA-based ionogel electrodes were able to achieve a device with a tuning range from 83% to 92%, causing the surface to change from translucent to transparent. However, the poor lifetime stability and incomplete surface wrinkling reversibility make the ionogels unsuitable for such a longer-term application. Moreover, the device using deformable PEDOT:PSS electrodes could electrically tune the transmittance from 79% to 85%, whilst the use of PEDOT:PSS/AgNWs compound electrodes could provide a lower transparency with a tuning range from 68% to 76%. Furthermore, the device with a stacked configuration using PEDOT:PSS/AgNWs electrodes showed another possible tuning range from 58% to 69%, although a much more complicated fabrication process was required. Therefore, based on all those experimental results, deformable PEDOT:PSS was selected as the optimal transparent electrode material to develop novel DEA-based adaptive optical devices (described in Chapters 4 and 5). This was because the PEDOT:PSS electrodes not only offered a high surface transparency, but also exhibited environmental stability and surface wrinkling reversibility and could be deposited using a relatively simple fabrication process.

One thing to point out is that all the optical transmittances mentioned in this chapter were measured based on the near-field method (Figure 3.2), which

quantifies the percentage of incident light transmitted as a whole, including both diffused transmitted and specular transmitted components. That includes any transmitted light whether it is scattered or not. As a result, any measured change in the near-field total transmittance is mainly attributed to the light reflection from the sample surface and the absorption within the sample. Thus, in order to properly and precisely identify the voltage-induced light scattering from the wrinkled surfaces, a far-field transmittance was required. Such measurement is discussed in more detail in Chapter 4 and Chapter 5.

Chapter 4 Electrically tuning soft membranes to both a higher and a lower transparency

4.1 Introduction

Smart membranes with optical transparency that can be electrically tuned are gathering growing interest for possible applications in various fields. For instance, controllable light diffusing filters that can continuously adjust the degree of light diffusion are used to either avoid eye damage from direct spot lights, hide details or obtain soft illumination (Ohzono et al., 2013). As another example, so-called smart windows are being employed to replace conventional sunlight shades, for instance in new-generation passenger airplanes (Williamson & Venables, 2013). Similarly, smart privacy glass is being used as a substitute for louver blinds in modern buildings (Mortimer et al., 2015). At present, the majority of such devices with electrically controllable transparency is based on electrochromic materials described in detail in Chapter 2, where an electric field-driven transport of ions between an ion storage film and an electrochromic film is used to modulate the optical transmittance (Claes G. Granqvist, 2014; Claes Goran Granqvist, 2005; Mortimer et al., 2015; Niklasson & Granqvist, 2007). Other types of devices are based on polymer-dispersed liquid crystals (PDLC) also described in Chapter 2, where the application of a voltage changes the alignment of liquid crystal molecules, so as to electrically switch the transparency (Cupelli et al.,

2009; Hosseinzadeh Khaligh et al., 2015; M. Kim et al., 2015; Nicoletta et al., 2005).

This chapter focuses on dielectric elastomer actuators (DEAs) that have been shown as an alternative promising technology to achieve large and continuous voltage-induced changes in optical transparency (Jun et al., 2017; Lin et al., 2017; Ong et al., 2015; Shian & Clarke, 2016; Shian et al., 2018; Shrestha et al., 2018; Van Den Ende et al., 2013; Yang et al., 2017). DEAs, which belong to the broader family of electromechanically active polymers (Carpi, 2016), essentially are electrically deformable capacitors, typically consisting of a dielectric elastomer membrane carrying two compliant electrodes. DEAs have also been used to electrically tune the optical transparency of soft insulating membranes, with various strategies, which can be grouped as presented in Figure 4.1. Note that the change of membrane thickness resulting from the actuation of each device is not shown for simplicity.

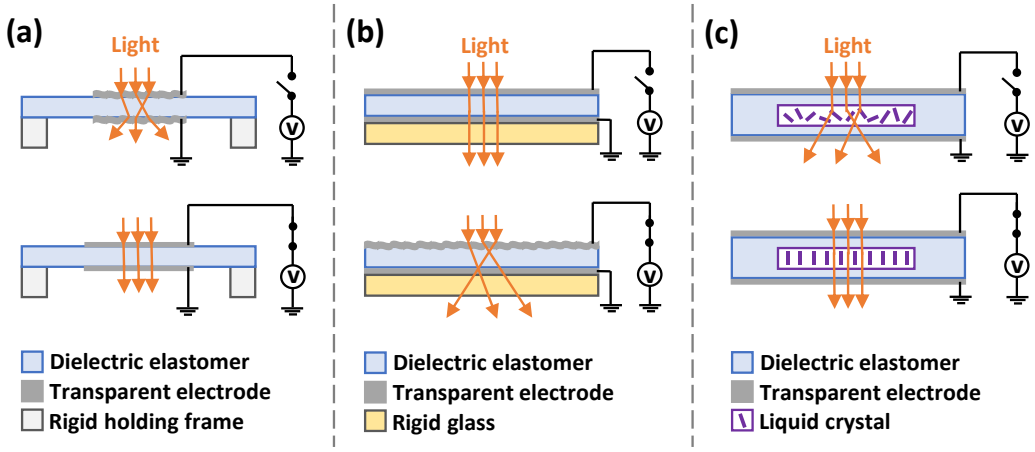

Figure 4.1 State-of-the-art strategies to achieve DEA-based devices with electrically tuneable optical transparency: (a) expansion of a soft membrane with wrinkled stretchable transparent electrodes; (b) cratering-type surface instability of a constrained soft membrane with transparent electrodes; (c) alignment of liquid crystals encapsulated within a soft matrix sandwiched between transparent electrodes.

The first strategy (Figure 4.1a) consists of coating the soft dielectric membrane with stretchable transparent electrodes, which are initially made translucent by mechanically inducing an electrode wrinkling and then are made more transparent by electrically inducing an electrode smoothing (Jun et al., 2017; Ong et al., 2015; Shrestha et al., 2018). In a second approach (Figure 4.1b), the transparency can be reduced by means of a cratering-type wrinkling of surface electromechanical instabilities of transparent electrodes covering the membrane fixed to a rigid substrate, typically requiring significant electric fields (Lin et al., 2017; Shian & Clarke, 2016; Shian et al., 2018; Van Den Ende et al., 2013). In a third approach (Figure 4.1c), voltage-controlled light shutters are obtained by encapsulating liquid crystals into the membrane and sandwiching it between transparent electrodes, to achieve an operation similar to that of PDLC windows, producing an on-off switching (Yang et al., 2017).

According to all these state-of-the-art approaches, by using electrical means the optical transparency can be either only increased or only decreased.

In this chapter, the first concept to make the optical transparency electrically tuneable to both higher and lower values within the same device is presented. The concept is applicable to any soft insulating membrane, by coating both of its surfaces with a central circle of transparent stretchable conductor, surrounded by a stretchable conducting ring. The device shows that the resulting transparency of the central area can be electrically modulated with dual operation, such that it can be both increased and decreased, depending on whether the electrical activation is used to generate an expansion or a contraction of the central area.

4.2 Experimental

4.2.1 Dielectric elastomer membrane

All the tests were performed using clear and adhesive acrylic-based elastomer membranes (VHB 4910, 3M, USA). The membranes were biaxially pre-stretched (to a range of values that are specified later), in order to achieve a well-known increase in the electromechanical transduction performance, as first documented by Pelrine et al (R. Pelrine, Kornbluh, Pei, et al., 2000) and later on explained in different ways by Brochu and Pei (Brochu & Pei, 2010) and Koh et al (Koh et al., 2011). The membrane had at rest a thickness of 1 mm, which then reduced to a lower value, depending on the amount of the applied pre-stretch, as detailed below.

4.2.2 Stretchable transparent conductive material

Stretchable, conductive and transparent layers on the dielectric elastomer membranes were obtained by spray coating a PEDOT:PSS compound, consisting of a 17.2 wt% aqueous PEDOT:PSS solution (Clevios PH 1000, Heraeus, Germany), 0.86 wt% dimethyl sulfoxide (DMSO, Sigma-Aldrich, UK), 6.9 wt% fluorosurfactant (Capstone FS-30, Apollo Scientific, UK) and 75 wt% isopropanol (2-Propanol, Sigma-Aldrich, UK). The compound solution was mixed using a vortex mixer (SA8, Stuart Equipment, UK) with a speed of 2000 rpm for 1 minute at room temperature.

4.2.3 Fabrication of the tuneable devices

The expansion-mode device was fabricated as follows. A volume of 25 µL of the PEDOT:PSS compound solution was used to spray on both sides of a 4-times pre-stretched VHB elastomer membrane a 28 mm-wide circular thin layer (with an estimated thickness lower than 100 nm after solvent evaporation), to be used as a transparent electrode. Then, the membrane was partially relaxed to a 3.5-times pre-stretch, making the PEDOT:PSS electrode wrinkle, due to its dissimilar modulus when compared with the elastomer membrane (Z. H. Chen, Fang, Li, & Guan, 2019). Then resulting -23.4% area strain corresponded to a reduction of the electrode diameter from 28 to 24.5 mm (Figure 4.2) and an increase of the membrane thickness from 62.5 to 81.6 µm (calculated values). Note that the change of membrane thickness resulting

from the actuation of each device is not shown for simplicity in Figure 4.2.The membrane was finally fixed to a support frame, exploiting its adhesive properties.

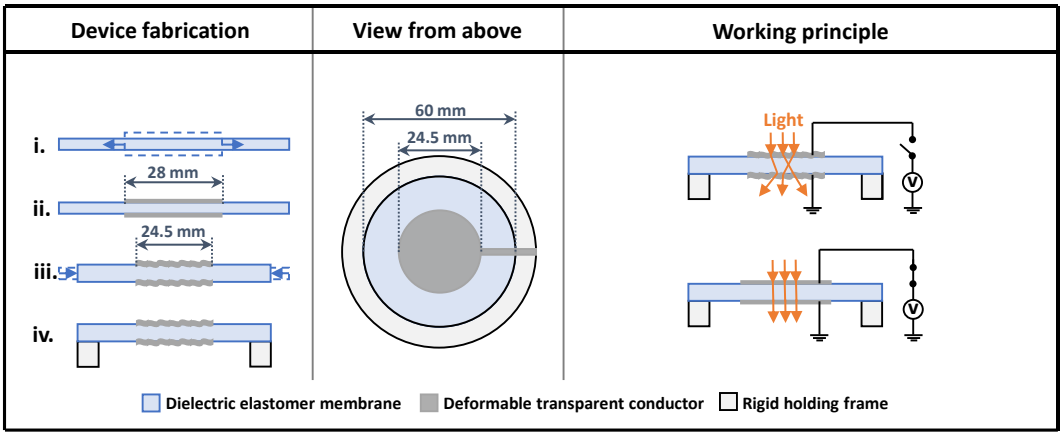

Figure 4.2 Concepts for a DEA-based electrical tuning of the optical transparency of a soft membrane working in an expansion mode.

The contraction-mode device was fabricated in the same way as the expansion-mode one, although without any reduction of the 4-times pre-stretch. So, the membrane thickness was about 62.5 μm and the PEDOT:PSS-coated central area had a diameter of 28 mm. A non-transparent stretchable conductor, consisting of conductive carbon grease (Carbon Conductive Grease 846, M.G. Chemicals, Canada), was carefully applied to the annular outer region of each side of the membrane, so as to obtain ring-shaped stretchable electrodes. The central circular area was separated by the outer annular area by a 2 mm gap (Figure 4.3). Note that the change of membrane thickness resulting from the actuation of each device is not shown for simplicity in Figure 4.3.

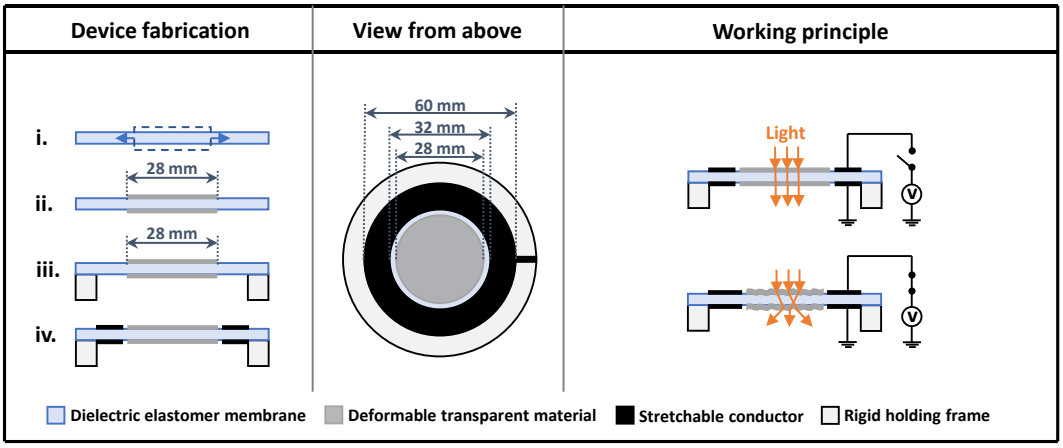

Figure 4.3 Concepts for a DEA-based electrical tuning of the optical transparency of a soft membrane working in a contraction mode.

The dual-mode device was fabricated combing the procedures described above. So, the membrane thickness was about 81.6 µm and the PEDOT:PSS electrode had a diameter of 24.5 mm. The gap between the circular and annular electrodes was 3.75 mm wide (Figure 4.4). Note that the change of membrane thickness resulting from the actuation of each device is not shown for simplicity in Figure 4.4.

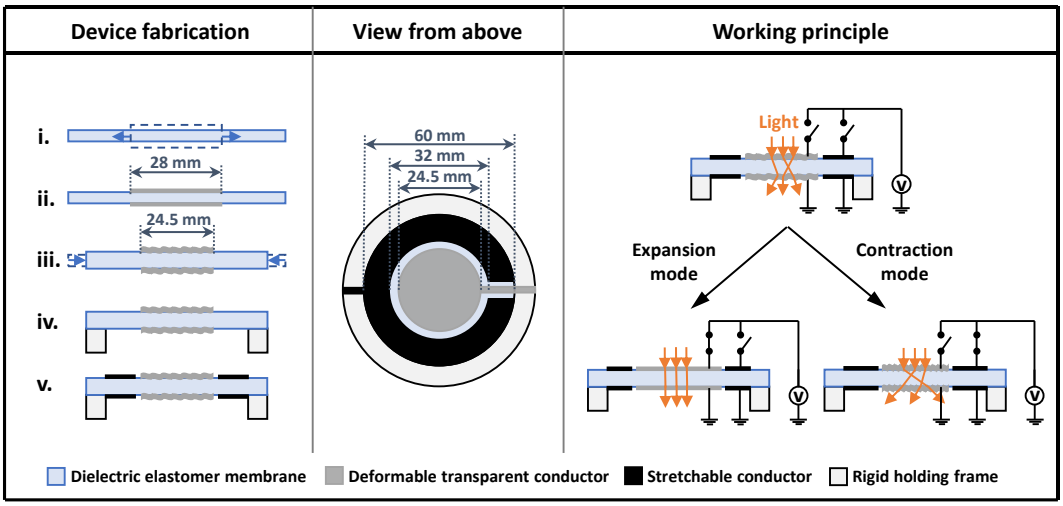

Figure 4.4 Concepts for a DEA-based electrical tuning of the optical transparency of a soft membrane working in a dual expansion-contraction mode.

For all the devices, the PEDOT:PSS layer was oven dried for 30 min at 80°C. A copper tape was used to connect each electrode to the high voltage source.

4.2.4 Characterisation

In order to drive the devices, a compact DC-DC high voltage converter (Q-series, EMCO High Voltage Corporation, USA) was used to produce voltages up to 6 kV, which were monitored with a high-voltage probe. Each voltage value was divided by the membrane's thickness at electrical rest (81.6 or 62.5 µm, as describe above), in order to calculate the applied (nominal) electric field.

Transmittance spectra of the tuneable devices were characterised, in the 400-800 nm visible range, using a Perkin Elmer Lambda 950 UV-vis spectrometer with a 10 cm-wide integrating sphere.

The actuation strains were calculated by processing images (taken at different driving voltages) with the software Image J.

The reversible formation of surface wrinkles that were mechanically induced within the PEDOT:PSS thin films at different area strains was investigated using an atomic force microscope - AFM (NanoWizard 4 BioAFM, JPK Instruments AG, Germany) and a scanning electron microscope - SEM (Inspect F50, FEI, USA). The AFM images were taken with a cantilever probe (NSG01, NT-MDT, Russia) having a resonant frequency of around 150 kHz and a spring constant of 3.5 N/m. The SEM images were taken at an acceleration voltage of 2 kV.

4.3 Results and discussion

4.3.1 Electrically induced expansions and contractions of a soft membrane to tune its transparency

The dual-operation concept proposed originates from the combination of the expansion-mode operation mentioned above (Figure 4.1a) with an additional contraction-mode operation, based on a different structure described below. The two operation modes and their integration into a dual-mode single device that can exploit both of them are schematically presented in Figure 4.4.

The expansion-mode device (Figure 4.2) is obtained as follows. The elastomeric membrane is first biaxially pre-stretched and then coated on both sides with a transparent deformable conductor to create electrodes, which define a circular DEA. By making the electrode’s stiffness higher than that of

the elastomer, it is possible to create wrinkles on the electrode layer when the pre-stretch is reduced. After that, the membrane is clamped to a rigid circular frame. At electrical rest, the wrinkled electrodes scatter the transmitted light, making the sandwich opaque. When a voltage is applied, the resulting surface expansion causes the wrinkles to flatten, thereby reducing the scattering and so leading to a higher optical transparency (Figure 4.2). Therefore, this configuration, known from the state of the art, translates increasing voltages into an increasing transparency.

On the other hand, if any given application requires that the membrane at electrical rest is transparent and then should become progressively opaque with increasing voltages, a different concept is required. To achieve this, a contraction-mode device presented in Figure 4.3 was envisaged. It is obtained by first biaxially pre-stretching the elastomeric membrane and coating both sides of it with a transparent deformable material on a central area. The membrane is then fixed to a rigid holding frame and a conductive stretchable material is applied, on both sides, creating an outer ring, separated from the central circle. That ring (which can be non-transparent) works as the stretchable electrode of an annular DEA, whilst the central circle (which can be non-conductive) acts as a deformable medium with strain-dependent scattering of the transmitted light. When the device is at electrical rest, the central coating is optically transparent. When a voltage is applied, the annular electrodes expand towards the centre (as they are constrained at their outer edge), causing the central area of the membrane to relax, due to a reduction of its pre-stretch. If the stiffness of the central coating is higher than that of the elastomer, the resulting effect is the creation of wrinkles, which scatter light

and so reduce the transparency (Figure 4.3). Therefore, this alternative configuration allows for using increasing voltages to reduce the transparency.

Nevertheless, there might be application scenarios where it could be of interest to electrically tune the transparency to both higher and lower values, within the same membrane. To address this need, an integration of the two concepts described above, leading to the dual-mode (expansion-contraction) device, which is shown in Figure 4.4, was conceived. It can be assembled using the same procedure adopted for the expansion-mode device (Figure 4.2), although in this case both the surfaces also host outer ring-shaped stretchable electrodes, to form an annular DEA, as for the contraction-mode device (Figure 4.3). Note that the central transparent material is not only deformable, as required by the contraction mode, but also electrically conductive, as required by the expansion mode. On each surface, the outer ring electrode encircles the central circular electrode without contact between them, so that the two can be electrically activated independently. Indeed, their independent driving enables a dual operation of the device: the transmitted light scattering caused by the wrinkled central area at electrical rest can be either increased or decreased, depending on whether the electrical activation concerns the annular DEA (contraction mode) or the circular DEA (expansion mode), respectively (Figure 4.4).

The three concepts described above were all built and optimised to investigate how the proposed dual-mode configuration performs as compared to the single-mode ones. The experiments were based on pre-stretched dielectric elastomer membranes made of a commercial acrylic elastomer film (VHB tape

series, by 3M), as detailed earlier. This elastomer was chosen because of its extensive usage within the DEA field as a test material, due to a high electromechanical transduction performance in quasi-static conditions and a simplification of manufacturing processes resulting from its adhesive properties (Brochu & Pei, 2010; Carpi et al., 2010, 2008; R. E. Pelrine et al., 1998; R. Pelrine, Kornbluh, Pei, et al., 2000).

The most challenging aspect of the implementation was the material to be used as transparent deformable conductor. The state of the art offers a range of different materials (McCoul et al., 2016), including silver nanowires (Shian & Clarke, 2016), metal oxide thin films (Ong et al., 2015; Shrestha et al., 2018), carbon nanotubes (Shian et al., 2018; Yuan et al., 2008), graphene (Zang et al., 2013), ionogels (B. Chen, Lu, et al., 2014) and conducting polymers (Son et al., 2012). Following the investigation in Chapter 3, PEDOT:PSS was selected as a conducting polymer. It is already widely adopted for transparent electrodes in flexible organic electronic devices (Lipomi et al., 2012). PEDOT:PSS can offer transparency and conductivity comparable to those of indium-tin oxide electrodes (Hau, Yip, Zou, & Jen, 2009; Y. H. Kim et al., 2011). Nevertheless, the order of magnitude of its Young's modulus in pure form is usually as high as 1 GPa (Tank, Lee, & Khang, 2009). This would prevent PEDOT:PSS from serving as an effective compliant electrode for DE actuation. However, the addition of dimethylsulfoxide (DMSO) and a zonyl fluorosurfactant into an aqueous PEDOT:PSS solution makes it possible to produce transparent PEDOT:PSS electrodes that are stretchable (Liu et al., 2012; Vosgueritchian et al., 2012), with reported retentions of conductivity for strains in excess to 180% (Lipomi et al., 2012). Therefore, in this work the

membrane was spray coated with a thin layer of PEDOT:PSS to create the central stretchable transparent conducting area, and for the contraction- and dual-mode devices a carbon grease was used to create the outer non-transparent stretchable electrodes. Details about materials and fabrication processes are all as have been reported previously in the thesis.

These materials were used to assemble the three devices described above. In order to obtain a roughly symmetrical behaviour and enable proper comparisons of their performance, they were carefully sized as follows. They all had the same membrane's outer diameter, so as to have the same size constraint. With respect to the reference configuration represented by the expansion-mode device, the PEDOT:PSS coated area of the contraction-mode device had at electrical rest the same diameter (28 mm) that the expansion-mode device had prior to wrinkling during manufacturing (Figure 4.2). With this choice, the contraction-mode device had at electrical rest the same transparency and same window size of the expansion-mode device when its wrinkles are electrically flattened; moreover, with an applied electric field sufficiently high to reduce the diameter to the same value that the reference device has at rest (24.5 mm), the contraction-mode device was developed to be able to reach the same opacity (wrinkling) of the reference device at rest (Figure 4.3). This behaviour was confirmed by the tests presented in the next section. For the dual-mode device, the PEDOT:PSS diameter was the same as that for the reference device (24.5 mm), so as to achieve the same effect when used in the expansion mode (Figure 4.4).

The size of the annular electrode in the contraction- and dual-mode devices was identical, in order to ensure an analogous effect. Indeed, for any given active strain of the annular surface, a wider annulus would have a larger deformation, inducing a higher strain of the central region. In particular, the annulus width (difference between its outer and inner diameters) was made identical (14 mm) to the radius of the PEDOT:PSS coated area of the expansion-mode device.

This sizing of the three devices enabled a comparative investigation of their performance, which is presented below.

4.3.2 Electrical tuneability of the soft membrane transparency

The electro-optical transduction performance of each device was characterised in the 400-800 nm visible range (as described previously), quantifying how different electrical activations changed the optical transmittance measured in both the near and far fields. According to the test equipment used in this research, near and far fields are here defined as a device-to-detector distance of 5 and 40 cm, respectively (Figure 4.5).

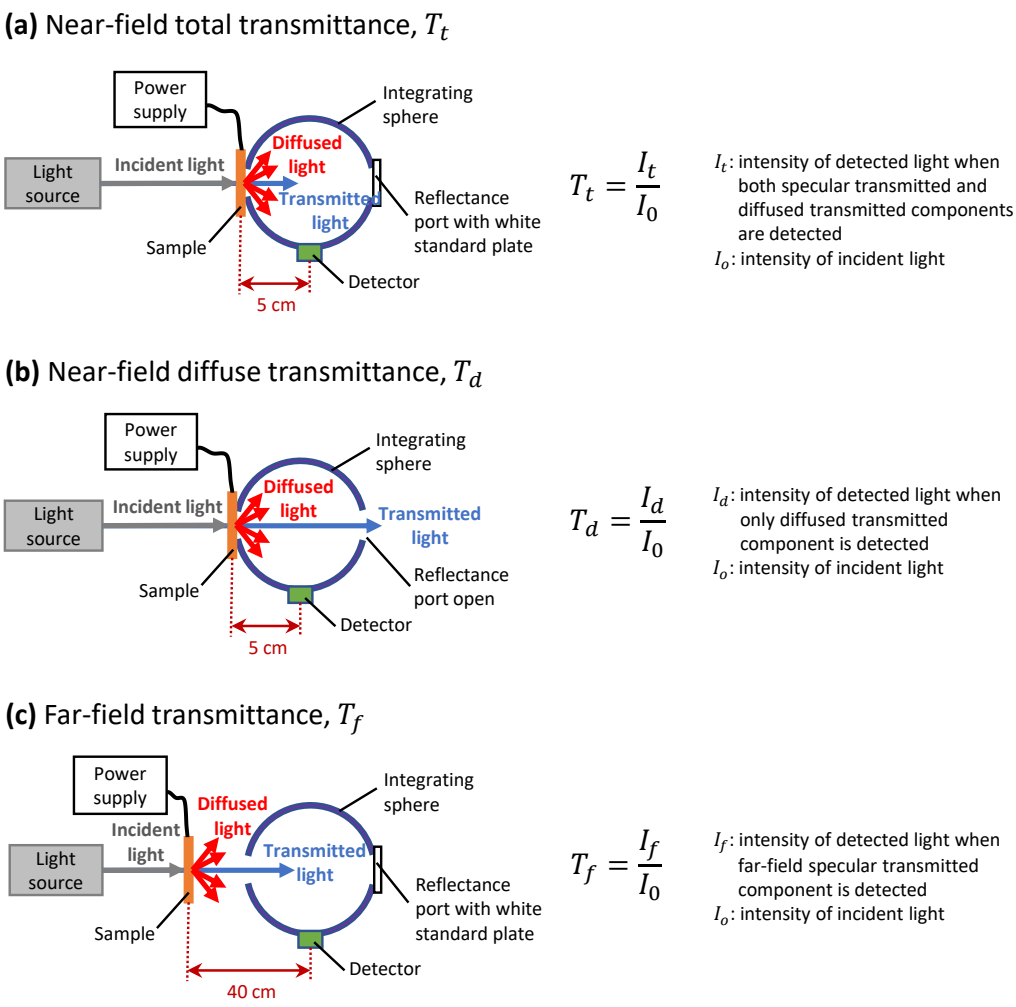

Figure 4.5 Schematic representation of the UV-Vis spectrometer set-up used to characterize the transmittance: (a) Near-field total transmittance measurement, with both specular transmitted and diffused transmitted light detected; (b) Near-field diffuse transmittance measurement, with only diffused transmitted light detected; (c) Far-field transmittance measurement, with only specular transmitted light detected.

In the near field, the measurements concerned both the diffuse transmittance T_d (percentage of incident light transmitted as diffused light) and the total transmittance T_t (percentage of incident light transmitted as a whole, including both diffused transmitted and specular transmitted components, which may or may not be scattered), which were detected as detailed in Figure 4.5. For the test of a near-field total transmittance, the transmission port was covered with

the sample, whilst the reflectance port was covered with a white standard plate (Figure 4.5a). For the test of a near-field diffuse transmittance, the transmission port was covered with the sample, whilst the reflectance port was left open (Figure 4.5b). The data were also used to calculate the transmission Haze, defined as the ratio between the near-field diffuse and total transmittances: $Haze = T_d/T_t$. The Haze value, representing the percentage of total transmitted light that propagates as diffused light, was used to give an indication of the cloudy appearance of the sample (Campo, 2008).

In the far field, a far-field transmittance was simply considered, without any further distinction between diffused and specular components, due to the fact that such a difference tends to progressively lose significance as the sample-to-detector distance increases (the diffused component tends to be lost by the measurement equipment). For the test of a far-field transmittance, the transmission port was left open, whilst the reflectance port was covered with a white standard plate (Figure 4.5c).

The near-field total and far-field transmittances of the pre-stretched acrylic elastomer membranes (without any coating) were approximately 92% at 550 nm, whilst their Haze value was lower than 0.5% at 550 nm. The optical spectra while using the membranes in the three described configurations to tune their transparency are presented in Figure 4.6, Figure 4.7 and Figure 4.8.

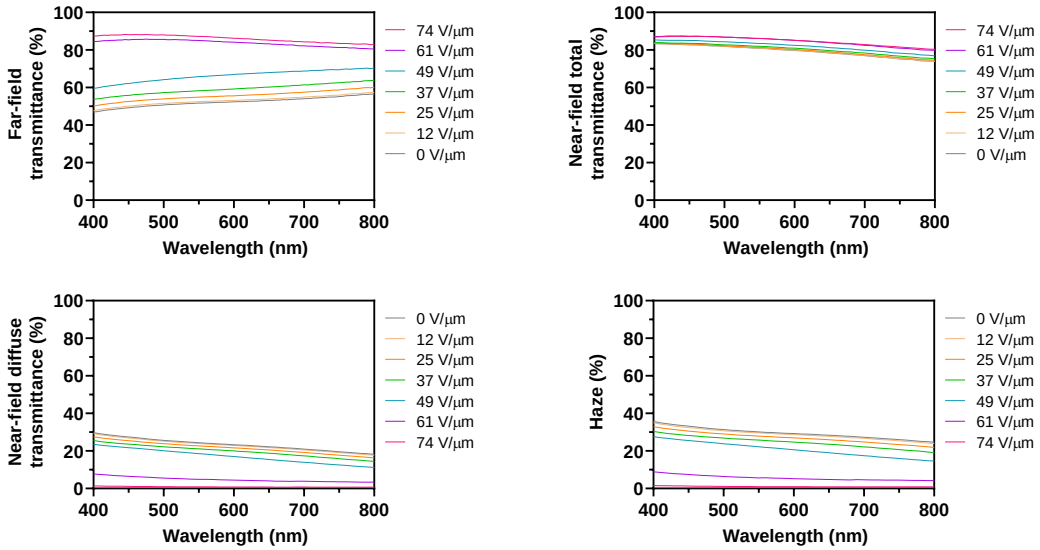

Figure 4.6 Visible-range spectra of the far-field transmittance, near-field total transmittance, near-field diffuse transmittance and Haze value of the soft membrane-based tuneable optical transparency device working in an expansion mode.

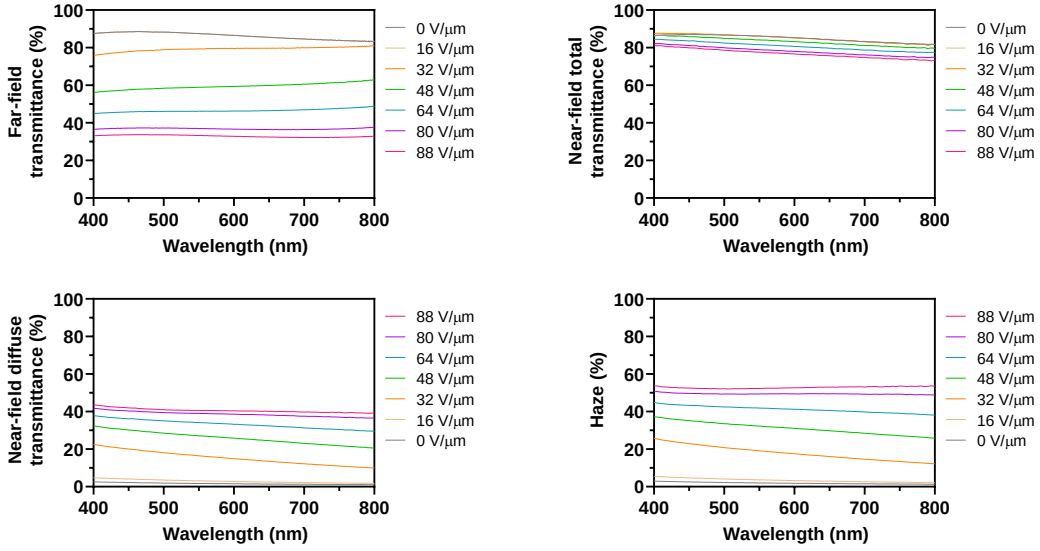

Figure 4.7 Visible-range spectra of the far-field transmittance, near-field total transmittance, near-field diffuse transmittance and Haze value of the soft membrane-based tuneable optical transparency device working in a contraction mode.

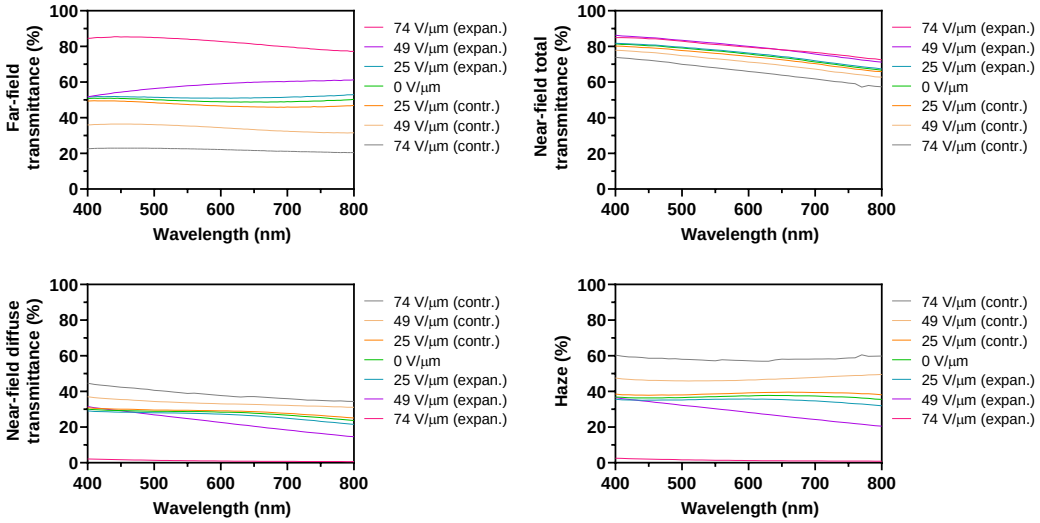

Figure 4.8 Visible-range spectra of the far-field transmittance, near-field total transmittance, near-field diffuse transmittance and Haze value of the soft membrane-based tuneable optical transparency device working in a dual expansion-contraction mode.

Also, their corresponding electro-optical transduction performance achieved is given in Figure 4.9, Figure 4.10 and Figure 4.11. In those three figures, for each configuration, the electrically-induced variations of the transmittances (near-field total, near-field diffuse and far-field) at 550 nm and the Haze number at different wavelengths are shown. Each data point represents the average value from three sample devices. Error bars corresponding to the standard deviation are included, although most of them are too small to be seen within the 0-100% range of the graph. The photographs visualise the change in transparency due to the specified electric fields, which caused the reported area strains of the PEDOT:PSS windows: the first photo set shows the device covering text 3 cm away, whereas the second set shows flowers approximately 100 cm away from a device attached to the camera lens.

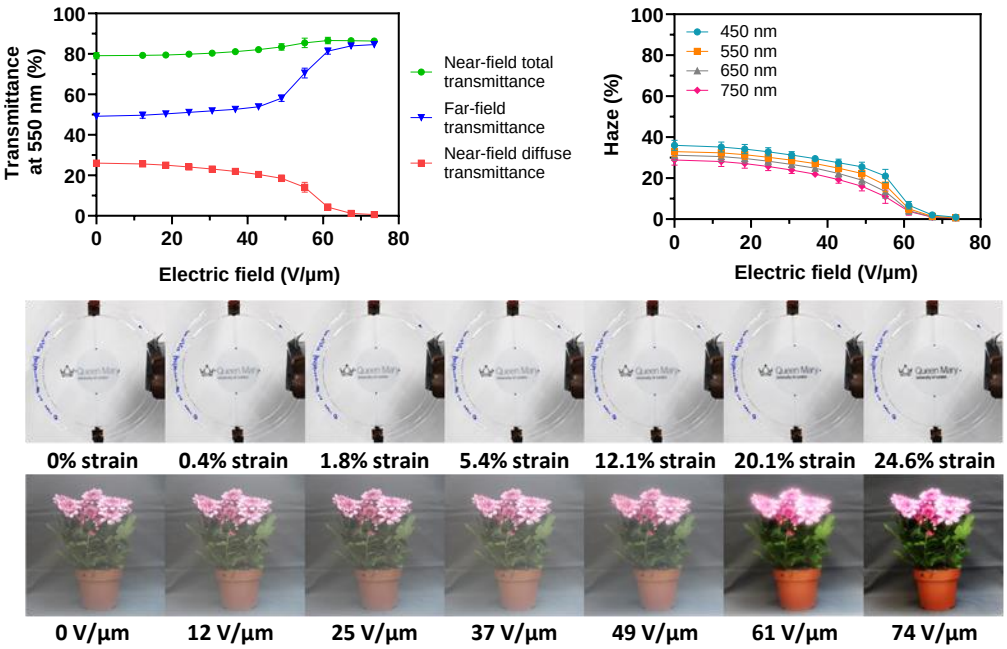

Figure 4.9 Electro-optical transduction performance of the tested soft membrane-based device working in an expansion mode.

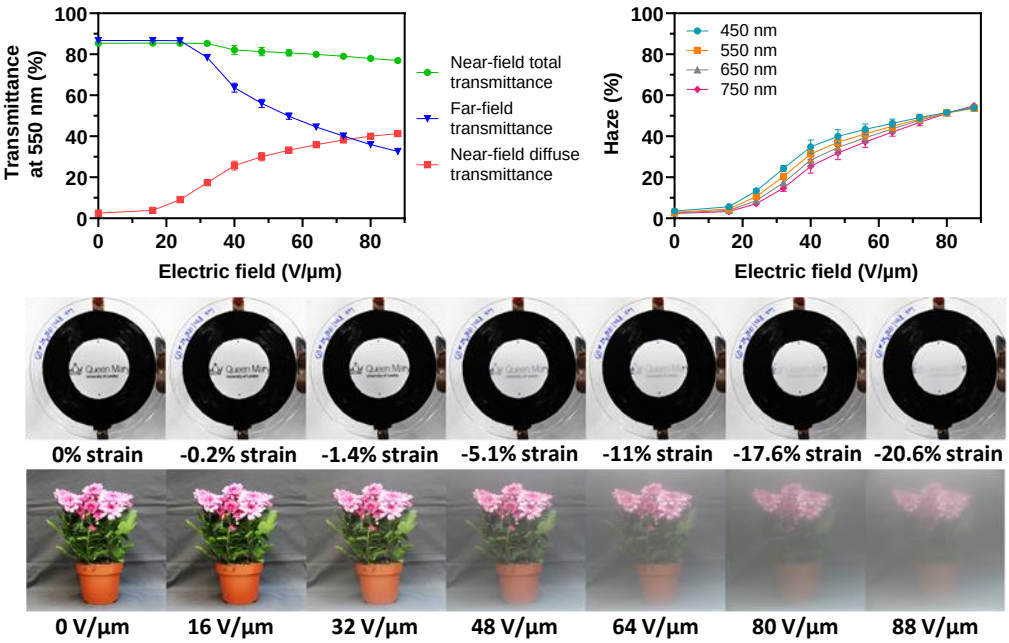

Figure 4.10 Electro-optical transduction performance of the tested soft membrane-based device working in a contraction mode.

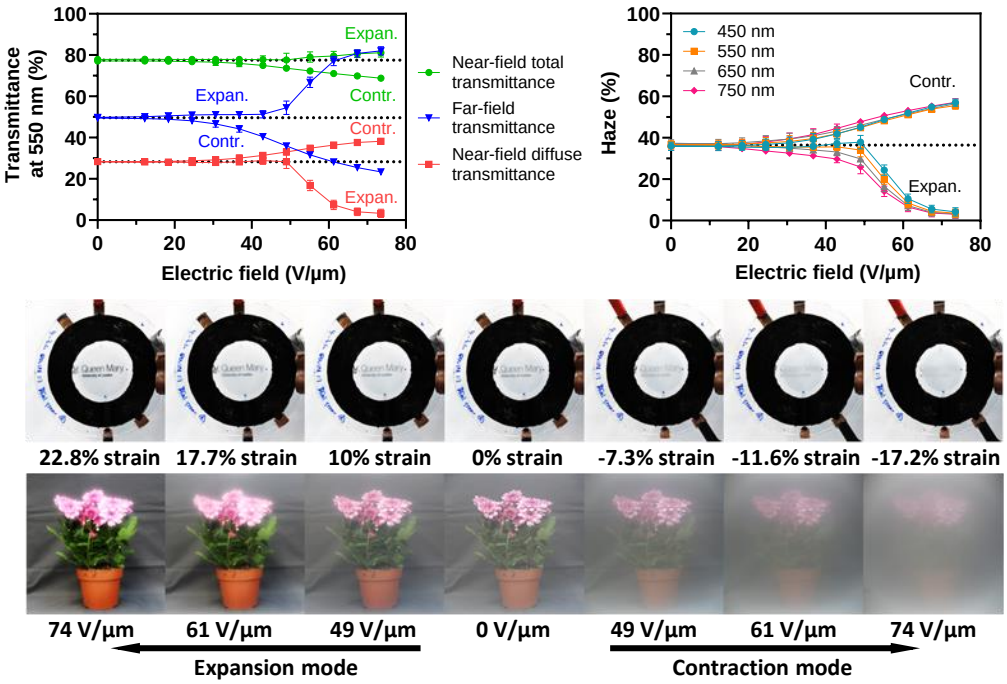

Figure 4.11 Electro-optical transduction performance of the tested soft membrane-based device working in a dual expansion-contraction mode.

Owing to the transparency of PEDOT:PSS thin film, all the devices had at electrical rest a rather high near-field total transmittance (around 80%), which could then be electrically increased or decreased, according to either the expansion or contraction mode, respectively. Any electrically-induced increase or decrease of the near-field total transmittance (green curves in Figure 4.9, Figure 4.10 and Figure 4.11) was due to a smoothening or a wrinkling of the surface, which caused a reduction or an increase of the near-field diffuse transmittance (red curves in Figure 4.9, Figure 4.10 and Figure 4.11) and an increase or a decrease of the far-field transmittance (blue curves in Figure 4.9, Figure 4.10 and Figure 4.11).

Interestingly, in all the cases the near-field total transmittance corresponded rather accurately (±5% error) to the sum of the near-field diffuse transmittance and the far-field one. This means that the sample-to-detector distance adopted in the far field (40 cm) was sufficiently long that in practice nearly all the diffuse component of the transmitted light was not detected (Figure 4.5), such that the far-field transmittance was essentially representative only of light that was specular transmitted, effectively the light that is not scattered. The so-achieved far-field transmittance then provides a quantification of the transparency that an observer can perceive while looking through the device window, perpendicularly to it, from that distance.

From a qualitative standpoint, the electrical tuneability of the transparency can be observed from the photos in Figure 4.9, Figure 4.10 and Figure 4.11, which were taken by arranging the devices either in front of a camera (to image the whole device and a text behind it, also showing the electrode deformation at different electric fields) or attached to its lens (to image a whole scene with flowers as seen through the device window). The cloudy appearance of the three devices, as a result of their electrically variable scattering of light, is quantified by the Haze-field plots.

The electrically induced area strains experienced by the PEDOT:PSS coated circles for devices operating in an expansion, a contraction and a dual expansion-contraction mode are presented in Figure 4.12, Figure 4.13 and Figure 4.14, respectively. Each data point represents the average value from three sample devices. Error bars corresponding to the standard deviation are included, although most of them are too small to be seen within the broad

range of the graph. In particular, strain-field and transmittance-field plots are shown with data sets taken both immediately after fabrication and up to eight weeks later.

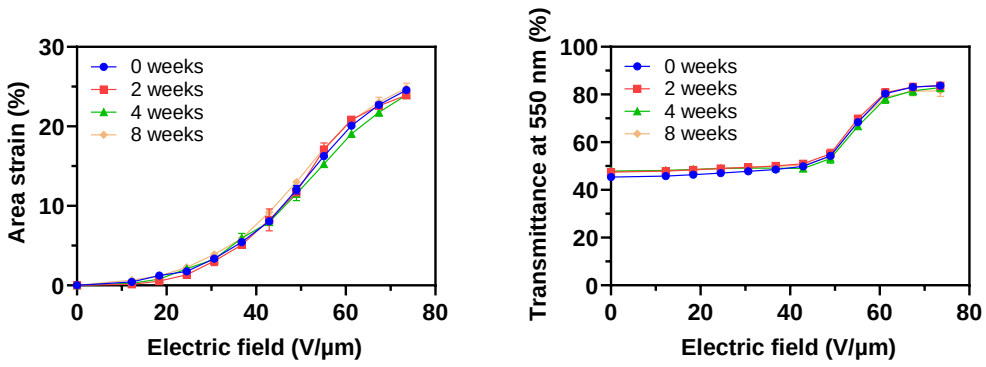

Figure 4.12 Electro-mechano-optical performance stability over time for the device operating in an expansion mode. The dependence on the applied electric field of both the area strain of the PEDOT:PSS-coated circle and its far-field transmittance at 550 nm are shown at different times after fabrication.

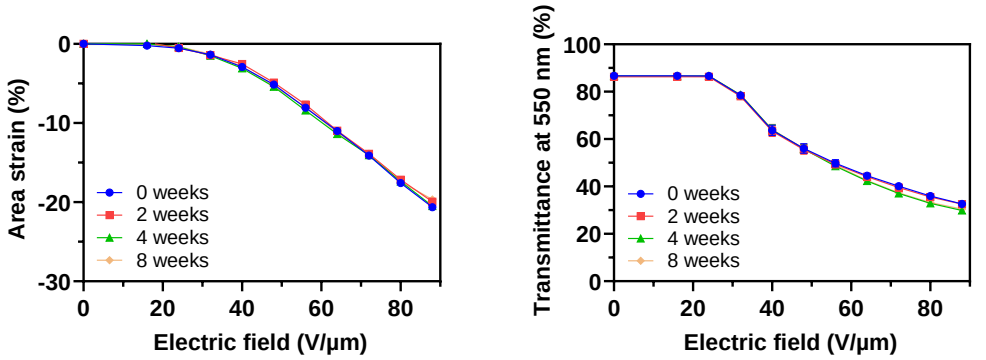

Figure 4.13 Electro-mechano-optical performance stability over time for the device operating in a contraction mode. The dependence on the applied electric field of both the area strain of the PEDOT:PSS-coated circle and its far-field transmittance at 550 nm are shown at different times after fabrication.

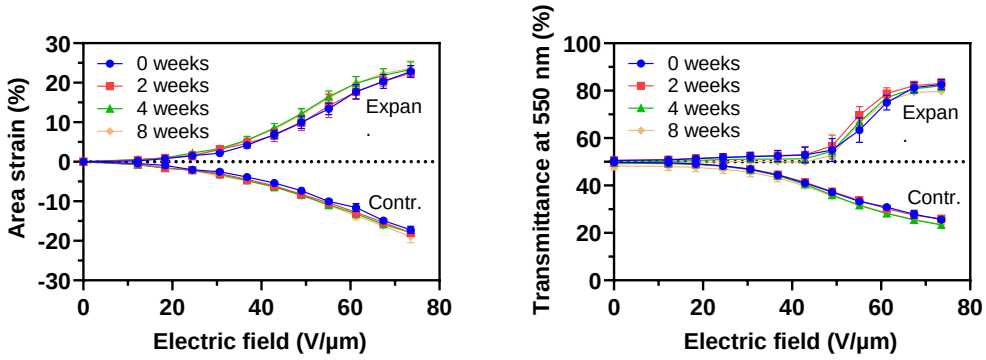

Figure 4.14 Electro-mechano-optical performance stability over time for the device operating in a dual expansion-contraction mode. The dependence on the applied electric field of both the area strain of the PEDOT:PSS-coated circle and its far-field transmittance at 550 nm are shown at different times after fabrication.

The first evidence is that the electro-mechano-optical performance was found to be particularly stable over the monitored time span. Moreover, the strain-field plots provide further insights on how the electrical actuation of the membrane in each configuration affects its transparency, as discussed below. For the sake of comparisons, data at a maximum applied field of 74 V/μm are considered, as it is the highest available for all the three cases.

For the expansion-mode device, the area strain at 74 V/μm (about 24.6%, Figure 4.12) corresponded to an increase of the PEDOT:PSS diameter from 24.5 to 27.4 mm, which was close to the size before the creation of the wrinkles during manufacturing (28 mm, Figure 4.2). Therefore, the electrical activation of the wrinkled electrodes could recover a nearly smooth surface. Moreover, as 28 mm was also the PEDOT:PSS diameter of the contraction-mode device at electrical rest (Figure 4.3), the transparency electrically reached by the expansion-mode device was basically the same as that of the contraction-

mode device at rest. This was confirmed by the transmittance measurements (Figure 4.12 and Figure 4.13).

For the contraction-mode device, the area strain at 74 V/µm (about -15%, Figure 4.13) corresponded to a reduction of the PEDOT:PSS diameter from 28 to 25.8 mm, which was close to the size of the expansion-mode device at electrical rest (24.5 mm, Figure 4.2). So, the electrical activation of the contraction-mode device was able to create a level of wrinkling comparable to that of the expansion-mode device at rest, and so also a comparable scattering of light. This was confirmed by the transmittance measurements (Figure 4.12 and Figure 4.13).

For the dual-mode device, the operation in expansion or contraction mode created at 74 V/µm a strain of 23% or –17.2%, respectively (Figure 4.14), changing the PEDOT:PSS diameter from 24.5 mm to either 27.2 or 22.3 mm, respectively. Therefore, when used in expansion mode, the device behaved like the single expansion-mode one; this was confirmed by the transmittance measurements (Figure 4.12 and Figure 4.14). When used in contraction mode, however, the lower strain achieved made the electrical reduction of the transmittance smaller than that occurring in the single contraction-mode device (Figure 4.13 and Figure 4.14).

The creation and relaxation of surface wrinkles underpinning this electro-mechano-optical performance was studied with a microscopic investigation, described next.

4.3.3 Microscopic investigations on the reversible surface wrinkling

Atomic force microscopy (AFM) and scanning electron microscopy (SEM) were used to investigate the reversible formation of surface wrinkles within the PEDOT:PSS thin films at different area strains. The strain values were selected as representatives of those experienced by the PEDOT:PSS-coated region in the three devices, either mechanically or electrically. To this end, the acrylic elastomer membrane was first biaxially pre-stretched up to 4 times its initial diameter and then coated with a thin circular layer of PEDOT:PSS. From this condition, the membrane was partially relaxed by reducing the stretch, such that the PEDOT:PSS circle was subject to area strains of -10%, -19% and -28%. Subsequently, the strains were reversed back to -19%, -10% and 0%, by progressively stretching the membrane again, so as to investigate the reversibility of the surface wrinkling. The results are presented in Figure 4.15.

As revealed by both the AFM and SEM images, the initial smooth surface of the as-created PEDOT:PSS film (Figure 4.15a) showed progressively increased wrinkling as the area progressively contracted (Figure 4.15b-d). In particular, the wrinkles increased in number (surface density) and height, with peak values ranging from about 0.3 μm at a -10% strain to about 1.5 μm at a -28% strain (Figure 4.15). These morphological surface changes were fully reversible, as shown by the images taken at strains that were progressively reverted back to 0% (Figure 4.15e-g).

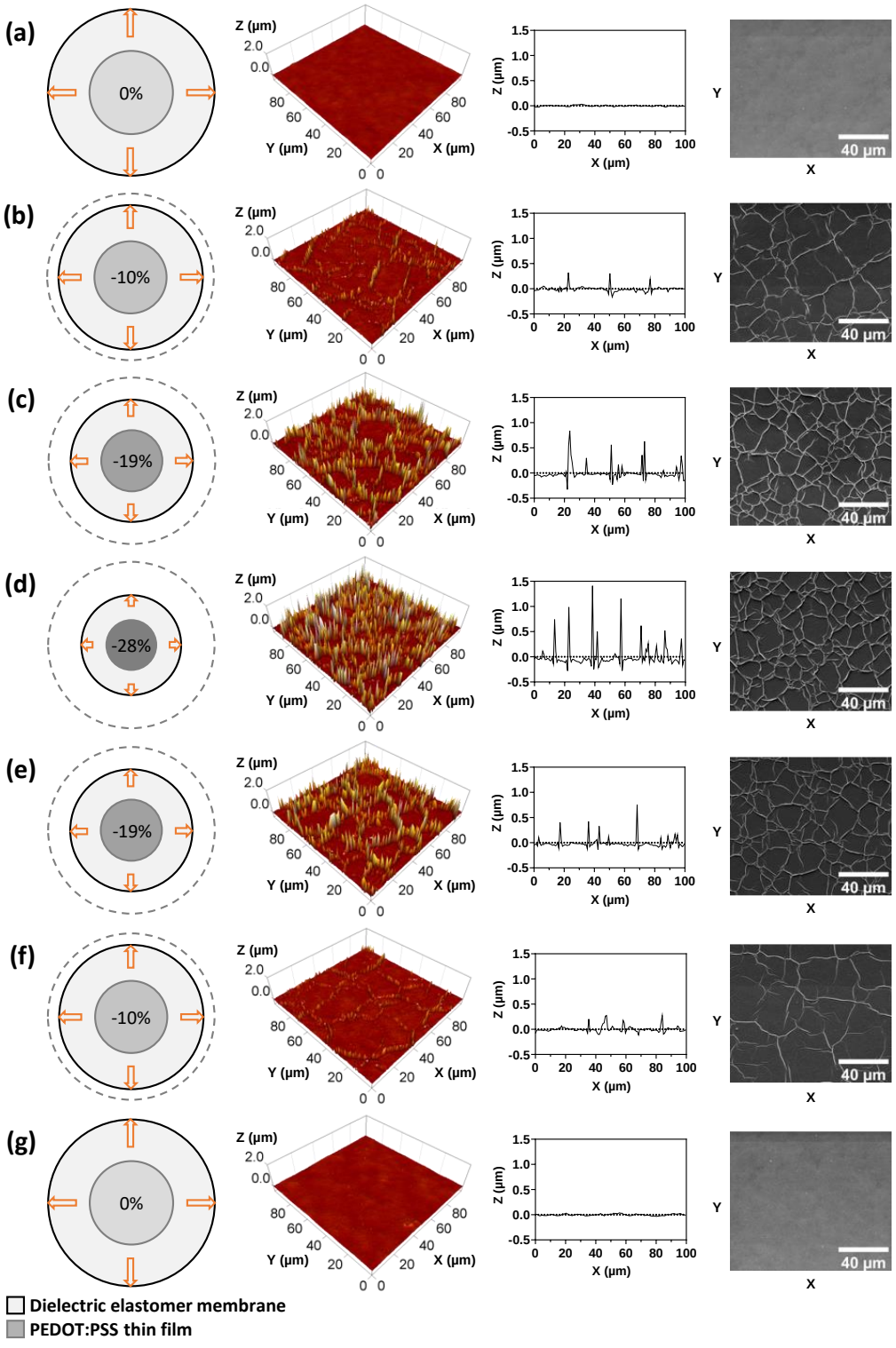

Figure 4.15 Investigation on the reversible surface wrinkling of the PEDOT:PSS thin film covering the elastomer membrane, as a result of different imposed strains. AFM plots (second and third columns) and SEM images (fourth column) of the surface are shown at an area strain of (a) 0%, (b) -10%, (c) -19% and (d) -28%, resulting from a progressive reduction of the membrane stretch, and then at an area strain of (e) -19%, (f) -10% and (g) 0%, resulting from a re-increase of the membrane stretch.

Therefore, as the electrical actuation of the membranes induced strains analogous to those used in these tests, these results provide evidence that the electrical tuning of the membrane transparency occurs via a surface wrinkling that shows up with topological patterns that can be controlled in a continuous and reversible manner.

4.3.4 Performance comparisons

In order to compare how the three driving modes affect the electro-optical performance, Figure 4.16a reports for the three cases the tuning ranges of the far-field transmittance and the Haze value (both at 550 nm), for electric fields up to 74 V/µm.

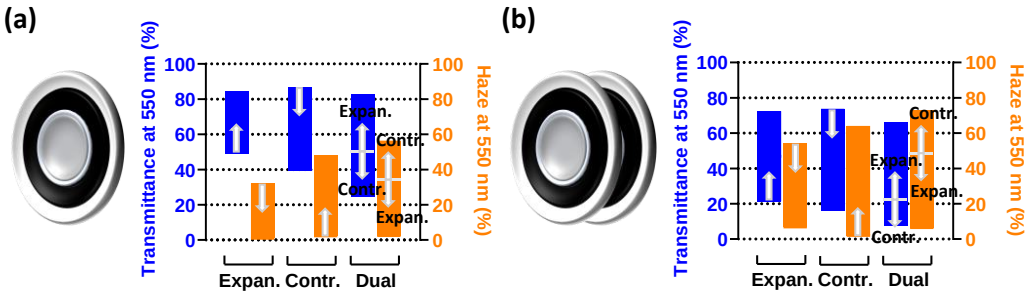

Figure 4.16 Tuning ranges of the far-field transmittance and Haze value at 550 nm for the three operating modes. Data are presented for (a) a single device and (b) two coaxially aligned devices. The arrows indicate the directions of variation for increasing electric fields, up to 74 V/µm.

Compared to the expansion-mode configuration, the contraction-mode one offered a wider tuning range, both for the transmittance and the Haze value. With respect to the contraction-mode device, the dual-mode configuration was capable of a broader range, both for the transmittance and the Haze (Figure 4.16a), although its main advantage clearly is the possibility to reach both higher and lower transparencies from the rest condition.

In order to increase the portion of scattered light and so increase the tuning range, the same investigations presented above were repeated on another set of three systems, each consisting of two coaxially-aligned, 3 mm-spaced devices, operating in parallel according to one of the three modes described above. Therefore, light was forced to pass through total four layers of wrinkled PEDOT:PSS films. The optical spectra of these systems are presented in Figure 4.17, Figure 4.18 and Figure 4.19.

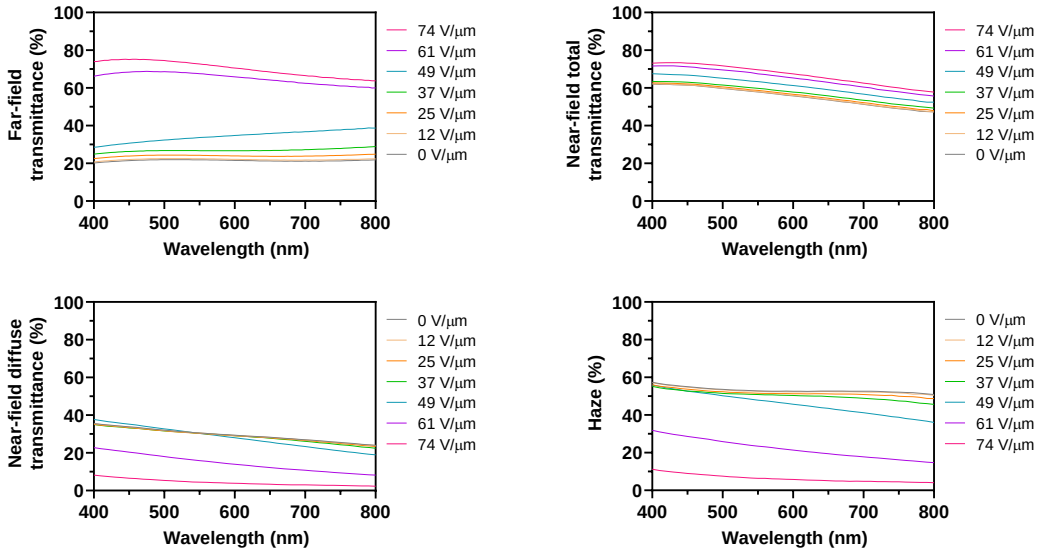

Figure 4.17 Visible-range spectra of the far-field transmittance, near-field total transmittance, near-field diffuse transmittance and Haze value of two coaxially-aligned tuneable optical transparency devices both working in an expansion mode.

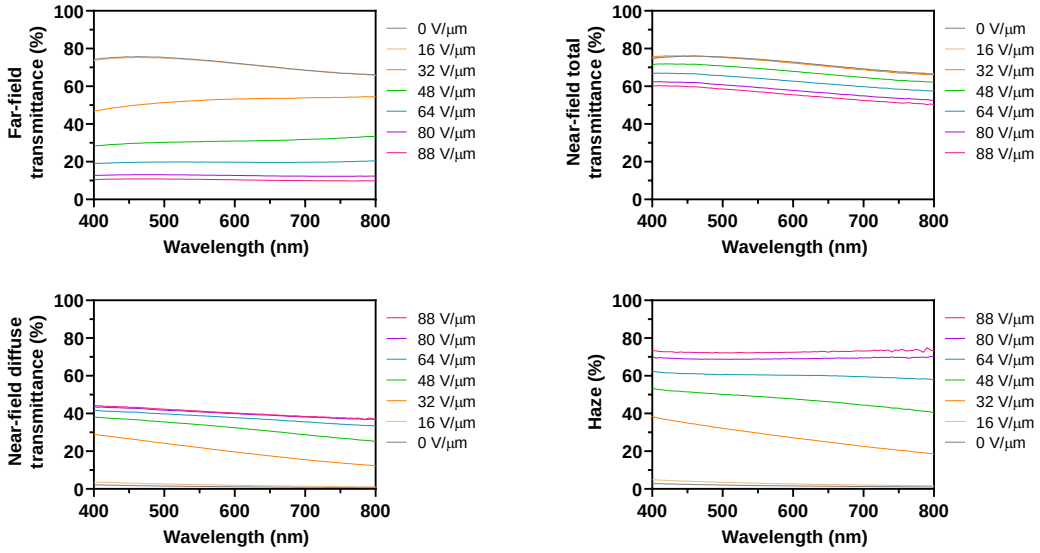

Figure 4.18 Visible-range spectra of the far-field transmittance, near-field total transmittance, near-field diffuse transmittance and Haze value of two coaxially-aligned tuneable optical transparency devices both working in a contraction mode.

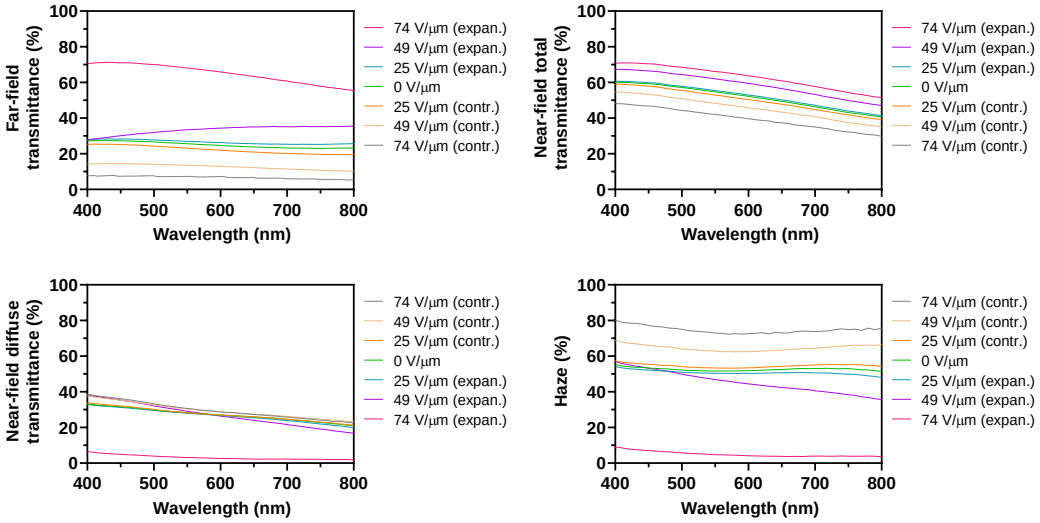

Figure 4.19 Visible-range spectra of the far-field transmittance, near-field total transmittance, near-field diffuse transmittance and Haze value of two coaxially-aligned tuneable optical transparency devices both working in a dual expansion-contraction mode.

The corresponding electro-optical transduction performance achieved of these systems is given in Figure 4.20, Figure 4.21 and Figure 4.22. For each configuration, the electrically-induced variations of the transmittances (near-field total, near-field diffuse and far-field) at 550 nm and the Haze number at different wavelengths are shown. Each data point represents the average value from three sample devices. Error bars corresponding to the standard deviation are included, although most of them are too small to be seen within the 0-100% range of the graph. The photographs visualise the change in transparency due to the specified electric fields, which caused the reported area strains of the PEDOT:PSS windows: the first photo set shows the device covering text 3 cm away, whereas the second set shows flowers approximately 100 cm away from a device attached to the camera lens. The resulting tuning ranges of these systems are summarised in Figure 4.16b.

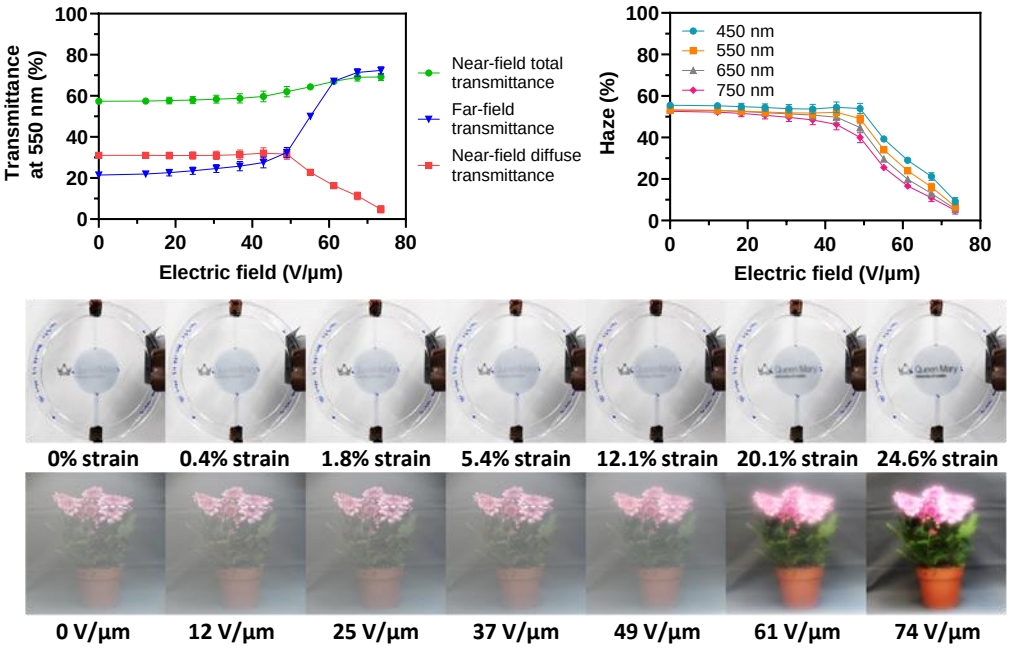

Figure 4.20 Electro-optical transduction performance of two coaxially-aligned soft membrane-based devices both working in an expansion mode.

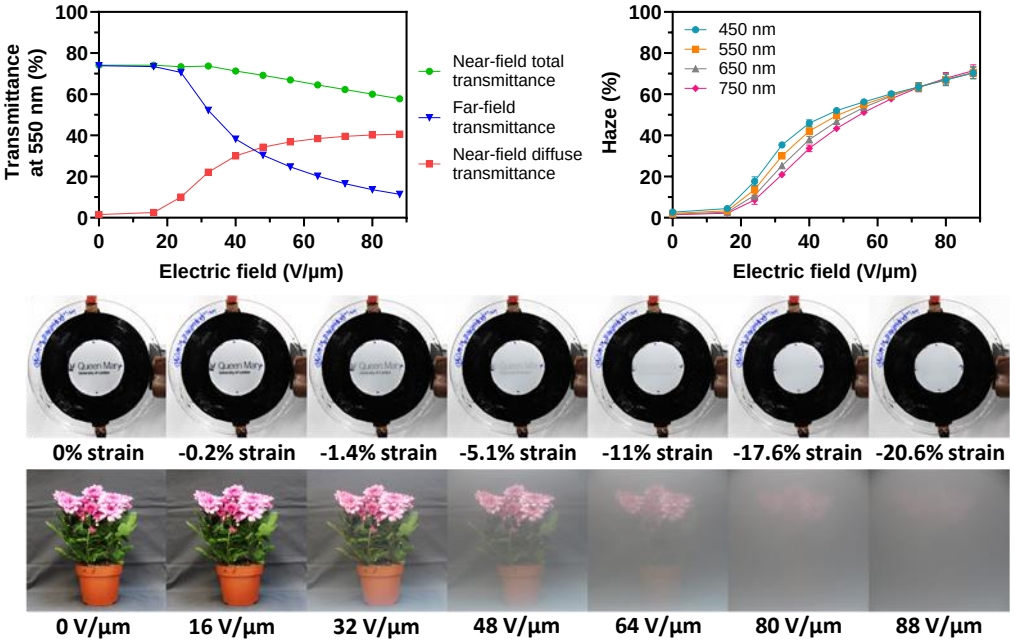

Figure 4.21 Electro-optical transduction performance of two coaxially-aligned soft membrane-based devices both working in a contraction mode.

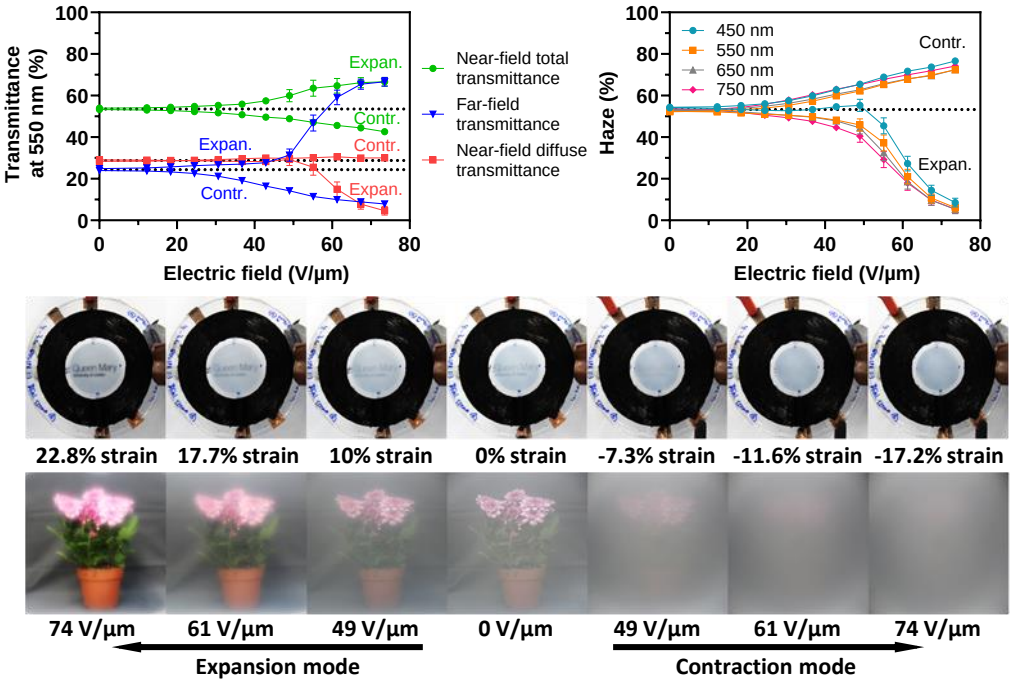

Figure 4.22 Electro-optical transduction performance of two coaxially-aligned soft membrane-based devices both working in a dual expansion-contraction mode.

It is evident that, for each driving mode, the double-membrane system outperformed the single-membrane one in terms of tuning range amplitude (Figure 4.16). However, the doubled number of wrinkled PEDOT:PSS layers reduced the maximum transmittance that can be achieved among the three devices, from more than 85% to about 75% (Figure 4.16). Therefore, doubling the number of membranes/aligned devices is a useful strategy to increase the tuning range, although at the cost of a reduced maximum transparency.

4.4 Conclusions

Three ways to electrically tune the optical transparency of soft elastomeric membranes, using dielectric elastomer actuation, were developed in this investigation and compared. The driving strategies were based on different methods to electrically modulate the surface topography of a transparent PEDOT:PSS thin film covering the membrane surface.

The configurations operating in expansion or contraction modes were used to electrically increase or decrease the light transmittance, whilst the dual-mode configuration enabled a modulation of transparency to both higher and lower values, with the broadest tuning range of far-field transmittance (25%-83%). Within the monitored time span of 8 weeks, all the implemented devices exhibited stable electro-mechano-optical performance.

Coaxially aligning two of such devices served to broaden the transmittance tuning range (7%-66%), although at the cost of reducing the maximum transmittance value.

As the wrinkles are randomly formed on soft elastomer membranes, this may lead to the non-uniform light scattering for each single device. Even within the same membrane, the light scattering could be slightly different in various measured regions. However, the experimental results showed that the impact of non-uniformity of wrinkles on optical response was very limited, with low deviations of optical transmittances (less than 5%) measured for several tested samples.

As an example of application, the various configurations described in this chapter to electrically tune the transparency of elastomeric membranes could be useful for tuneable ‘windows’. They are here generically defined as any interface that separates distinct environments and is able to transmit light. So, they are not necessarily limited to conventional windows used in buildings and vehicles. Depending on the specific type of system/application of interest, and, so, the specific functionality required, a device configuration could be more advantageous than others. For instance, for a window of a building, the need is usually not to enable both increases and decreases of the transparency, but, rather, just to reduce it (for example on a bright sunny day) from a high value at rest. So, in this case, the contraction-mode device would be more useful. Differently, there might be other systems/applications, such as windows acting as light filters in optical machines, where the need for commuting both to lower or higher transparencies could justify the use of the dual-mode device, even at the cost of requiring a constant voltage to achieve the maximum-transparency state.

Therefore, as for any other technology, the selection of a configuration for a given application should weight the pros and cons according to the functional needs. For that selection, moreover, the energy consumption requirements should be considered as well. With regard to this, it is worth stressing that driving any of the proposed configurations with a constant voltage would consume very limited current (just leakage current) and so, very limited power, due to the capacitive nature of the load (as for any DEA). This property, combined with the characteristic thin structure, low specific weight and

acoustically silent operation, makes this technology attractive to electrically control the transparency of soft membranes.

Chapter 5 Directionally-controlled light diffusion using dielectric elastomer actuation

5.1 Introduction

In the previous chapter a smart DEA device that was capable of tuning optical transmittance with the control of a voltage was demonstrated. In the previous section we demonstrated a state-of-the-art approach whereby the DEA-driven devices electrically control the optical transmittance based on two different working principles. In a first approach, DE membranes with wrinkled stretchable transparent electrodes initially show translucent, and the transparency can then be increased via the voltage-induced expansion of the structures, flattening the wrinkled electrodes. The second approach uses transparent electrodes covering DE membranes that are fixed to rigid glass substrates, and by applying very high electric fields the transparency can then be reduced due to the cratering-type surface electromechanical instabilities of the electrodes. To broaden the transmittance tuning range novel dual systems that exploit both modes or configurations whereby multiple devices in parallel have also been demonstrated.

DE membranes are usually processed with pre-stretch prior to the application of electrode materials in order to achieve an increase in the electromechanical transduction performance (Brochu & Pei, 2010; Koh et al., 2011; R. Pelrine, Kornbluh, Pei, et al., 2000). Several DEA-based devices developed from the above described approaches have applied the equi-biaxial pre-stretch,

although some others (adopting the second approach) have been built without any pre-stretch. As a result, the uniform deformation of actuation in all directions upon electrical activation have led to those devices to only produce the isotropic changes in optical transparency over the entire DE membrane surface.

Therefore, a new concept is to be proposed here with the aim of achieving directionally-controlled light diffusion based on dielectric elastomer actuation. This would mean that you can not only electrically adjust the amount of light transmitted in a designated direction but also achieve the electrical tuning of optical transparency with a comparatively broad range. The directional control of optical transmittance is gained by uniaxially pre-stretching a DE membrane and coating both of its surfaces with a deformable transparent polymer thin film (as a medium with strain-dependent scattering of the transmitted light) separated by two rectangular non-transparent stretchable conductors along the membrane's pre-stretched direction. Two such structures are aligned orthogonally with respect to each other to form the whole device, leading to the multi-directionally controlled light diffusion. This chapter describes how the light passing through the membranes can be diffused either transversely or longitudinally, depending on whether the electrical activation is used to actuate the single structure either at the back or at the front. This is potentially useful as a directional light beam spreader for optical light shaping. The device can be used in front of a light source to electrically spread the light in any desired direction, particularly in green-screen studios to avoid unwanted defined shadows. In addition to this, when both the back and front structures are simultaneously actuated, the device can diffuse the light in both directions,

causing the clear membranes to become completely opaque. Such DEA-based device can also be attractive to electrically control the surface transparency of soft membranes.

5.2 Experimental

5.2.1 Materials

All the tests were carried out using clear and adhesive acrylic-based dielectric elastomer membranes (VHB 4905, 3M, USA) with a thickness of 500 µm at electrical rest. Deformable transparent thin films on the dielectric elastomer membranes were obtained by spray coating a PEDOT:PSS compound, consisting of a 17.2 wt% aqueous PEDOT:PSS solution (Clevios PH 1000, Heraeus, Germany), 0.86 wt% dimethyl sulfoxide (DMSO, Sigma-Aldrich, UK), 6.9 wt% fluorosurfactant (Capstone FS-30, Apollo Scientific, UK) and 75 wt% isopropanol (2-Propanol, Sigma-Aldrich, UK). The compound solution was mixed using a vortex mixer (SA8, Stuart Equipment, UK) with a speed of 2000 rpm for 1 minute at room temperature. Non-transparent stretchable conductors that are regularly used for DEAs were conductive carbon grease (Carbon Conductive Grease 846, M.G. Chemicals, Canada).

5.2.2 Fabrication of tuneable directional light diffusers

The single directional light diffuser was fabricated as shown in Figure 5.1a. A VHB elastomer membrane (60 x 15 mm) was first uniaxially pre-stretched by

4 times, and then fixed to a support frame (60 x 60 mm), taking advantage of its adhesive properties. The pre-stretch reduced the membrane thickness from 500 µm to 125 µm (calculated value). A volume of 32 µL of the PEDOT:PSS compound solution was used to spray on both sides of the pre-stretched membrane a thin layer (30 x 30 mm, estimated thickness lower than 100 nm after solvent evaporation) at the centre, to be used as a deformable transparent thin film. Conductive carbon grease (13 x 60 mm) was smeared along the uniaxially pre-stretched direction on the two rectangular outer regions for each side of the membrane, so the deformable transparent thin film was situated in between the non-transparent stretchable electrodes. The central transparent coating was separated from the outer non-transparent conductors by a gap of 2 mm (Figure 5.1a). Such fabricated structure was then oven dried for 30 min at 80°C. A copper tape was used to connect each electrode to the high voltage source.

The proposed electrically-induced tuneable multi-directional light diffusing device was also then fabricated by attaching two of these simpler single direction light diffusers orthogonally to each other, which is described in more detail later.

In order to drive the devices, a compact DC-DC high voltage converter (Q50, EMCO High Voltage Corporation, USA) was used to produce voltages up to 4 kV, which were monitored with a high-voltage probe. Each voltage value was divided by the elastomer membrane's thickness at electrical rest (125 µm) to calculate the applied (nominal) electric field.

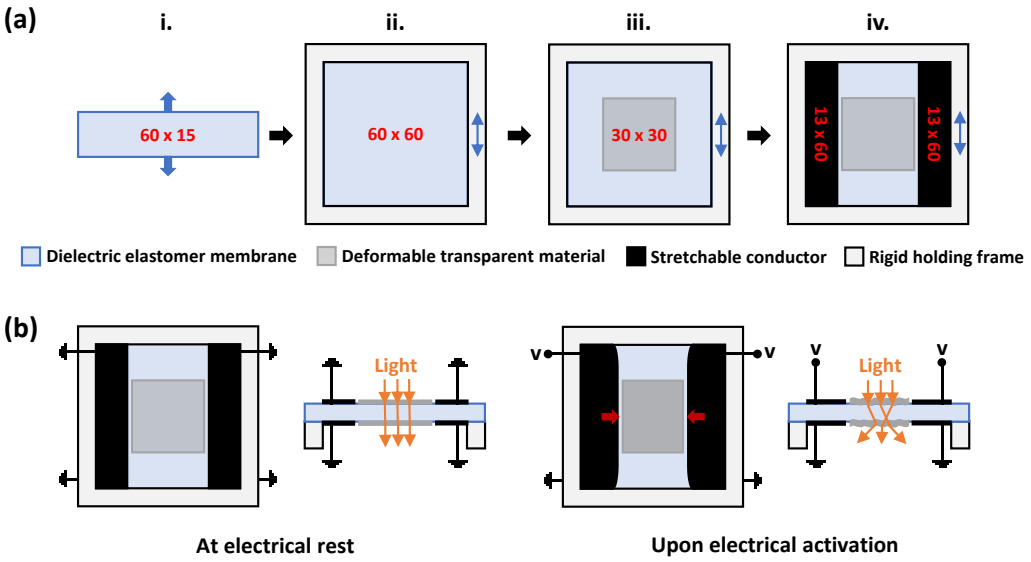

Figure 5.1 Concept for a DEA-based electrical tuning of the directional light scattering from a soft membrane. (a) Fabrication of a single directional light diffuser. Numbers in red colour indicate the dimensions of the structure in mm. (b) Working principle of the single directional light diffuser with the top and cross-sectional views.

5.2.3 Characterisation

The optical transparency of all the tuneable diffusers were characterised in the 400-800 nm visible range using a Perkin Elmer Lambda 950 UV-vis spectrometer with a 10 cm-wide integrating sphere.

The actuation axial strains exerted on the central transparent coatings were estimated by measuring the distance between the inner edges of two rectangular carbon grease electrodes. Such values at different driving voltages were calculated by processing images taken with the software Image J.

The formation of surface wrinkles that were mechanically induced within the PEDOT:PSS thin films at different axial strains, which is described in more

detail later, was investigated using an atomic force microscope – AFM (NanoWizard 4 BioAFM, JPK Instruments AG, Germany) and a scanning electron microscope – SEM (Inspect F50, FEI, USA). The AFM images were taken with a cantilever probe (NSG01, NT-MDT, Russia) having a resonant frequency of around 150 kHz and a spring constant of 3.5 N m^{-1}. The SEM images were taken at an acceleration voltage of 2 kV.

5.3 Results and discussion

5.3.1 Electrically-induced tuneable light diffusion in one direction

The concept of electrically tuneable multi-directional light diffusion within a device originates from the combination of two single tuneable directional light diffusers orthogonally aligned with respect to each other. The fabrication and operation of a single tuneable directional diffuser are shown in Figure 5.1a. The elastomeric membrane is first uniaxially pre-stretched and is clamped to a rigid rectangular holding frame. A square shape of transparent deformable material is then coated on both sides of the membrane in its central area. After that, a non-transparent conductive stretchable material is applied to both sides of the membrane, parallel to the direction in which the membrane is pre-stretched, to create two rectangular conductors that are constrained by the frame and separated from the central transparent coating. The two non-transparent conductors work as the stretchable electrodes of two rectangular DEAs, whilst the central transparent coating (which can be non-conductive) acts as a deformable medium with strain-dependent scattering of the transmitted light. When the single diffuser is at electrical rest, the central

transparent coating allows light to pass through the elastomer membrane. Because the uniaxial pre-stretch induces a high strain in the stretched direction and nearly no strain in the direction 90 degree from the stretched direction, the elastomer membrane thus tends to be stiffened in the high pre-strained direction, causing the membrane to actuate primarily in the softer and non-pre-strained direction (R. Pelrine, Kornbluh, Pei, et al., 2000). Therefore, when a voltage is applied across the two rectangular electrodes, the DEAs will effectively expand orthogonally to the pre-stretched direction and both electrodes will deform toward the centre (as they are constrained at their outer edge by a rigid frame), causing the central area of the membrane to undergo an axial contraction in the non-pre-strained direction, illustrated in Figure 5.1b. Note that the change of membrane thickness resulting from the actuation is not shown for simplicity. If the stiffness of the central coating of deformable transparent material is higher than that of the elastomer, the resulting effect generates wrinkles aligned along the pre-stretched direction (Z. H. Chen et al., 2019), which scatters the light perpendicular to the pre-stretched direction and so reduces the transparency of the membrane.

The tested dielectric elastomer membranes in this work were based on a commercially available acrylic elastomer film (VHB tape series, by 3M), as detailed in Section 5.2.1. This elastomer is extensively selected as a test material within the DEA field, because it has a high electromechanical transduction performance in quasi-static conditions and a simplification of manufacturing processes resulting from its adhesive properties (Brochu & Pei, 2010; Carpi et al., 2010, 2008; R. E. Pelrine et al., 1998; R. Pelrine, Kornbluh, Pei, et al., 2000). The deformable transparent thin layers used as the central

coating is another challenging aspect for the light diffusers. In the experiments, the PEDOT:PSS compound (as described in Section 5.2.1) was chosen because PEDOT:PSS can offer high transparency and is widely used for transparent electrodes in flexible organic electronic devices (Lipomi et al., 2012). With the doping of dimethyl sulfoxide (DMSO) and zonyl fluorosurfactant solutions, the produced PEDOT:PSS thin films were shown to also be highly stretchable, transparent and conductive (Lipomi et al., 2012; Liu et al., 2012; Vosgueritchian et al., 2012). Also, PEDOT:PSS normally has a high refractive index, which allows its wrinkled surfaces to effectively scatter light, offering a broad tuning range of optical transmittance. Thus, in this work the uniaxially pre-stretched membrane was spray coated with a thin layer of PEDOT:PSS to create the central deformable transparent conducting area. In fact, such coating area is primarily designed to act as a deformable medium with strain-dependent scattering of the transmitted light rather than an electrode. Therefore, any applicable non-conductive deformable transparent material can also be chosen to assemble the proposed light diffusing devices.

5.3.2 Electro-mechano-optical transduction performance of single directional light diffuser

The electrically-induced changes in the optical transmittance of elastomer membranes were quantified in the 400-800 nm visible range using both the near-field and far-field measurements, where the sample-to-detector distances in the test instrument were set to 5 cm and 40 cm, respectively (see Figure 4.5 in Chapter 4). In the near-field measurement, both the total

transmittance T_t and the diffuse transmittance T_d were detected. These were used to calculate the behaviour as in Chapter 4. Therefore, the total transmittance was calculated as the percentage of incident light transmitted as a whole, including both diffused transmitted and specular transmitted components, both the light that is scattered and not scattered. The diffuse transmittance was given by the percentage of incident light transmitted as diffused light, which is only the scattered light. The ratio between the near-field diffuse and near-field total transmittance was used to determine the transmission Haze $H = T_d/T_t$. Therefore, the Haze value, which expressed as the proportion of diffused light in total transmitted light, was used to indicate the cloudy appearance of the sample (Campo, 2008). In the far-field measurement, because the sample-to-detector distance was sufficiently long, the diffused transmitted component was lost by the measuring instrument and only the specular transmitted component was able to be detected, as illustrated in Figure 4.5 in Chapter 4. Thus, the measured data were used to define the far-field transmittance T_f, representing the percentage of incident light transmitted as specular component, which is not scattered. Theoretically, the near-field total transmittance (diffused and specular transmitted components) should be the sum of the near-field diffuse transmittance (diffused transmitted component) and the far-field transmittance (specular transmitted component), which gives $T_t = T_d + T_f$. In general, the far-field transmittance provides a quantification of the transparency that an observer can perceive while looking through the device window, perpendicularly to it, from a certain distance, whereas the near-field total transmittance is more

suited to indicate the visibility when an object is just situated behind the device window without any distance.

For comparison, the uniaxially pre-stretched acrylic elastomer membranes (without any coating) were measured and showed the near-field total and far-field transmittances were both about 92% at a wavelength of 550 nm, and the Haze value of about 0.5% at 550 nm. The optical spectra of a single tuneable directional light diffuser are presented in Figure 5.2, whereas its corresponding electro-optical transduction performance achieved is given in Figure 5.3. At electrical rest the diffuser had a very high level of near-field total and far-field transmittances around 86% due to the transparency of PEDOT:PSS thin film. As the increase of applied electric fields to the maximum value of 32 V μm^{-1} (the highest available for the fabricated devices), the far-field transmittance continuously reduced to around 20%, owing to a wrinkling of the surface resulting in the extensive scattering of transmitted light, although the near-field total transmittance remained almost unchanged, presumably due to no further light reflection and absorption occurred during the surface wrinkling. Also, the near-field diffuse transmittance gradually increased because of the electrically-induced wrinkling produced the light diffusion. Such spectral data experimentally confirmed that the near-field total transmittance corresponded accurately (to within a ±5% error) to the sum of the near-field diffuse and the far-field transmittances in all the cases. The electrical tuneability of the transparency can be observed from the photos in Figure 5.3 that the membrane surface was clear enough to show the text behind it at electrical rest, whilst the cloudy appearance as a result of the electrically variable scattering of light, which is quantified by the Haze-field plot, progressively

caused the text to become blurry rather than invisible, as a consequence of the anisotropic light diffusion.

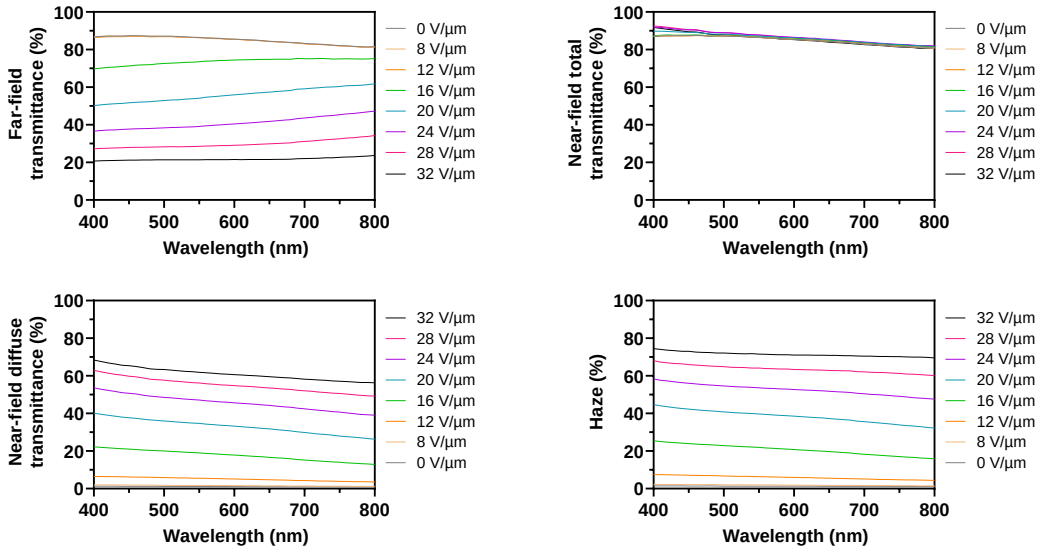

Figure 5.2 Visible-range spectra of the far-field transmittance, near-field total transmittance, near-field diffuse transmittance and Haze value of the soft membrane-based single tuneable directional light diffuser.

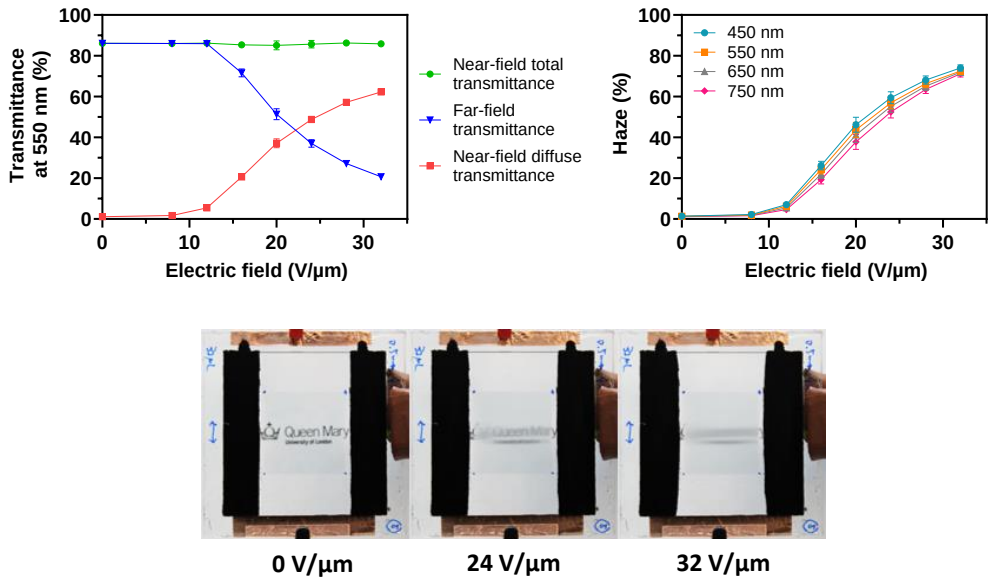

Figure 5.3 Electro-optical transduction performance of the single tuneable directional light diffuser. The text logo is located 30 mm behind the elastomer membrane.

The electro-mechanical transduction performance of the tuneable unidirectional light diffuser was investigated by the actuation strains perpendicular to the membrane's pre-stretched direction. The corresponding axial strains exerted on the central transparent coating at various electric fields were measured based on the distances between the edges of two deformable rectangular DEAs. Due to the frame constraint, the deformation of actuation was non-uniform along the edges, with the maximum value at the middle of each rectangular DEA (photos in Figure 5.3), which was thus selected to calculate the so-called axial strains in the central region. With the increase of applied electric fields on the two DEAs simultaneously, the generated electrostatic forces caused the rectangular non-transparent areas to both gradually expand towards the centre of the elastomer membrane. This increasingly created the compressive strains (shown as the negative values in

the strain-field plot in Figure 5.4) on the central transparent coatings to form surface wrinkles due to the dissimilar moduli between the elastomer membrane and the PEDOT:PSS coatings.

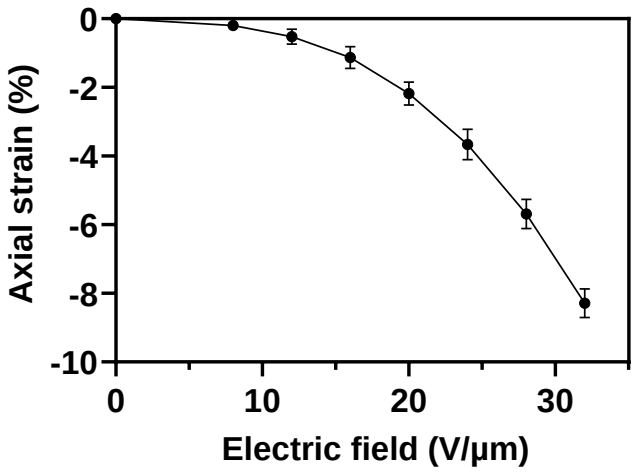

Figure 5.4 The effect of the applied electric field on the axial strain that was exerted on the central PEDOT:PSS-coated region for the single tuneable directional light diffuser.

5.3.3 Microscopic investigation of the surface wrinkling

Microscopic characterisation of the formation of surface wrinkles within the PEDOT:PSS thin films at various axial strains were performed using atomic force microscopy (AFM) and scanning electron microscopy (SEM). The strain values were selected as representative of those experienced by the PEDOT:PSS-coated central area in the tuneable directional light diffuser under electrical activation. To this end, the acrylic elastomer membrane was first uniaxially pre-stretched by 4 times and fixed to a rigid holding frame, and then coated with a thin layer of PEDOT:PSS at the centre, whose

concentration and thickness remained the same as that used to fabricate the tuneable diffuser. From this condition, the membrane was progressively contracted in the direction 90 degree from the direction of pre-stretch by mechanically pulling two small acrylic bars, which were attached to the elastomer membrane and placed next to the two sides of the coated central layer, towards each other, such that the deformable PEDOT:PSS film was subject to the axial strains of -2.5%, -5%, -7.5% and -10%. In addition, the axial strain was reversed back to 0%, by completely releasing the contraction, so as to investigate the surface wrinkling reversibility. The results are presented in Figure 5.5.

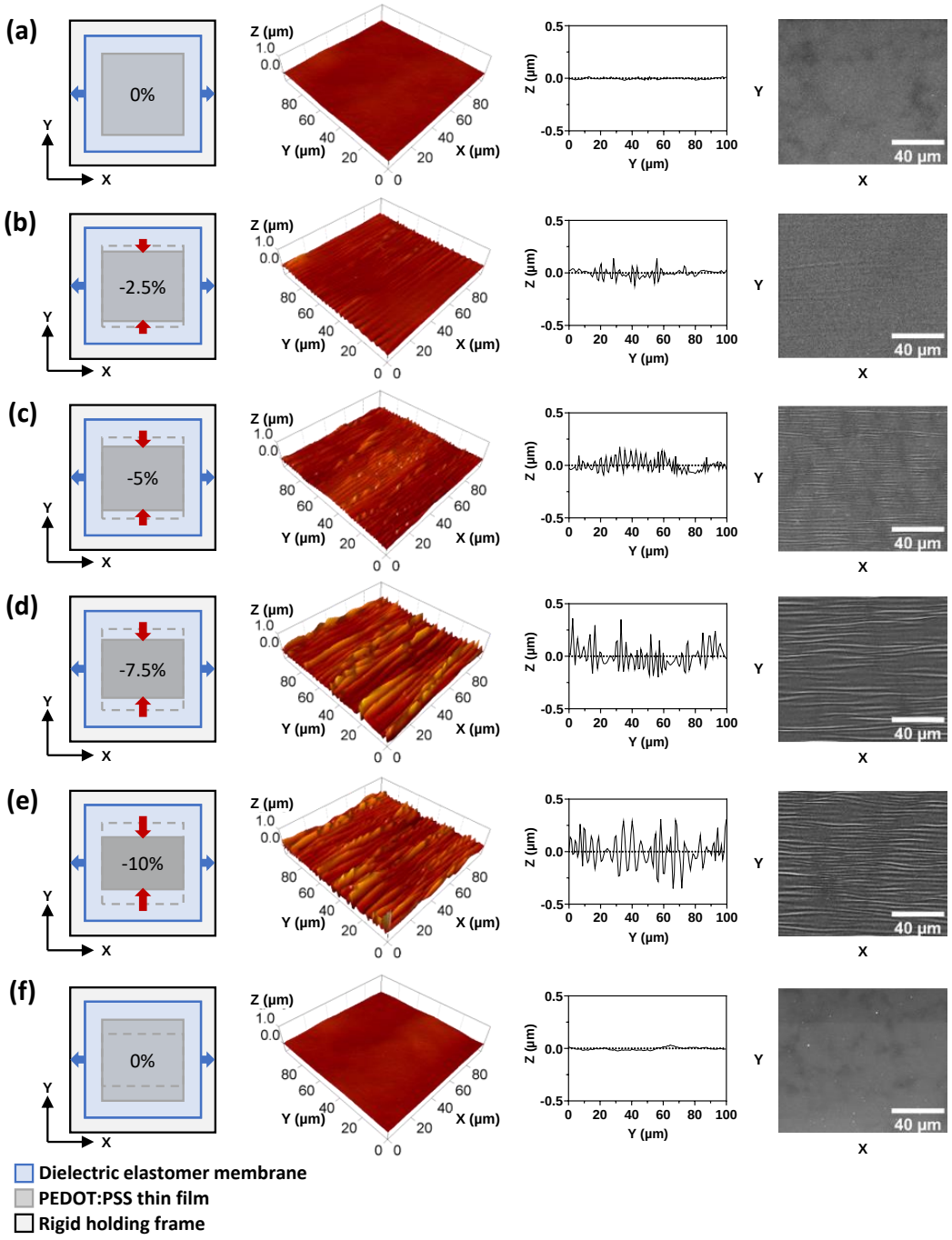

Figure 5.5 Microscopic investigation on the surface wrinkling of deformable PEDOT:PSS thin film covering the elastomer membrane uniaxially pre-stretched by 4 times in the X direction (blue arrows), as a result of different imposed compressive axial strains (red arrows) orthogonal to the pre-stretch of the membrane. AFM plots (second and third columns) and SEM images (fourth column) of the surface are shown at an axial strain of a) 0%, b) -2.5%, c) -5%, d) -7.5% and e) -10%, resulting from a progressive contraction of the membrane in the Y direction (red arrows), and then at an axial strain back to f) 0%, resulting from a complete release of the contraction in the Y direction.

The AFM and SEM images show that the surface of the coated PEDOT:PSS thin film was initially smooth (Figure 5.5a). As the film was progressively contracted the surface wrinkles progressively developed and aligned orthogonal to the direction of thin film contraction (Figure 5.5b-e). Also, the increase in the compressive axial strains gradually increased the number (surface density) and height (amplitude) of the formed wrinkles, with peak values ranging from about 0.1 μm at a -2.5% axial strain to about 0.4 μm at a -10% strain. In comparison with the previous work in Chapter 4 (in which the acrylic elastomer membrane was equi-biaxially pre-stretched and then equi-biaxially contracted to form randomly oriented wrinkles), under the same axial strains, the surface wrinkles created in this work (in which the membrane was uniaxially pre-stretched and then uniaxially contracted) were directionally aligned and showed a greater quantity of wrinkles over the same region, although the heights of those wrinkles was smaller. In addition, these morphological surface changes were fully reversible, as shown by the microscopy images taken at the axial strain that was reverted back to 0% (Figure 5.5f). Therefore, as the electrical actuation of the membranes induced strains analogous to those used in the microscopic analyses, these results demonstrate that the membrane transparency is electrically tuneable as a consequence of the changes in the topographic patterns of surface wrinkling that can be continuously and reversibly controlled.

5.3.4 Electrically-induced light diffusion in multiple direction

For the above described single directional light diffuser, the surface wrinkles were formed along the membrane's pre-stretched direction during electrical actuation, and the scattering of light occurred orthogonal to the wrinkles. As the result, the control of light diffusion was observed to take place in a single given direction, so the single diffuser blurred the image behind the elastomer membrane in that direction. It is envisioned that there are application scenarios where it would be of benefit to electrically tune the light to diffuse or spread in more than one direction without having to rotate the device. To address this need, an integration of two single directional light diffusers was conceived, leading to a tuneable multi-directional light diffusing device, without significantly impairing the surface transparency at electrical rest as a consequence of having increased the number of PEDOT:PSS film layers. As shown in Figure 5.6, such a device could be assembled by adopting the same procedure used for the fabrication of the single directional light diffuser (Figure 5.1) and aligning two such diffusers orthogonally with respect to each other. The use of carbon grease conductors made the surrounding region non-transparent and therefore the degree of light diffusion for the whole device was primarily controlled by the central coated transparent layers. The lower single directional diffuser had the elastomer membrane pre-stretched in the longitudinal direction, whereas the upper second directional diffuser had the membrane pre-stretched in the transverse direction. The distance between the bottom and top elastomer membrane was set at 3 mm. Such design could be used to electrically active each diffuser independently (Figure 5.6). When the lower diffuser was actuated, the coated PEDOT:PSS films on both sides of the

lower elastomer membrane contracted and formed wrinkles in the longitudinal direction, whilst when the upper diffuser was actuated, the coated films on both sides of the top elastomer membrane were contracted to create wrinkles in the transverse direction. Thus, the multi-directional control of light diffusion was achieved. Additionally, both directional diffusers at the bottom and the top could be electrically activated simultaneously. Under this situation, the surface wrinkling of the coated films on the bottom and top membranes diffused light in both longitudinal and transverse directions, which was able to prevent light passing through the device and thus rendering the image behind it completely invisible for the possible application of electrically tuning optical transparency.

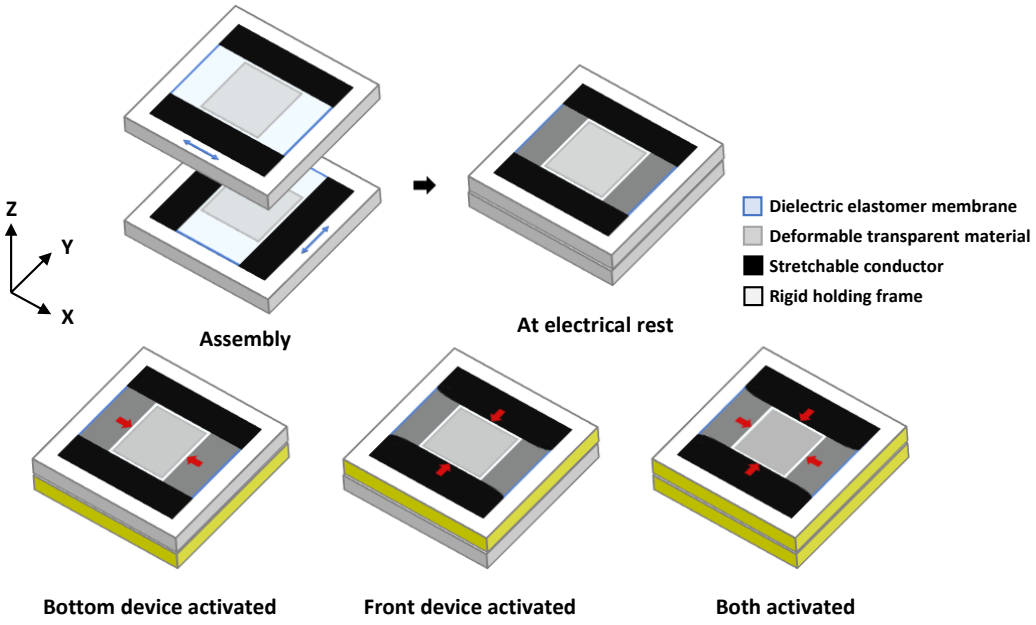

Figure 5.6 Assembly of tuneable multi-directional light diffusing device, based on two single direction light diffusers aligned orthogonally to each other, with three different working principles upon electrical actuation. Blue arrows indicate the pre-stretched direction of elastomer membranes. Red arrows represent the deformation of actuation for the rectangular DEAs.

5.3.5 Electro-optical transduction performance of multi-directional light diffusing device

The optical spectra of the tuneable multi-directional light diffusing device while electrically actuating the bottom diffuser, the top diffuser and the both together to adjust their optical transparency are shown in Figure 5.7, Figure 5.8 and Figure 5.9, respectively, where their corresponding electro-optical transduction performance achieved is given in Figure 5.10, Figure 5.11 and Figure 5.12. Since the proposed multi-directional light diffusing device consisted of two aligned single diffusers, light was therefore forced to pass through a total of four layers of PEDOT:PSS thin film with two elastomer membranes. However, the transparency was not significantly impaired at electrical rest and the objects behind the device window were still clear to be observed (as shown in Figure 5.10, Figure 5.11 and Figure 5.12), although the doubled number of PEDOT:PSS layers reduced the maximum transmittance at 550 nm from 86% to 75%.

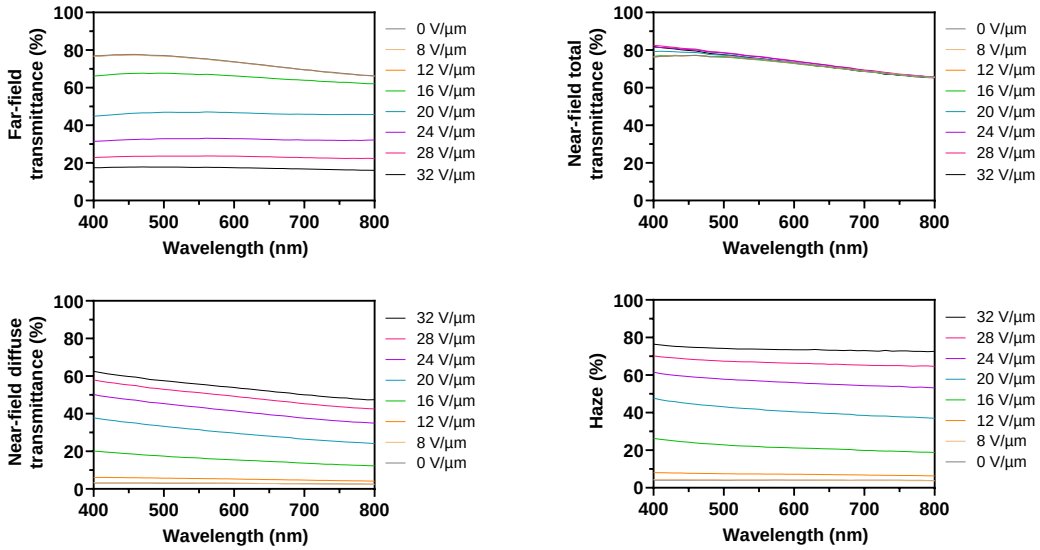

Figure 5.7 Visible-range spectra of the far-field transmittance, near-field total transmittance, near-field diffuse transmittance and Haze value of the soft membrane-based tuneable multi-directional light diffusing devices, upon electrical actuation of the diffuser at the back.

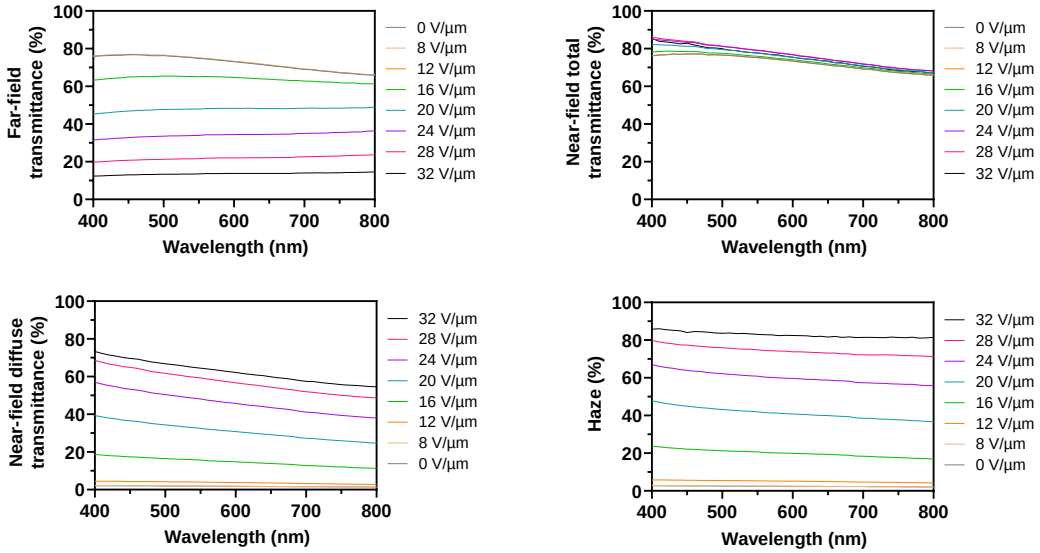

Figure 5.8 Visible-range spectra of the far-field transmittance, near-field total transmittance, near-field diffuse transmittance and Haze value of the soft membrane-based tuneable multi-directional light diffusing devices, upon electrical actuation of the diffuser at the front.

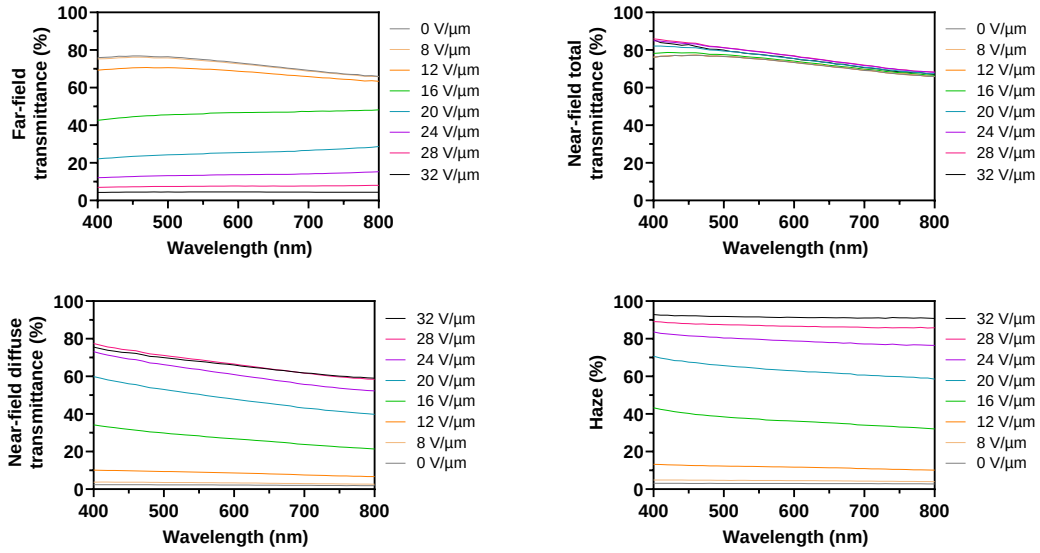

Figure 5.9 Visible-range spectra of the far-field transmittance, near-field total transmittance, near-field diffuse transmittance and Haze value of the soft membrane-based tuneable multi-directional light diffusing devices, upon electrical actuation of both the back and front diffusers.

In the situation of electric fields applied only to the lower diffuser, the central transparent coatings on the bottom elastomer membrane were contracted to form surface wrinkles in the longitudinal direction as previously described in the microscopic investigation section, causing the light to scatter in the transverse direction. Such an effect is observed in the second-row photos in Figure 5.10 showing that a point light was electrically spread horizontally. By further increasing the applied electric fields, the bottom membrane was further contracted to create more surface wrinkles, leading to the reduction of the light transmittance and an increase in the Haze value for the whole device, given by the transmittance-field and Haze-field plots in Figure 5.10. Interestingly, due to the unidirectional light scattering, the grid photos (first row in Figure 5.10) show that the vertical lines progressively disappeared while the horizontal lines remained visible. Apparently, the device with directional light diffusion is suited

to the application where the membrane can progressively make the objects behind the device window become blurry with increasing voltages rather than invisible (third-row photos in Figure 5.10), for instance, creating a blurring effect for photography. Additionally, the device is potentially useful to control the direction of light diffusion, which has an application for use as a directional light beam spreader, and under this circumstance, to spread the bright light in the transverse direction, avoiding the formation of defined shadows.

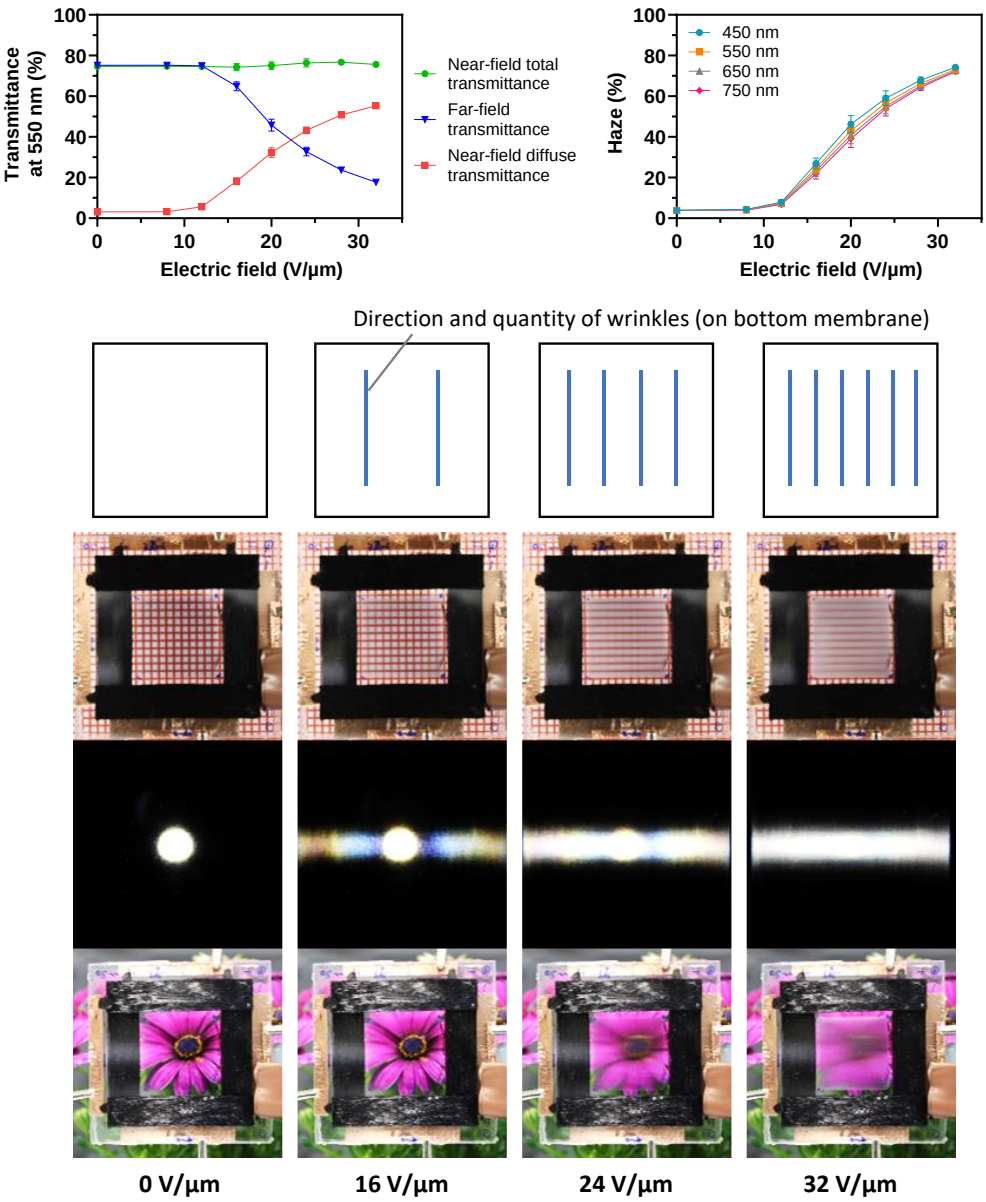

Figure 5.10 Electro-optical transduction performance of the multi-directional light diffusing device upon electrical actuation of the diffuser at the back. A schematic indicates voltage-induced wrinkles are aligned in the longitudinal direction on the bottom membrane while photos show light is thus diffused in the transverse direction. The grid (first-row photos), spotlight (second-row photos) and flower (third-row photos) are all located 30 mm behind the device.

By contrast, when the upper diffuser was electrically activated only, the central transparent coatings on the upper elastomer membrane contracted to form surface wrinkles in the transverse direction, leading to the scattering of light in the longitudinal direction (second-row photos in Figure 5.11). By increasing the electric fields, the light transmittance progressively reduced while the Haze value increased accordingly (Figure 5.11), owing to an increasing amount of surface wrinkles resulted from the contraction of the top membrane. In this situation, it was observed from the grid photos (first row in Figure 5.11) that the horizontal lines gradually disappeared whilst the vertical lines were still visible. As a result, such electrically-induced directional light scattering caused light to spread in the longitudinal direction without requiring the device to be rotated. This made the clear image become blurred longitudinally (second-row and third-row photos in Figure 5.11).

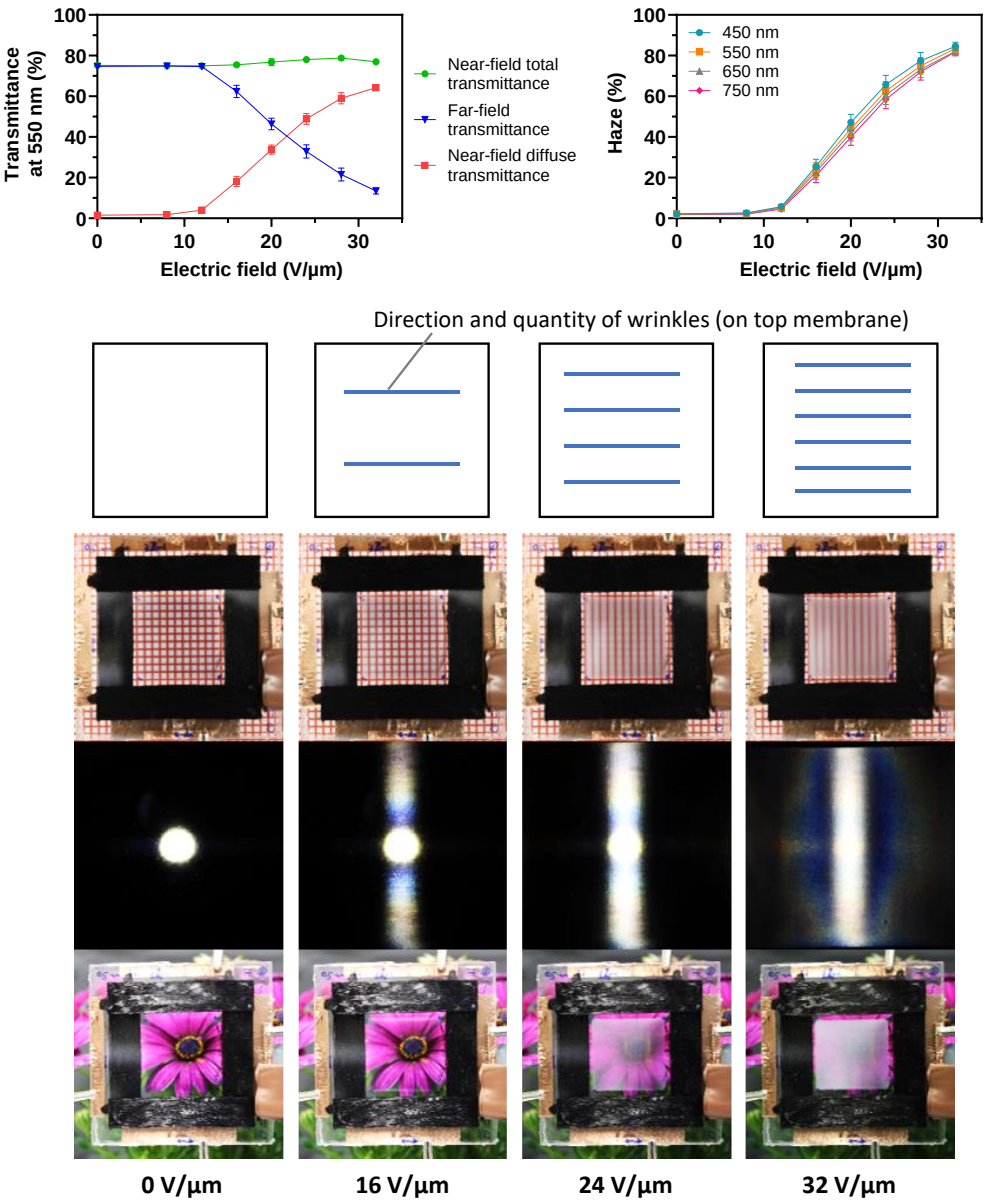

Figure 5.11 Electro-optical transduction performance of the multi-directional light diffusing device upon electrical actuation of the diffuser at the front. A schematic indicates voltage-induced wrinkles are aligned in the transverse direction on the top membrane while photos show light is thus diffused in the longitudinal direction. The grid (first-row photos), spotlight (second-row photos) and flower (third-row photos) are all located 30 mm behind the device.

While the main advantage of the tuneable multi-directional light diffusing device was clearly to control the light scattering in either transverse or longitudinal direction individually, it could be additionally used as a tuneable optical transparency window to continuously adjust the light transmittance if both the bottom and top diffusers were electrically activated simultaneously. This effect is shown in Figure 5.12, where the increase in the electrical fields was seen to increase the light scattering of the device under this condition. Consequently, both horizontal and vertical lines in the grid photos (first row in Figure 5.12) vanished progressively as the voltage is increased. The most impressive feature was that when a maximum electric field was applied this device could substantially reduce the optical transmittance, leading to the surface transparency tuned from clear to completely opaque, which can be seen from the photos and the Haze value over 90% at 32 V μm^{-1} (Figure 5.12). Such device created an extremely broad tuning range of optical transparency, causing the far-field transmittance at 550 nm to electrically reduce from 75% to 4%.

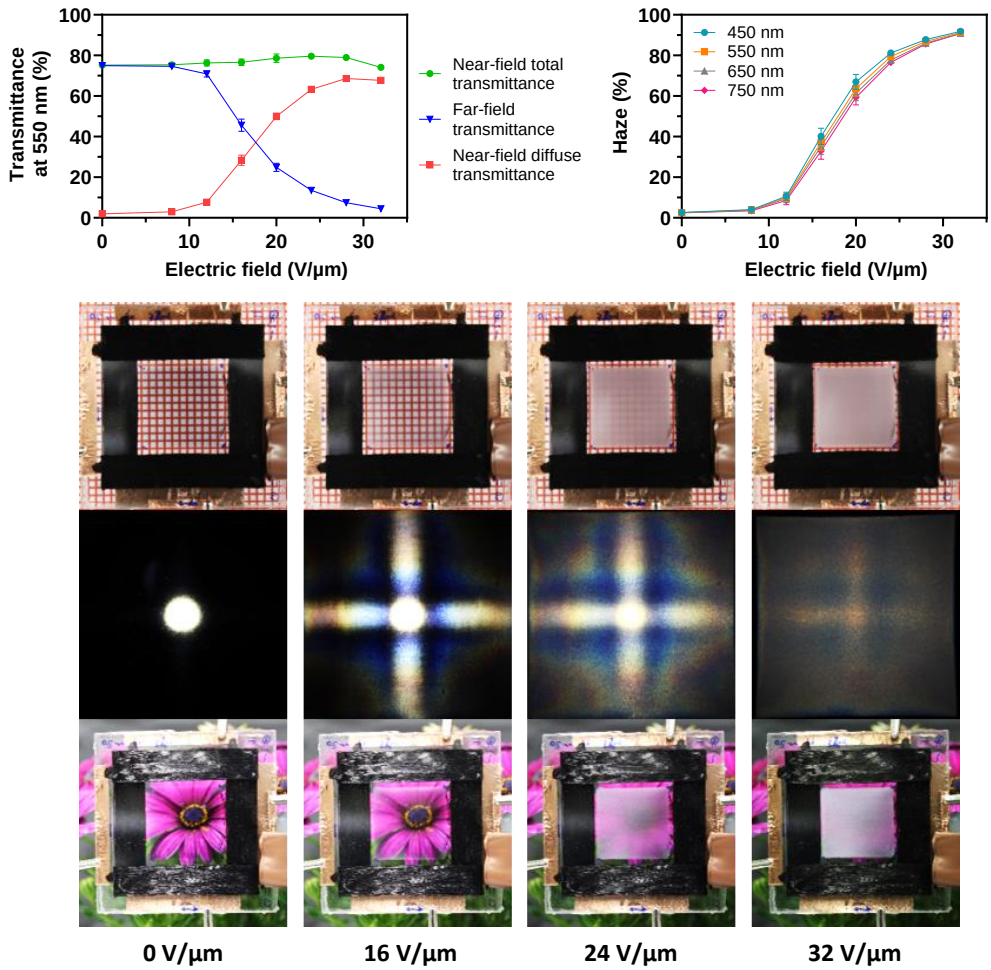

Figure 5.12 Electro-optical transduction performance of the multi-directional light diffusing device upon electrical actuation of both the back and front diffusers, showing the changes in surface transparency between clear and opaque. The grid (first-row photos), spotlight (second-row photos) and flower (third-row photos) are all located 30 mm behind the device.

5.4 Conclusions

The electrically controllable directional light diffusion on soft elastomeric membranes using the DEA technology has been developed. While the tuning of the optical transparency was achieved by the light scattering from the voltage-induced wrinkling of a deformable transparent PEDOT:PSS thin film covering the membrane surface, the anisotropic light diffusion was caused by

the controllable alignment of surface wrinkles that are formed by electrical actuation.

The single directional light diffuser was fabricated by uniaxially pre-stretching the dielectric elastomer membrane and coating on both sides of it with a deformable transparent polymer film at the centre separating two rectangular DEAs. The central transparent coatings were electrically contracted by the surrounding DEAs to form surface wrinkles aligned with the pre-stretched direction, leading to the electrical tuning of light scattering perpendicular to the wrinkles. A single direction diffuser device could therefore simply obtain voltage-induced changes in light diffusion in a single direction.

In order to achieve the controllable light diffusion in more than one direction without significantly impairing the surface transparency of the whole device at electrical rest, two single directional light diffusers were assembled together aligned orthogonally to each other. The resulting device was able to electrically tune the light scattering in either transverse or longitudinal direction individually, depending on whether the electrical activation concerned the lower or upper single directional diffuser. Additionally, the two diffusers could be actuated simultaneously to produce light scattering in both directions. Under this situation, a maximum applied electric field resulted in the extremely low degree of surface transparency, allowing a very broad tuning range of far-field transmittance between 4% and 75%.

Such type of device with the electrically-induced directional light diffusion could be not only potentially useful in spreading light in a desired direction but also attractive to control the surface transparency of soft membranes. Another

possible application could find in polarisers which filter a beam of light of undefined or mixed polarisation into a beam of well-defined polarisation.

Chapter 6 Conclusions and future work

6.1 Conclusions

Electroactive polymers that deform in response to electrical stimulation is currently at the forefront of developing electrically adaptive devices. Dielectric elastomer actuators (DEAs), which belong to the broader family of electromechanically active polymers, essentially are deformable capacitors consisting of a dielectric elastomer (DE) membrane coated on both sides with two compliant electrodes. By applying an electric field across the membrane, the structure can continuously and reversibly deform, showing surface expansion and thickness compression. In general, the adaptive devices designed using the DEA technology can exhibit large actuation strains, fast response speed, light weight, high resilience, high energy efficiency and no acoustic noise.

Smart devices capable of tuning optical transmittance with the control of a voltage are gathering increasing interest for possible applications varying from aerospace to automotive applications. Recently, DEAs have been used as a promising technology to electrically modulate the optical transparency of soft insulating membranes. The major focus of this thesis is to develop variable optical transmission DEA driven devices that use reliable transparent conductors, with the aim of achieving the electrically-induced large and continuous changes in the degree of surface transparency.

First, it has been necessary to study the fundamental aspects of DEAs. Therefore, the background of electroactive polymer technology has been reviewed, and a comprehensive survey on DEAs, including working principles, dielectric elastomer materials, compliant electrode materials, pre-stretch effects, electromechanical instability and device configurations, has also been conducted. Then, the state-of-the-art technologies that can be applied in smart-window applications and their principles of operation to electrically control light transmittance have been carefully reviewed. Those technologies include commercially available electrochromic, PDLC and SPD windows, as well as more recently developed DEA-based electrically tuneable transparency devices.

Since the most challenging part of this work was to develop a material that could be used as transparent deformable conductor, the reliability and electrically tuning performance of several transparent electrode materials for use with DEAs have been experimentally investigated. Those devices have been tested based on a planar DEA configuration consisting of clear dielectric elastomer membranes with various transparent electrodes, and all operated by an expansion-mode working principle to electrically control light transmittance. It has been found that AgNWs electrodes scatter light even on the flat elastomer membrane, and thus can only change the surface transparency from opaque to translucent. The PAAm-based hydrogels containing LiCl as transparent electrodes were also proposed due to the material's high transparency. But such prototype was unsuccessful, because the hydrogels were too hydrophobic to bond with the elastomer membrane and tended to progressively dry out in open air. After that, PMMA-based

ionogels were evaluated. Such highly transparent electrodes, however, have failed to provide good lifetime stability and surface wrinkling reversibility, and therefore were not suitable for the long-term use. Eventually, deformable PEDOT:PSS electrodes successfully exhibited the strain-dependent scattering of transmitted light. More importantly, such conducting polymer can be made as very transparent thin films, exhibit good environmental stability and offer reversible formation of surface wrinkles. Therefore, PEDOT:PSS was selected as the optimal transparent electrode material used to develop DEA-based adaptive optical devices.

After identifying the most suitable transparent conductor, many different ways to electrically tune the optical transparency of soft elastomeric membranes, using dielectric elastomer actuation, were developed and have been presented and compared in this thesis. The driving strategies have been based on different methods to electrically modulate the surface topography of a transparent PEDOT:PSS thin film covering the membrane surface. It has been found that the configurations operating in expansion and contraction modes can be used to electrically increase and decrease the light transmittance, respectively. Furthermore, the concept of dual-mode configuration integrating expansion and contraction strategies has been developed. This enables a modulation of transparency to both higher and lower values within the same device, with a very broad tuning range of far-field transmittance (25%-83%). Additionally, coaxially aligning two of such dual-mode devices can serve to broaden the transmittance tuning range (7%-66%), although at the cost of reducing the maximum value of transmittance. Within

the monitored time span of 8 weeks, all the implemented devices exhibited stable electro-mechano-optical performance.

Moreover, the concept of electrically-induced directional light diffusion using the DEA technology has been developed. While the tuning of optical transparency is still achieved by electrically changing the surface topography of a deformable transparent PEDOT:PSS thin film coated on the elastomer membrane, the anisotropic tuning of light diffusion is primarily caused by the uniaxial pre-stretch of the elastomer membrane to form the alignment of surface winkles upon electrical activation. Multi-directional light diffusion has also been obtained by attaching two single direction light diffusers using dielectric elastomer actuation orthogonally to each other. This type of device has been shown to electrically control the light scattering in either transverse or longitudinal direction individually, depending on whether the electrical activation concerns the single directional diffuser at the back or the front. Besides, the two diffusers can be actuated simultaneously to allow the light scattering to occur in both directions. Under this condition, the device can offer a more isotropic change to the optical transparency, with an even broader tuning range of far-field transmittance (4%-75%) than that of the above described dual-mode device.

Overall, the DEA-based tuneable optical transparency devices and directional light diffusing devices developed in this work have shown thin structures, fast response within a second, low specific weight and acoustically silent operation. Therefore, they could be potentially useful in electrically tuneable privacy

windows, controllable light diffusers and directional beam spreaders with light shaping.

6.2 Future work

For the electrically tuneable optical transparency device operated by dual-mode configuration described in Chapter 4, future developments could improve its performance by optimising the area ratio of the two independent electrodes, according to application-driven specifications in terms of required window size and acceptable device size. To this aim, a useful tool would be represented by computational models, such as that by Lu et al (Lu, Cai, Wang, & Suo, 2013).

Furthermore, improvements could also concern the use of conductive deformable transparent materials with an even higher refractive index, in order to increase the scattering of light when the surface is wrinkled, and so further extend the transmittance tuning range. The significant diversity of stretchable transparent materials available today, as recalled in the Section 3.1 in Chapter 3, offers a wide range of choices to be explored for possible improvements. In addition, for the tuneable transparency device operated by contraction mode described in Chapter 4 and the directional light diffusing device described in Chapter 5, PEDOT:PSS has primarily acted as a deformable medium with strain-dependent scattering of the transmitted light, rather than a transparent electrode. In fact, this material could be replaced by any applicable non-

conductive deformable polymer thin film with a high refractive index, which should definitely be further investigated to create a lower cost membrane.

Moreover, the use of membranes made of silicone elastomers is expected to lead to devices capable of the highest possible tuning speeds due to their lower glass transition temperature and much-reduced mechanical losses, as it can be inferred from previous investigations on tuneable lenses driven by dielectric elastomer actuation (Maffli et al., 2015).

References

Anderson, I. A., Gisby, T. A., McKay, T. G., O'Brien, B. M., & Calius, E. P. (2012). Multi-functional dielectric elastomer artificial muscles for soft and smart machines. *Journal of Applied Physics*, *112*(4), 041101. doi: 10.1063/1.4740023

Aschwanden, M., Beck, M., & Stemmer, A. (2007). Diffractive transmission grating tuned by dielectric elastomer actuator. *IEEE Photonics Technology Letters*, *19*(14), 1090–1092. doi: 10.1109/LPT.2007.900055

Bar-Cohen, Y. (2004). *Electroactive Polymer (EAP) Actuators as Artificial Muscles: Reality, Potential, and Challenges, Second Edition* (Vol. 5; Y. Bar-Cohen, ed.). doi: 10.1117/3.547465

Beck, M., Fiolka, R., & Stemmer, A. (2009). Variable phase retarder made of a dielectric elastomer actuator. *Optics Letters*, *34*(6), 803–805. doi: 10.1364/OL.34.000803

Bonsor, K. (2001). How smart windows work. Retrieved October 24, 2019, from https://home.howstuffworks.com/home-improvement/construction/green/smart-window.htm

Brochu, P., & Pei, Q. (2010). Advances in dielectric elastomers for actuators and artificial muscles. *Macromolecular Rapid Communications*, *31*(1), 10–36. doi: 10.1002/marc.200900425

Campo, E. A. (2008). Physical Properties of Polymeric Materials. In *Selection of Polymeric Materials* (pp. 175–203). doi: 10.1016/B978-081551551-7.50007-3

Carpi, F. (2016). *Electromechanically Active Polymers: A Concise Reference*. doi: 10.1007/978-3-319-31530-0

Carpi, F., Anderson, I., Bauer, S., Frediani, G., Gallone, G., Gei, M., … Shea, H. (2015). Standards for dielectric elastomer transducers. *Smart Materials and Structures*, *24*(10), 105025. doi: 10.1088/0964-1726/24/10/105025

Carpi, F., Bauer, S., & De Rossi, D. (2010). Stretching dielectric elastomer performance. *Science*, *330*(6012), 1759–1761. doi: 10.1126/science.1194773

Carpi, F., De Rossi, D., Kornbluh, R., Pelrine, R., & Sommer-Larsen, P. (2008). *Dielectric Elastomers as Electromechanical Transducers: Fundamentals, Materials, Devices, Models and Applications of an Emerging Electroactive Polymer Technology*. doi: 10.1016/B978-0-08-047488-5.X0001-9

Carpi, F., Frediani, G., Turco, S., & De Rossi, D. (2011). Bioinspired tunable lens with muscle-like electroactive elastomers. *Advanced Functional Materials*, *21*(21), 4152–4158. doi: 10.1002/adfm.201101253

Carpi, F., Kornbluh, R., Sommer-Larsen, P., & Alici, G. (2011). Electroactive polymer actuators as artificial muscles: are they ready for bioinspired applications? *Bioinspiration & Biomimetics*, *6*(4), 045006. doi: 10.1088/1748-3182/6/4/045006

Chen, B., Bai, Y., Xiang, F., Sun, J. Y., Mei Chen, Y., Wang, H., … Suo, Z. (2014). Stretchable and transparent hydrogels as soft conductors for dielectric elastomer actuators. *Journal of Polymer Science, Part B: Polymer Physics*, *52*(16), 1055–1060. doi: 10.1002/polb.23529

Chen, B., Lu, J. J., Yang, C. H., Yang, J. H., Zhou, J., Chen, Y. M., & Suo, Z. (2014). Highly stretchable and transparent ionogels as nonvolatile conductors for dielectric elastomer transducers. *ACS Applied Materials and Interfaces*, *6*(10), 7840–7845. doi: 10.1021/am501130t

Chen, Z. H., Fang, R., Li, W., & Guan, J. (2019). Stretchable transparent conductors: from micro/macromechanics to applications. *Advanced Materials*, *31*(35), 1900756. doi: 10.1002/adma.201900756

Choi, H. R., Jung, K., Chuc, N. H., Jung, M., Koo, I., Koo, J., … Lee, Y. (2005). Effects of prestrain on behavior of dielectric elastomer actuator. *Proc.SPIE*, *5759*. Retrieved from https://doi.org/10.1117/12.599363

Cupelli, D., Nicoletta, F. P., Manfredi, S., Vivacqua, M., Formoso, P., De Filpo, G., & Chidichimo, G. (2009). Self-adjusting smart windows based on polymer-dispersed liquid crystals. *Solar Energy Materials and Solar Cells*, *93*(11), 2008–2012. doi: 10.1016/j.solmat.2009.08.002

Ding, Y., Zhang, J., Chang, L., Zhang, X., Liu, H., & Jiang, L. (2017). Preparation of High-Performance Ionogels with Excellent Transparency, Good Mechanical Strength, and High Conductivity. *Advanced Materials*, *1704253*, 1704253. doi: 10.1002/adma.201704253

Fang, Z. H., Punckt, C., Leung, E. Y., Schniepp, H. C., & Aksay, I. A. (2010). Tuning of structural color using a dielectric actuator and multifunctional compliant electrodes. *Applied Optics*, *49*(35), 6689–6696. doi: 10.1364/AO.49.006689

Granqvist, Claes G. (2014). Electrochromics for smart windows: oxide-based thin films and devices. *Thin Solid Films*, *564*, 1–38. doi: 10.1016/j.tsf.2014.02.002

Granqvist, Claes Goran. (2005). Electrochromic devices. *Journal of the European Ceramic Society*, *25*(12), 2907–2912. doi: 10.1016/j.jeurceramsoc.2005.03.162

Hau, S. K., Yip, H. L., Zou, J., & Jen, A. K. Y. (2009). Indium tin oxide-free semi-transparent inverted polymer solar cells using conducting polymer as both bottom and top electrodes. *Organic Electronics: Physics, Materials, Applications*, *10*(7), 1401–1407. doi: 10.1016/j.orgel.2009.06.019

Hosseinzadeh Khaligh, H., Liew, K., Han, Y., Abukhdeir, N. M., & Goldthorpe, I. A. (2015). Silver nanowire transparent electrodes for liquid crystal-based smart windows. *Solar Energy Materials and Solar Cells*, *132*, 337–341. doi: 10.1016/j.solmat.2014.09.006

Huang, M., Tunnicliffe, L. B., Zhuang, J., Ren, W., Yan, H., & Busfield, J. J. C. (2016). Strain-Dependent Dielectric Behavior of Carbon Black Reinforced Natural Rubber. *Macromolecules*, *49*(6), 2339–2347. doi: 10.1021/acs.macromol.5b02332

Ig Mo Koo, Kwangmok Jung, Ja Choon Koo, Jae-Do Nam, Young Kwan Lee, & Hyouk Ryeol Choi. (2008). Development of Soft-Actuator-Based Wearable Tactile Display. *IEEE Transactions on Robotics*, *24*(3), 549–558. doi: 10.1109/TRO.2008.921561

Ji, X., Rosset, S., & Shea, H. R. (2016). Soft tunable diffractive optics with multifunctional transparent electrodes enabling integrated actuation. *Applied Physics Letters*, *109*(19), 191901. doi: 10.1063/1.4967001

Jun, K.-W., Kim, J.-N., Jung, J.-Y., & Oh, I.-K. (2017). Wrinkled graphene–AgNWs hybrid electrodes for smart window. *Micromachines*, *8*(2), 43. doi: 10.3390/mi8020043

Keplinger, C., Sun, J.-Y. Y., Foo, C. C., Rothemund, P., Whitesides, G. M., & Suo, Z. (2013). Stretchable, transparent, ionic conductors. *Science*, *341*(6149), 984–987. doi: 10.1126/science.1240228

Kim, M., Park, K. J., Seok, S., Ok, J. M., Jung, H. T., Choe, J., & Kim, D. H. (2015). Fabrication of microcapsules for dye-doped polymer-dispersed liquid crystal-based smart windows. *ACS Applied Materials and Interfaces*, *7*(32), 17904–17909. doi: 10.1021/acsami.5b04496

Kim, Y. H., Sachse, C., MacHala, M. L., May, C., Müller-Meskamp, L., & Leo, K. (2011). Highly conductive PEDOT:PSS electrode with optimized solvent and thermal post-treatment for ITO-free organic solar cells. *Advanced Functional Materials*, *21*(6), 1076–1081. doi: 10.1002/adfm.201002290

Kofod, G., Sommer-Larsen, P., Kornbluh, R., & Pelrine, R. (2003). Actuation Response of Polyacrylate Dielectric Elastomers. *Journal of Intelligent Material Systems and Structures*, *14*(12), 787–793. doi: 10.1177/104538903039260

Koh, S. J. A., Li, T., Zhou, J., Zhao, X., Hong, W., Zhu, J., & Suo, Z. (2011). Mechanisms of large actuation strain in dielectric elastomers. *Journal of Polymer Science Part B: Polymer Physics*, *49*(7), 504–515. doi: 10.1002/polb.22223

Kornbluh, R. D., Pelrine, R., Pei, Q., Heydt, R., Stanford, S., Oh, S., & Eckerle, J. (2002). Electroelastomers: applications of dielectric elastomer transducers for actuation, generation, and smart structures. In A.-M. R. McGowan (Ed.), *Smart Structures and Materials 2002: Industrial and Commercial Applications of Smart Structures Technologies* (Vol. 4698, pp. 254–270). doi: 10.1117/12.475072

Kovacs, G., & Düring, L. (2009). Contractive tension force stack actuator based on soft dielectric EAP. In Y. Bar-Cohen & T. Wallmersperger (Eds.), *Proc.SPIE* (Vol. 7287, p. 72870A). doi: 10.1117/12.815195

Kovacs, G., Lochmatter, P., & Wissler, M. (2007). An arm wrestling robot driven by dielectric elastomer actuators. *Smart Materials and Structures*, *16*(2), S306–S317. doi: 10.1088/0964-1726/16/2/S16

Lam, T., Tran, H., Yuan, W., Yu, Z., Ha, S., Kaner, R., & Pei, Q. (2008). Polyaniline nanofibers as a novel electrode material for fault-tolerant dielectric elastomer actuators. *Proc.SPIE*, *6927*. Retrieved from https://doi.org/10.1117/12.776817

Lau, G.-K., Goh, S. C.-K., & Shiau, L.-L. (2011). Dielectric elastomer unimorph using flexible electrodes of electrolessly deposited (ELD) silver. *Sensors and Actuators A: Physical*, *169*(1), 234–241. doi: 10.1016/j.sna.2011.04.037

Lee, Y. R., Kwon, H., Lee, D. H., & Lee, B. Y. (2017). Highly flexible and transparent dielectric elastomer actuators using silver nanowire and carbon nanotube hybrid electrodes. *Soft Matter*, *13*(37), 6390–6395. doi: 10.1039/C7SM01329A

Lin, I. T., Wang, T., Zhang, F., & Smoukov, S. K. (2017). Fault-tolerant electro-responsive surfaces for dynamic micropattern molds and tunable optics. *Scientific Reports*, *7*(1), 12481. doi: 10.1038/s41598-017-12899-y

Lipomi, D. J., Lee, J. A., Vosgueritchian, M., Tee, B. C.-K., Bolander, J. A., & Bao, Z. (2012). Electronic properties of transparent conductive films of PEDOT:PSS on stretchable substrates. *Chemistry of Materials*, *24*(2), 373–382. doi: 10.1021/cm203216m

Liu, J., Davis, N. R., Liu, D. S., & Hammond, P. T. (2012). Highly transparent mixed electron and proton conducting polymer membranes. *Journal of Materials Chemistry*, *22*(31), 15534–15539. doi: 10.1039/c2jm32296j

Lu, T., Cai, S., Wang, H., & Suo, Z. (2013). Computational model of deformable lenses actuated by dielectric elastomers. *Journal of Applied Physics*, *114*(10), 104104. doi: 10.1063/1.4821028

Madden, J. D. W., Vandesteeg, N. A., Anquetil, P. A., Madden, P. G. A., Takshi, A., Pytel, R. Z., … Hunter, I. W. (2004). Artificial Muscle Technology: Physical Principles and Naval Prospects. *IEEE Journal of Oceanic Engineering*, *29*(3), 706–728. doi: 10.1109/JOE.2004.833135

Madsen, F. B., Daugaard, A. E., Hvilsted, S., & Skov, A. L. (2016). The Current State of Silicone-Based Dieletric Elastomer Transducers. *Macromolecular Rapid Communications*, *37*, 378–413. doi: 10.1002/marc.201500576

Maffli, L., Rosset, S., Ghilardi, M., Carpi, F., & Shea, H. (2015). Ultrafast all-polymer electrically tunable silicone lenses. *Advanced Functional Materials*, *25*(11), 1656–1665. doi: 10.1002/adfm.201403942

McCoul, D., Hu, W., Gao, M., Mehta, V., & Pei, Q. (2016). Recent advances in stretchable and transparent electronic materials. *Advanced Electronic Materials*, *2*(5), 1–51. doi: 10.1002/aelm.201500407

Mortimer, R. J., Rosseinsky, D. R., & Monk, P. M. S. (2015). *Electrochromic Materials and Devices*. John Wiley & Sons.

Nicoletta, F. P., Chidichimo, G., Cupelli, D., De Filpo, G., De Benedittis, M., Gabriele, B., … Fazio, A. (2005). Electrochromic polymer-dispersed liquid-crystal film: a new bifunctional device. *Advanced Functional Materials*, *15*(6), 995–999. doi: 10.1002/adfm.200400403

Niklasson, G. A., & Granqvist, C. G. (2007). Electrochromics for smart windows: thin films of tungsten oxide and nickel oxide, and devices based on these. *Journal of Materials Chemistry*, *17*(2), 127–156. doi: 10.1039/b612174h

O'Halloran, A., O'Malley, F., & McHugh, P. (2008). A review on dielectric elastomer actuators, technology, applications, and challenges. *Journal of Applied Physics*, *104*(7), 071101. doi: 10.1063/1.2981642

Ohzono, T., Suzuki, K., Yamaguchi, T., & Fukuda, N. (2013). Tunable optical diffuser based on deformable wrinkles. *Advanced Optical Materials*, *1*(5), 374–380. doi: 10.1002/adom.201300128

Ong, H.-Y., Shrestha, M., & Lau, G.-K. (2015). Microscopically crumpled indium-tin-oxide thin films as compliant electrodes with tunable transmittance. *Applied Physics Letters*, *107*(13), 132902. doi: 10.1063/1.4932115

Palakodeti, R., & Kessler, M. R. (2006). Influence of frequency and prestrain on the mechanical efficiency of dielectric electroactive polymer actuators. *Materials Letters*, *60*(29–30), 3437–3440. doi: 10.1016/j.matlet.2006.03.053

Pei, Q., Rosenthal, M., Stanford, S., Prahlad, H., & Pelrine, R. (2004). Multiple-degrees-of-freedom electroelastomer roll actuators. *Smart Materials and Structures*, *13*(5), N86–N92. doi: 10.1088/0964-1726/13/5/N03

Pelrine, R. E., Kornbluh, R. D., & Joseph, J. P. (1998). Electrostriction of polymer dielectrics with compliant electrodes as a means of actuation. *Sensors and Actuators A: Physical*, *64*(1), 77–85. doi: 10.1016/S0924-4247(97)01657-9

Pelrine, R., Kornbluh, R., & Kofod, G. (2000). High-Strain Actuator Materials Based on Dielectric Elastomers. *Advanced Materials*, *12*(16), 1223–1225. doi: 10.1002/1521-4095(200008)12:16<1223::AID-ADMA1223>3.0.CO;2-2

Pelrine, R., Kornbluh, R., Pei, Q., & Joseph, J. (2000). High-speed electrically actuated elastomers with strain greater than 100%. *Science*, *287*(5454), 836–839. doi: 10.1126/science.287.5454.836

Plante, J.-S., & Dubowsky, S. (2006). Large-scale failure modes of dielectric elastomer actuators. *International Journal of Solids and Structures*, *43*(25–26), 7727–7751. doi: 10.1016/j.ijsolstr.2006.03.026

Roentgen, W. C. (1880). About the changes in shape and volume of dielectrics caused by electricity. *Annual Physics and Chemistry Series*, *11*, 771–786.

Rosset, S., Araromi, O. A., Schlatter, S., & Shea, H. R. (2016). Fabrication Process of Silicone-based Dielectric Elastomer Actuators. *Journal of Visualized Experiments*, (108), 1–13. doi: 10.3791/53423

Rosset, S., Niklaus, M., Dubois, P., & Shea, H. R. (2009). Metal ion implantation for the fabrication of stretchable electrodes on elastomers. *Advanced Functional Materials*, *19*(3), 470–478. doi: 10.1002/adfm.200801218

Rosset, S., O'Brien, B. M., Gisby, T., Xu, D., Shea, H. R., & Anderson, I. A. (2013). Self-sensing dielectric elastomer actuators in closed-loop operation. *Smart Materials and Structures*, *22*(10), 104018. doi: 10.1088/0964-1726/22/10/104018

Rosset, S., & Shea, H. R. (2013). Flexible and stretchable electrodes for dielectric elastomer actuators. *Applied Physics A*, *110*(2), 281–307. doi: 10.1007/s00339-012-7402-8

Rosset, S., & Shea, H. R. (2016). Small, fast, and tough: Shrinking down integrated elastomer transducers. *Applied Physics Reviews*, *3*(3), 031105. doi: 10.1063/1.4963164

Sheng, J., Chen, H., Qiang, J., Li, B., & Wang, Y. (2012). Thermal, Mechanical, and Dielectric Properties of a Dielectric Elastomer for Actuator Applications. *Journal of Macromolecular Science, Part B*, *51*(10), 2093–2104. doi: 10.1080/00222348.2012.659617

Shian, S., & Clarke, D. R. (2016). Electrically tunable window device. *Optics Letters*, *41*(6), 1289–1292. doi: 10.1364/OL.41.001289

Shian, S., Diebold, R. M., & Clarke, D. R. (2013). Tunable lenses using transparent dielectric elastomer actuators. *Optics Express*, *21*(7), 8669–8676. doi: 10.1364/OE.21.008669

Shian, S., Diebold, R. M., McNamara, A., & Clarke, D. R. (2012). Highly compliant transparent electrodes. *Applied Physics Letters*, *101*(6), 12–16. doi: 10.1063/1.4742889

Shian, S., Kjeer, P., & Clarke, D. R. (2018). Electric-field induced surface instabilities of soft dielectrics and their effects on optical transmittance and scattering. *Journal of Applied Physics*, *123*(11), 113105. doi: 10.1063/1.5018858

Shrestha, M., Asundi, A., & Lau, G. K. (2018). Smart window based on electric unfolding of microwrinkled TiO2 nanometric films [Research-article]. *ACS Photonics*, *5*(8), 3255–3262. doi: 10.1021/acsphotonics.8b00486

Son, S., Pugal, D., Hwang, T., Choi, H. R., Koo, J. C., Lee, Y., … Nam, J.-D. (2012). Electromechanically driven variable-focus lens based on transparent dielectric elastomer. *Applied Optics*, *51*(15), 2987–2996. doi: 10.1364/AO.51.002987

Tang, C., Li, B., Zou, C., Liu, L., & Chen, H. (2018). Voltage-induced wrinkle performance in a hydrogel by dielectric elastomer actuation. *Polymers*, *10*(7), 697. doi: 10.3390/polym10070697

Tank, D., Lee, H. H., & Khang, D. Y. (2009). Elastic moduli of organic electronic materials by the buckling method. *Macromolecules*, *42*(18), 7079–7083. doi: 10.1021/ma900137k

Van Den Ende, D., Kamminga, J. D., Boersma, A., Andritsch, T., & Steeneken, P. G. (2013). Voltage-controlled surface wrinkling of elastomeric coatings. *Advanced Materials*, *25*(25), 3438–3442. doi: 10.1002/adma.201300459

Vosgueritchian, M., Lipomi, D. J., & Bao, Z. (2012). Highly conductive and transparent PEDOT:PSS films with a fluorosurfactant for stretchable and flexible transparent electrodes. *Advanced Functional Materials*, *22*(2), 421–428. doi: 10.1002/adfm.201101775

Wang, Q., Tahir, M., Zang, J., & Zhao, X. (2012). Dynamic electrostatic lithography: multiscale on-demand patterning on large-area curved surfaces. *Advanced Materials*, *24*(15), 1947–1951. doi: 10.1002/adma.201200272

Wang, Y., Zhou, J., Sun, W., Wu, X., & Zhang, L. (2014). Mechanics of dielectric elastomer-activated deformable transmission grating. *Smart Materials and Structures*, *23*(9), 095010. doi: 10.1088/0964-1726/23/9/095010

Wei, K., Domicone, N. W., & Zhao, Y. (2014). Electroactive liquid lens driven by an annular membrane. *Optics Letters*, *39*(5), 1318. doi: 10.1364/OL.39.001318

Williamson, M., & Venables, M. (2013). Special report: 50th Paris Air Show. *Engineering & Technology*, *8*(7), 18–19. doi: 10.1049/et.2013.0709

Yang, C. H., Zhou, S., Shian, S., Clarke, D. R., & Suo, Z. (2017). Organic liquid-crystal devices based on ionic conductors. *Materials Horizons*, *4*(6), 1102–1109. doi: 10.1039/C7MH00345E

Yuan, W., Hu, L. B., Yu, Z. B., Lam, T., Biggs, J., Ha, S. M., … Pei, Q. (2008). Fault-tolerant dielectric elastomer actuators using single-walled carbon nanotube electrodes. *Advanced Materials*, *20*(3), 621–625. doi: 10.1002/adma.200701018

Yuan, W., Lam, T., Biggs, J., Hu, L., Yu, Z., Ha, S., … Pei, Q. (2007). New electrode materials for dielectric elastomer actuators. *Proc.SPIE*, *6524*. Retrieved from https://doi.org/10.1117/12.715383

Yun, S., Niu, X., Yu, Z., Hu, W., Brochu, P., & Pei, Q. (2012). Compliant Silver Nanowire-Polymer Composite Electrodes for Bistable Large Strain Actuation. *Advanced Materials*, *24*(10), 1321–1327. doi: 10.1002/adma.201104101

Zang, J., Ryu, S., Pugno, N., Wang, Q., Tu, Q., Buehler, M. J., & Zhao, X. (2013). Multifunctionality and control of the crumpling and unfolding of large-area graphene. *Nature Materials*, *12*(4), 321–325. doi: 10.1038/nmat3542

Zhao, Q., Haines, A., Snoswell, D., Keplinger, C., Kaltseis, R., Bauer, S., … Baumberg, J. J. (2012). Electric-field-tuned color in photonic crystal elastomers. *Applied Physics Letters*, *100*(10), 101902. doi: 10.1063/1.3691930

Zhao, X., & Suo, Z. (2010). Theory of Dielectric Elastomers Capable of Giant Deformation of Actuation. *Physical Review Letters*, *104*(17), 178302. doi: 10.1103/PhysRevLett.104.178302

Appendix I Details of collaboration and publications

1. Chen, L., Busfield, J.J.C., & Carpi, F. (2020). Electrically tunable directional light scattering from soft thin membranes. *Optics Express*, *28*(14), 20669-20685. doi: 10.1364/OE.392015

2. Chen, L., Ghilardi, M., Busfield, J.J.C., & Carpi, F. (2019). Electrically tuning soft membranes to both a higher and a lower transparency. *Scientific Reports*, *9*(1), 20125. doi: 10.1038/s41598-019-56505-9

3. Chen, L., Ghilardi, M., Carpi, F., & Busfield, J.J.C. (2019). Changes in optical transparency of a soft membrane using a dielectric elastomer actuator. *Proceedings of IRC 2019 – International Rubber Conference.* (IRCO Best Paper Presentation Award)

4. Chen, L., Ghilardi, M., Carpi, F., & Busfield, J. (2019). Changes in optical transmission of a soft membrane using a dielectric elastomer actuator. *Proceedings of EuroEAP 2019 – Ninth International Conference on Electromechanically Active Polymer (EAP) Transducers & Artificial Muscles.*

5. Chen, L., Carpi, F., & Busfield, J. (2018). Voltage-induced changes in optical transmission based on dielectric elastomer actuators. *Proceedings of EuroEAP 2018 – Eighth International Conference on Electromechanically Active Polymer (EAP) Transducers & Artificial Muscles.*

6. Chen, L., Carpi, F., & Busfield, J. (2017). Tuneable optical transmission devices based on dielectric elastomer actuators. *Proceedings of EuroEAP 2017 – Seventh International Conference on Electromechanically Active Polymer (EAP) Transducers & Artificial Muscles*.